UNIVERSIDADE DE LISBOA
FACULDADE DE FARMÁCIA

The therapeutic potential of small molecules p53-MDM protein-protein interaction inhibitors

Rute Cláudia Correia Sacadura Nunes

Dissertação orientada pela Doutora Maria Manuel Duque Vieira Marques dos Santos e coorientada pela Doutora Joana São José Dias Amaral

Mestrado em Ciências Biofarmacêuticas

2016

UNIVERSIDADE DE LISBOA
FACULDADE DE FARMÁCIA

The therapeutic potential of small molecules p53-MDM protein-protein interaction inhibitors

Rute Cláudia Correia Sacadura Nunes

Dissertação orientada pela Doutora Maria Manuel Duque Vieira Marques dos Santos e coorientada pela Doutora Joana São José Dias Amaral

Mestrado em Ciências Biofarmacêuticas

2016

RESUMO

Ao longo dos anos, vários estudos científicos têm comprovado a importância da proteína supressora de tumor p53 na homeostase celular. Esta proteína encontra-se inativada em aproximadamente 50% dos tumores humanos, quer seja por mutação ou por deleção do seu gene. Por outro lado, a inativação da p53 por inibição reversível é frequentemente observada nos tumores que expressam a forma selvagem da proteína. Esta inativação pode resultar da sobre-expressão dos seus reguladores negativos, tais como a proteínas MDM2 e MDMX, conduzindo a patologias oncogénicas caracterizadas principalmente pela expressão da p53 do tipo selvagem. Vários estudos têm demonstrado que a interação da p53 com as MDM's envolve três aminoácidos hidrofóbicos (Phe_{19}, Trp_{23} e Leu_{26}) da proteína p53. Além disso, sabe-se que a reativação da p53 é facilitada pela inibição destas interações. Nos últimos anos, várias famílias de compostos têm sido concebidas e desenvolvidas como moduladoras da atividade da p53. No entanto, o objetivo de desenvolver uma terapia anti-tumoural baseada na inibição das interações p53-MDM's, e consequentemente na reativação da p53, encontra-se ainda no início, com apenas alguns candidatos em ensaios clínicos. Deste modo, torna-se premente a descoberta e desenvolvimento de inibidores mais potentes e seletivos para a interação entre a p53 e os seus reguladores negativos.

Nos últimos anos, o nosso grupo de investigação tem vindo a investigar o potencial de várias famílias de spirooxindoles com anéis de cinco membros para o tratamento do cancro. Trabalhos anteriormente desenvolvidos pelo grupo, mostraram que as spiropirazolinas e spiroisoxazolina oxindoles apresentam propriedades anticancerígenas *in vitro*. O anel spiro encontrado nestes compostos funciona como uma estrutura heterocíclica rígida, a partir da qual podem ser projetados os três grupos lipofílicos que mimetizam a Phe_{19}, Trp_{23} e Leu_{26} da p53. Estudos mais detalhados sobre o mecanismo de ação das spiroisoxazolina oxindoles mostraram que estes compostos inibem a interação p53-MDM2. No entanto, estes compostos apenas induziram moderada atividade anti-proliferativa (IC_{50} cerca de 35 μM) para a linha celular de cancro colo-retal humano HCT-116. Estudos de química computacional indicaram que esta moderada atividade resulta provavelmente da orientação espacial do oxindole nestes compostos não permitir que mimetizasse o resíduo Trp_{23} da p53, fundamental para ocorrer a ligação à proteína MDM2. Em particular, os estudos de *docking* molecular mostraram que o oxindole é projetado para a cavidade que seria ocupada pela Phe19 da proteína p53, enquanto os grupos aromáticos ligados ao anel de isoxazolina são projetados para as cavidades Trp_{23} e Leu_{26} da p53. A substituição do átomo de oxigénio do anel de isoxazolina por um grupo *N*-Ar, poderia permitir não só a inclusão de mais um substituinte no anel de 5 membros, como uma reorientação dos substituintes do anel de 5 membros de forma a ocuparem as cavidades da MDM2 a que se ligam os aminoácidos da p53.

Por esse motivo, foi desenvolvida uma família de spiropirazolina oxindoles que foi testada nas linhas celulares de cancro da mama humano, MCF-7 e MDA-MB-231. Os compostos mais ativos apresentaram um valor de IC_{50} cerca de 7 μM. Adicionalmente, estes compostos apresentaram seletividade para a linha celular MDA-MB-231 e não foram tóxicos em células não tumorais Hek-293T. Nesta dissertação, otimizou-se esta família de compostos (spiropirazolina oxindoles) e avaliou-se em mais detalhe os seus efeitos biológicos. As

spiropirazolina oxindoles foram obtidas através de uma reação de cicloadição 1,3-dipolar entre 2-indolinonas e nitrilo iminas (formadas *in situ* a partir de cloretos de hidrazonoílo). Esta nova biblioteca de compostos foi caracterizada e posteriormente avaliada quanto ao seu potencial anti-proliferativo *in vitro*, utilizando as linhas celulares humanas de cancro colo-retal HCT-116 e cancro da mama MCF-7 e MDA-MB-231, e glioma de murino GL-261. Para a linha de cancro colo-retal os compostos apresentaram atividades entre os 11-13 μM, e para as linhas de cancro da mama MCF-7 e MDA-MB-231 apresentaram atividades de 7-12 μM e 6-11 μM, respetivamente. No caso da linha celular de glioma de murino, apenas um composto apresentou valores de atividade anti-proliferativa na mesma gama de valores com um IC_{50} de 19 μM. De salientar, a inclusão de um grupo *N*-Ar aumentou para mais do dobro a capacidade anti-proliferativa em HCT-116 $p53^{(+/+)}$, quando é feita uma comparação direta entre os compostos equivalentes de spiroisoxazolina oxindoles.

Com o intuito de avaliar o potencial citotóxico dos compostos em células saudáveis, foi realizado o ensaio de viabilidade celular em fibroblastos de colon humano normal e em culturas primárias de astroglia de murino. Como resultado, dois compostos (**2e** e **2m**) pertencentes à família spiropirazolina oxindoles não apresentaram citotoxicidade nas células saudáveis, apesar de serem citotóxicos nas linhas celulares de cancro. O mesmo não se verificou para o composto **2q**, para o qual foi observada citotoxicidade tanto em células normais como cancerígenas. Os compostos não citotóxicos em células normais foram então avaliados quanto à sua capacidade de indução de apoptose e paragem do ciclo celular na linha celular HCT-116. Os resultados demonstraram que estes compostos induzem tanto a morte por apoptose como a paragem do ciclo celular na fase G0/G1, estando ambos os fenómenos dependentes do tempo de exposição ou concentração de composto utilizada.

Com a finalidade de confirmar a capacidade desta família de compostos para induzir a morte celular, foram ainda avaliados os níveis de libertação da enzima citoplasmática lactato desidrogenase (LDH) indicativos do grau de rutura da membrana celular e, por conseguinte, de morte. Os resultados obtidos corroboraram o ensaio de apoptose, confirmando assim a capacidade de indução de morte dependente da concentração. As spiropirazolina oxindoles apresentaram ainda a capacidade de aumentar os níveis de expressão da p53 e induzir a inibição da MDM2, através da diminuição dos seus níveis de expressão proteica. Adicionalmente, a aptidão destes compostos para inibir a interação p53-MDM2 foi observada através do ensaio de complementação de fluorescência bimolecular (BiFC), e foi ainda verificada uma boa estabilidade em PBS (pH 7.4). Por último, foi observado um efeito sinergético entre um agente quimioterapêutico amplamente utilizado na clínica e um dos compostos em estudos.

As spiropirazolina oxindoles foram também avaliadas quanto à capacidade de induzir apoptose e paragem do ciclo celular na linha de glioma de murino GL-261. No entanto, os resultados obtidos não demonstraram qualquer evidência de indução de apoptose ou paragem do ciclo celular nestas células, indicando que estes compostos não têm potencial terapêutico neste tipo de tumores.

No âmbito desta tese foi também estudado em mais detalhe o mecanismo de ação de três spirotriazolina oxindoles previamente desenvolvidas no grupo como potenciais agentes anticancerígenos. Resultados obtidos anteriormente, tinham demonstrado que esta família apresentava boa seletividade para as linhas de cancro da mama MCF-7 e MDA-MB-231, sem apresentar citotoxicidade na linha não-tumoral Hek-293T. Observou-se ainda a capacidade destes compostos para inibir a interação p53-MDM2, ativar as caspases-3 e -7 e, consequentemente, induzir apoptose. Por último, uma boa estabilidade em plasma já tinha sido observada para os compostos em estudo.

De forma a estudar o eventual mecanismo de ação desta família de compostos como potenciais agentes anticancerígenos, na presente dissertação, testaram-se os compostos mais promissores de spirotriazolina oxindoles em células da linha de cancro colo-retal HCT-116, tendo-se verificado que estes compostos induzem apoptose e clivagem da PARP, assim como a paragem do ciclo celular na fase G0/G1, sendo esta dependente do tempo de exposição ou da concentração de composto utilizada. Adicionalmente, avaliou-se a capacidade destes compostos para ativar a p53 e diminuir os níveis de expressão de MDM2, indicando uma potencial inibição da interação p53-MDM2. A indução de apoptose e paragem do ciclo celular foi também avaliada na linha celular de cancro da mama MDA-MB-231. Contudo, os resultados obtidos não demonstraram qualquer indução de apoptose após 72 horas de exposição das células ao composto. Porém, às 48 horas de exposição das células ao composto foi possível verificar a ativação das caspases-3 e -7 e paragem do ciclo celular na fase G2/M. Por último, os compostos mais promissores de spirotriazolina oxindoles foram testados em fibroblastos de colon humano normal, não se tendo verificado citotoxicidade para as concentrações testadas.

Em suma, nesta dissertação demonstrou-se o potencial de cinco compostos (**2e**, **2m**, **7f**, **7h** e **7z**) pertencentes a duas famílias de spirooxindoles, contendo anéis heterocíclicos de 5 membros, como agentes anticancerígenos e inibidores da interação proteína-proteína p53-MDM2.

Palavras-chave: Spirooxindoles, cancro, p53, MDM's.

ABSTRACT

Over the years, several scientific studies have been proving the importance of the p53 tumour suppressor protein, in cellular homeostasis. This protein is found inactivated in approximately 50% of human cancers, by mutation or deletion of its gene. Moreover, the inactivation of p53 by reversible inhibition is frequently observed in various human cancers, especially in those expressing wild type p53. This inactivation results from overexpression of its negative regulators such as MDM2 and MDMX, leading to oncogenic pathologies, mostly characterized by expression of a p53 wild type form. Several studies have shown that p53 interaction with its negative regulators involves three main hydrophobic amino acids (Phe_{19}, Trp_{23} and Leu_{26}) in the p53 protein. Moreover, it is known that p53 reactivation is facilitated by inhibition of its negative regulators. In recent few years, several families of compounds were designed and developed as modulators of p53. However, the development of a p53 reactivating cancer therapy through inhibition of p53–MDM´s interaction is still at the beginning, with only a few candidates entering clinical trials. Therefore, the discovery of more powerful and selective p53–MDM´s interaction inhibitors are still an unmet need.

The work developed in this master thesis aimed at developing new anticancer agents containing a spirooxindole scaffold having a pyrazoline ring. The spiro ring works as the rigid heterocyclic scaffold, from which the three lipophilic groups can be projected to mimic the p53 amino acids. The first goal included the development and optimization of a potential new anticancer agent by 1,3-dipolar cycloaddition reaction, complemented with biological activity studies, such as evaluation of cell death and cell cycle progression, and analysis of p53-MDM2 interaction. In addition, studies of combination therapy using the newly synthetized molecules and a chemotherapeutic agent commonly used in the clinic, were also performed and finally, the stability of the compound in a saline solution was assessed. The second main goal of this thesis was to understand the effect of changing the carbon atom by a nitrogen atom in position 4´ of the pyrazoline ring.

The results presented here reveal the potential anticancer activity of the new molecules, as shown by the ability to induce apoptosis and cell cycle arrest, inhibit the interaction between p53 and MDM2, while presenting good stability in PBS and no cytotoxic effects in normal human cells. Furthermore, a synergistic effect with the chemotherapeutic agent was observed.

The change of the carbon atom for a nitrogen atom in position 4´ (pyrazoline ring replaced by a tryazoline ring) led to a new family of small molecules that has the ability to increase the expression of p53, thus leading to apoptosis and cell cycle arrest. In addition, these compounds were not cytotoxic in human normal cells.

Key-words: Spirooxindoles, cancer, p53, MDM´s.

ACKNOWLEDGEMENTS/AGRADECIMENTOS

Primeiro de tudo gostaria de agradecer à minha orientadora Doutora Maria M. M. Santos pela oportunidade e ajuda concedida no âmbito desta dissertação, e pelas oportunidades concedidas anexamente a esta dissertação. Agradeço também à Doutora Joana Amaral, minha co-orientadora, por todo o apoio e ajuda no decorrer da dissertação, especialmente no decorrer dos ensaios biológicos e realização dos ensaios com a linha de gliomas de ratos.

Gostaria de agradecer ao Carlos Ribeiro pela realização do ensaio de BiFC e pela síntese dos compostos (**7f**, **7h** e **7z**) que utilizei para os estudos do mecanismo de ação. Gostaria ainda de agradecer ao Ângelo Monteiro pela síntese dos compostos **2a**-**2f**, **2h**-**2m**, **2p**, **2q**, **2s**, **2t**, **3c**, **3h**, **4b** e **4c**.

Agradeço à Doutora Lídia Gonçalves (iMed.ULisboa) por ter realizado os ensaios anti-proliferativos de MTT em células MCF-7, MDA-MB-231 e Hek-293T, e pela cedência das células MDA-MB-231 utilizadas para os restantes ensaios descritos nesta dissertação.

Quero também agradecer a todos as pessoas do grupo Cellular Function and Therapeutic Targeting (iMed.ULisboa) por toda a ajuda prestada no laboratório e análise de dados. Gostaria também de agradecer à Doutora Dora Brites pela cedência da linha celular GL-261.

Gostaria, ainda, de agradecer a todo o grupo de química medicinal por toda a ajuda, boa disposição e diversão passada com eles, e especialmente à minha colega Margarida pela ajuda no laboratório e pelas diversas explicações sobre a parte química.

Agradeço especialmente a toda a minha família e amigos, principalmente à minha mãe Otília pelo apoio, carinho e por nos momentos de desânimo ter sempre uma palavra reconfortante. Aos meus irmãos Paulo e Cristina pela animação e pelo apoio de todos os dias. Agradeço também ao meu namorado André João pela ajuda, paciência, amizade, carinho e todo o apoio incondicional. Sem vocês não teria sido possível.

Obrigada a todos.

ABBREVIATIONS

^{o}C	Celsius degrees
% (w/v)	Weight/volume percentage
5-Fu	5-Fluorouracil
7-AAD	7-Aminoactinomycin
Abs	Absorbance
Apaf-1	Apoptosis protease activating factor-1
ATP	Adenosine-5'-triphosphate
Bax	Bcl-2-associated X protein
Bcl-2	B-cell lymphoma protein 2
BiFC	Bimolecular fluorescence complementation assay
BSA	Bovine serum albumin
C	Carbon atom
Ca^{2+}	Calcium
Caspase	Cysteine-aspartic protease
CCD-18Co	Human normal colon fibroblasts cell line
CDI	Coefficient Drug Interaction
CH_2Cl_2	Dichloromethane
CO_2	Carbon dioxide
CRC	Colorectal cancer
DISC	Death inducing signaling complex
DCIS	Ductal carcinoma *in situ*
DMEM	Dulbecco's Modified Eagle Medium
DMSO	Dimethyl sulfoxide
DNA	Deoxyribonucleic acid
DTT	Dithiothreitol
EDTA	Ethylenediamine tetraacetic acid
EGFR	Epidermal growth factor receptor
Et_3N	Triethylamine
EtOAc	Ethyl Acetate
FBS	Fetal Bovine Serum
FITC	Fluorescein Isothiocyanate
G0/G1	phase Growth 0/ phase Growth 1 or Gap 0 phase/ Gap 1 phase
G2/M	phase Growth 0/ Mitotic phase
GL-261	Mouse glioma 261 cell line
H	Hydrogen atom
H_2O	Water
HER2+	Human epidermal growth factor receptor 2+
HCT-116	Colorectal carcinoma cell line
HCT-116 *p53*$^{(-/-)}$	Human colorectal cancer cell line with null p53
HCT-116 *p53*$^{(+/+)}$	Human colorectal cancer cell line with wild-type p53
Hek-293T	Human embryonic kidney cell line
KOH	Potassium hydroxide

HPLC	High-performance liquid chromatography
HR+	Hormone receptors
Hz	Hertz
IC_{50}	50% of maximal inhibitory concentration
kDa	KiloDalton
LCIS	Lobular carcinoma *in situ*
LDH	Lactate dehydrogenase
Leu	Leucine
MCF-7	Human breast adenocarcinoma cell line
MDA-MB-231	Human breast adenocarcinoma cell line
MDM2	Murine double minute-2
MDMX	Murine double minute-X
Me	Methyl
mTOR	Mammalian target of rapamycin
MTS	3-(4,5-dimetiltiazol-2-il)-5-(3-carboximetoxifenil)-2-(4-sulfofenil)-2H-tetrazólio
MTT	3-(4,5-dimethylthiazol-2-yl)-2,5-diphenyltetrazolium bromide
N	Nitrogen atom
NaCl	Sodium chloride
$NaHCO_3$	Sodium Bicarbonate
NCS	N-Chlorosuccinimide
NP-40	Nonyl phenoxypolyethoxylethanol
NMR	Nuclear magnetic resonance
PARP	Poly ADP ribose polymerase
PBS	Phosphate Buffered Saline
Ph	Phenyl
Phe	Phenylalanine
PI	Propidium Iodide
PMS	Phenazine Methosulphate
PPIs	Protein-protein interactions
ppm	parts per million
PS	Phospholipid phosphatidylserine
RNase A	Ribonuclease Ribonuclease A
ROS	Reactive oxygen species
r.t.	Room temperature
SAR	Structure-activity relationship
SDS	Sodium dodecyl sulfate
SD	Standard Deviation
SEM	Standard Error of the Mean
SI	Selectivity index
S phase	Synthesis phase
TBS	Tris-buffered saline
TEA	Triethylamine
temp.	Temperature

THF	Tetrahydrofuran
TLC	Thin layer chromatography
TNF	Tumour necrosis factor
TP53	p53 protein encoding gene
Tris-HCl	Tris-Hidroclorite
Trp	Tryptophan
UV	Ultraviolet
VEGF	Vascular endothelial growth factor
Wt	Wild-type

GENERAL CONTENTS

FIGURE INDEX

TABLE INDEX

SCHEME INDEX

Chapter 1

STATE OF THE ART

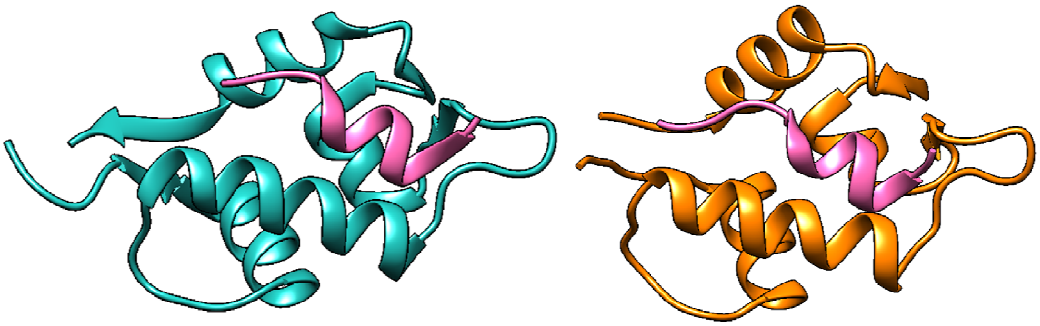

Mdm2 (orange)-p53 (pink) complex (PDB ID: 1YCR) and Mdmx (blue)-p53 (pink) complex (PDB ID: 3DAB). Image obtained using the UCSF Chimera software.

1.1. CANCER: ORIGIN, INCIDENCE AND THERAPEUTIC OPTIONS

The maintenance of cellular homeostasis is essential for tissue integrity in multicellular organisms. In this regard, apoptosis, a form of regulated cell death, is an highly conserved mechanism that has evolved to maintain cell number and cellular positioning within tissues, therefore acting as a natural barrier to cancer development[1,2].

Cancer is a multifaceted and multifactorial disease comprised of complex genetic and epigenetic aberrations that destabilize the normal balance of cellular life and death[3]. The main causes for cancer development are the nutrition habits, specific infections such as Helicobacter pylori, Hepatitis B and C viruses, and Human papillomaviruses, genetic determinants, and others factors[4–6]. According to the World Health Organization, cancer is a leading cause of death worldwide accounting for 8.2 millions of deaths each year. Female breast and colorectal cancers are among the five most diagnosed cancers and they are also the main contributors for mortality and loss of healthy life[4,6].

In terms of the therapies available, they differ according to the type of cancer. Overall, surgery, chemotherapy, and radiation therapy are the most common treatments used against cancer. Chemotherapy usually refers to the use of medicines or drugs as the therapeutic agent and act throughout the body, meaning that it can kill cancer cells that have spread (metastasized) in parts of the body away from the original (primary) tumour[7]. Surgery and radiation therapy remove, kill, or damage cancer cells in a certain area. These three types of therapy can and are currently used in combination for better efficiency of therapy[8,9].

More recently, new forms of cancer treatment have emerged, including targeted therapy that uses drugs or other substances to more precisely attack cancer cells causing minor damage to normal cells, and immunotherapy that relies in the use of an individual's own body immune system to tackle cancer. Immunotherapy may function in different ways: it can stimulate the immune system, or it can help the immune system to attack cancer cells. Finally, immunotherapy may also be used in combination with other types of treatment[7].

Cancer research has been a topic of great interest for the past decades; however, investment in cancer control, prevention, diagnosis and treatment is still an urgent need[5].

1.1.1. Colorectal Cancer

Colorectal cancer (CRC) is one of the most commonly diagnosed cancers and presents the highest cause of cancer deaths[10,11]. CRC develops in the colon or in the rectum, also known as the large intestine.

Most of the times, CRC begins as a noncancerous growth called polyp or adenoma that develops on the inner lining of the colon or rectum. Although all adenomas have the capacity to become cancerous, fewer than 10% are estimated to progress to invasive cancer. Cancer

that develops in glandular cells is called adenocarcinoma, which is approximately 96% of colorectal cancers[12].

Surgery is one of the primary options for CRC treatment, often in combination with radiation therapy and chemotherapy. The most often used drugs for colorectal cancer include: 5-Fluorouracil (5-FU); Capecitabine, which is in pill form and once in the body is converted to 5-FU; Irinotecan; Oxaliplatin; and Trifluridine and tipiracil (Lonsurf), a combination drug in pill form. Sometimes, two or more of these drugs are combined to achieve more efficacy.

Targeted therapy drugs work differently from standard chemotherapy drugs. Sometimes they are effective when standard chemotherapeutics drugs are not, and they often have different and less severe side effects. Currently, the most commonly used target cells with EGFR changes and the blood vessel formation (VEGF) where the Cetuximab (Erbitux) and the Bevacizumab (Avastin) are used. These drugs can be used in combination with chemotherapeutic drugs or alone if chemotherapeutic drugs are no longer effective[13].

1.1.2. Breast Cancer

Breast cancer is a heterogeneous disease with a wide spectrum of clinical, pathologic, and molecular features. Although it is much more frequent in women, men can also develop the disease[14]. The majority of breast cancers begin in the lobules and ducts where the mammary glands are located[15,16]. Breast cancer can be defined as *in situ* or invasive depending on its extension.

In situ breast cancer

Ductal carcinoma *in situ* (DCIS) is when abnormal cells replace the normal epithelial cells of the breast ducts. It is considered a non-invasive form of breast cancer and is the most common type of *in situ* breast cancer, representing about 83% of diagnosed cases. DCIS may or may not progress to invasive cancer and, in fact, some of these tumours grow so slowly that they may not affect the woman's health even without treatment.

Lobular carcinoma *in situ* (LCIS), also known as lobular neoplasia, generally is not considered a precursor of invasive cancer. Instead, it represents an indicator for increased risk for developing invasive cancer. LCIS accounts for about 13% of all female *in situ* breast cancers diagnosed.

Invasive breast cancer

The majority of breast cancer cases are invasive, or infiltrating, meaning that they have broken through the walls of the glands or ducts where they were originated, and have grown

into the surrounding breast tissue. Based on comprehensive gene expression profiling, breast tumours are classified into several subtypes: luminal and human epidermal growth factor receptor 2+ (HER2+), depending on if they express hormone receptors (HR+) and HER2, respectively[15,16]. Approximately 74% of all breast cancers are Luminal A (HR+/HER2-). These tumours tend to grow slowly and are less aggressive than other subtypes, probably because they are responsive to hormonal therapy[16,17]. Conversely, the triple negative tumours (HR-/HER2-) are the most aggressive, in part due to lack of specific therapies[16,17].

The majority of breast cancers are treated surgically, which can be often combined with radiation therapy, chemotherapy, hormonal (endocrine) therapy, and/or targeted therapy[16,18]. The benefit of different types of therapies depend on multiple factors, such as the size of the tumour, the number of lymph nodes involved, the presence of estrogen or progesterone receptors, and the amount of HER2 protein produced by cancer cells. For example, the triple negative and HER2+ breast cancers tend to be more sensitive to chemotherapy. Some examples of chemotherapeutics used are Paclitaxel, Carboplatin, 5-fluorouracil, Docetaxel among others[16,18].

There is yet, targeted therapy which is divided in two principal targets: targeted therapy aimed at HER2-positive where Trastuzumab, Pertuzumabre are used and targeted therapy for hormone receptor-positive using Everolimus and Palbociclib[16,18].

1.1.3. Glioblastoma

The brain is the most complex organ in vertebrates. It is composed primarily of two broad classes of cells, neurons and glial cells, which can develop into different types of tumours. The majority of brain tumours develop from glial cells that include astrocytes, oligodendrocytes, microglia and ependymal cells. Therefore, glioma is a generic term used to describe the different types of glial tumours: astrocytoma, oligodendroglioma, and glioblastoma. The most frequent and malignant of all is glioblastoma[19].

All the types of treatment referred before can be used in brain and spinal cord tumours. Each treatment is based on the type of tumour and other factors, and often, more than one type of treatment is used. Some of the chemotherapeutic drugs used to treat brain tumours include cisplatin, irinotecan and others, such as temozolomide. For example, temozolomide acts by inducing cytotoxicity through pro-autophagic processes and also through the induction of apoptosis. Of note, autophagy is a type II programmed cell death that represents an alternative mechanism to overcome, at least in part, the resistance of many cancers to apoptosis-related therapies. On the other hand, targeted therapy targets vascular endothelial growth factor (VEGF) and (mammalian target of rapamycin) *mTOR*[18,20,21].

1.2. CANCER BIOLOGY: PATHWAYS AND MECHANISMS

Tumourigenesis is a multistep process of acquiring successive genetic mutations that transform a normal cell into a cancer cell. These mutations give rise to hyperproliferative signals that sustain and enable the immortality of cells through an unlimited replicative potential, the invasion and metastization ability, the insensitivity to growth suppression signals, the resistance to cell death and the induction of tumour angiogenesis[2,22]. Deregulated expression of transcription factors during tumourigenesis is essential for the promotion of proliferation and differentiation of a neoplastic population[22].

1.2.1. Apoptosis

Cell death by apoptosis, is the principal strategy to control tumour development, in which cells receive specific stimuli to die. These stimuli are part of an important program of cell growth control, characterized by morphologic as well as biochemical changes. Apoptosis can occur by two major signalling pathways, the death receptors or extrinsic pathway, and the mitochondrial or intrinsic pathway. Overall, these two pathways are distinct, but ultimately converge to the same mechanism. The apoptotic process culminates in activation of a series of cysteine aspartyl-specific proteases, or caspases, that cleave key cellular proteins like polyADP-ribose polymerase (PARP) (Figure 1). Activation of caspases is considered the point of no-return, in which cell death becomes an irreversible process[23,24].

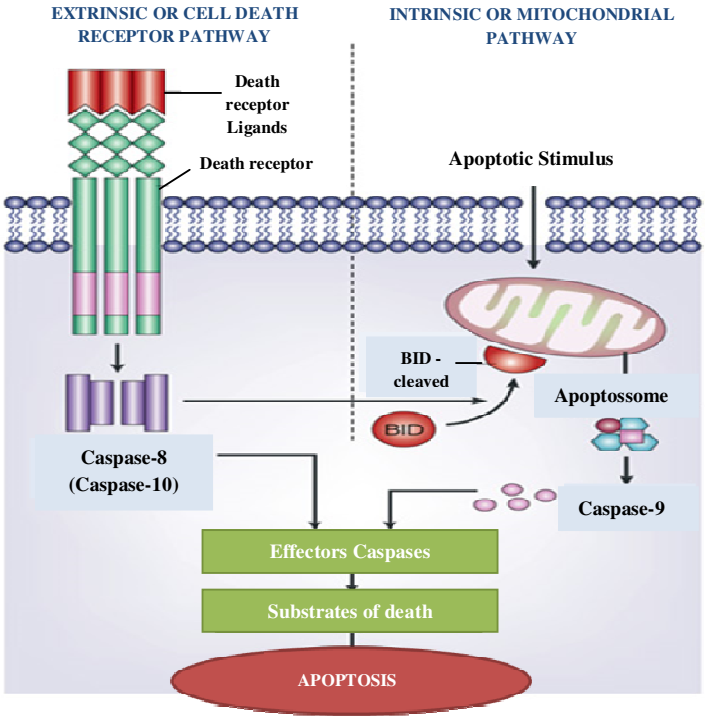

Figure 1 - Illustration of the two major apoptotic signalling pathways. Apoptosis can be initiated by two alternative pathways: via death receptors on the cell surface (extrinsic pathway) or by mitochondria (intrinsic pathway). In both pathways, induction of apoptosis leads to the activation of an initiator caspase. The two pathways are correlated since caspase-8 (extrinsic pathway) activates the intrinsic pathway for cleavage of Bid, Bcl2 family member. Adapted from [116].

Extrinsic or Cell Death Receptor Pathway

The extrinsic or cell death receptor pathway is initiated by extracellular signals, resulting in binding of ligands to specific transmembrane receptors, collectively known as death receptors, belonging to the tumour necrosis factor (TNF) family. The death receptors are cell surface receptors that transmit apoptotic signals from the cell surface to activate intracellular signalling pathways[25].

All death receptors work in a similar manner, via conformational changes that allow the assembly of a large multiprotein complex known as DISC (Death-Inducing Signalling Complex), ultimately leading to the activation of the caspase cascade. Pro-caspases are recruited to the DISC and subsequently are cleaved to result in active initiator caspases, including caspase-8 and -10, this initiator caspases have the ability to cleave and activate effectors caspases, such as caspase-3 and -7. Importantly, the extrinsic pathway is able to crosstalk with the intrinsic or mitochondrial pathway, thus amplifying the death signal[25–27].

Intrinsic or Mitochondrial Pathway

The intrinsic apoptotic pathway is initiated by a non-receptor mediated stimuli that triggers intracellular signalling. Mitochondria activation in the intrinsic pathway is mediated by the Bid protein, a pro-apoptotic member of the Bcl-2 family. Bid is cleaved indirectly by p53 and directly by active caspase-8, and subsequently translocated to the mitochondria. The presence of cleaved Bid in the mitochondrial membrane regulates mitochondria permeabilization. When an apoptotic stimuli reach the mitochondria, a variation of the inner mitochondrial membrane potential occurs, as well as changes in the membrane permeability, leading to the passage of water and consequently organelle's rupture. Consequently, mitochondria release pro-apoptotic factors into the cytoplasm, including cytochrome *c,* which together with the destabilization of the membrane potential leads to loss of cellular homeostasis, disruption of ATP synthesis and increased reactive oxygen species (ROS) production. The increase of ROS levels then leads to lipid, protein and nucleic acid oxidation by increasing the collapse of the inner mitochondrial membrane potential. Cytosolic cytochrome *c* also interacts with apoptotic protease activating factor 1 (Apaf-1) and pro-caspase 9, in the presence of ATP, to form a complex known as apoptosome. After that, caspase-9 is activated and subsequently activates effector caspases for the execution of apoptosis[25–28].

1.3. p53 – THE TUMOUR SUPPRESSOR PROTEIN AND TUMOURIGENESIS

p53 tumour suppressor protein is regarded as a key player in tumour suppression, as it promotes growth arrest, apoptosis and cellular senescence, while also blocking angiogenesis[29,30]. Strikingly, half of all human tumours carry p53 inactivated by mutation [30–32], while the other half refers to tumours in which the p53 pathway is partially abrogated by

inactivation of other signaling components, such as p53 endogenous negative regulators *m*urine *d*ouble *m*inute 2 (MDM2) and/or MDMX [29,32,33].

In some cases, frameshift or nonsense mutations result in the loss of p53 protein expression. However, missense mutations that lead to the substitution of a single amino acid in the p53 protein, can be stably expressed in tumours cells resulting in novel functions for p53[34,35]. These substitutions may occur throughout all the structural domains of p53 protein, but they are more frequently clustered within the DNA binding region of p53. These mutations generally lead to a loss or diminution of the wild-type activity of p53[34]. Although mutations have been detected in almost all of the p53 amino acids, a number of hotspot sites have been identified, especially at residues R175, G245, R248, R249 and R273[33,36].

p53 has been called "guardian of the genome", due to its central role in coordinating the cellular response to a wide range of cellular stress[37]. One of the main functions of p53 is as transcription factor that both activates and represses an ample range of target genes[37]. The regulation of p53 function has been described at multiple levels and consists in an array of post-translational modifications, that lead to protein accumulation and increase of its transcriptional activity, both during normal homeostasis as in stress-induced responses[31,37] (see Figure 2). Even though, the key mechanism by which p53 is regulated is through control of its protein stability, mediated primarily by MDM2.

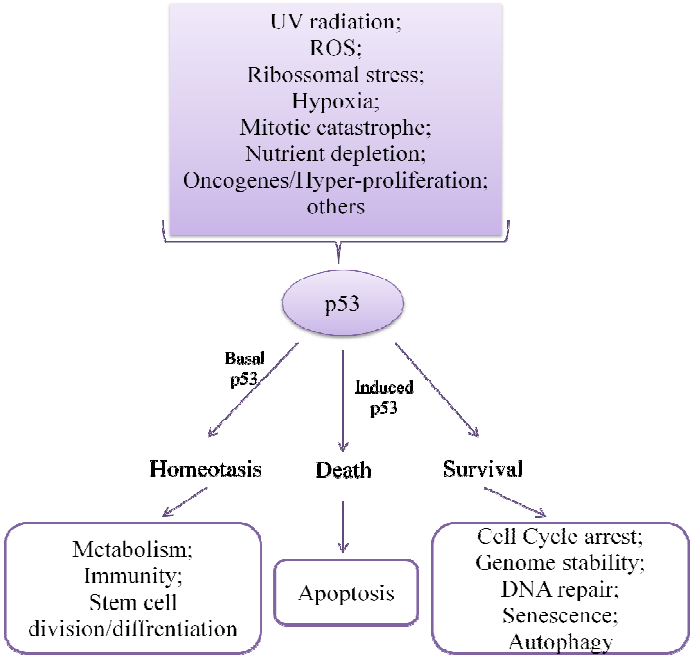

Figure 2 - Action of p53. A wide range of cellular stress stimuli induce p53, leading to co-ordinated changes in gene expression and various biological outcomes, depending on the cell type and the type, intensity and duration of the activating stress. Those events that induce p53 through the DNA-damage-response pathways are highlighted on the left-hand side in lilac. Regulation of some biological events may occur in a homoeostatic manner mediated by basal or low levels of p53. Adapted from[117].

As the p53 is frequently mutated or inactivated in cancer, this tumour suppressor has turned into a highly attractive therapeutic target for the treatment of the disease. Several studies have shown that p53 interaction with MDM2 and MDMX involves three main hydrophobic amino acids (Phe_{19}, Trp_{23} and Leu_{26}) in the p53 protein[38–40]. In case of cellular stress, these interactions should be inhibited to activate the p53 response[31]. For that purpose, small molecules that mimic the three amino acid residues of p53-MDMs binding pocket have been widely developed and tested as potential antitumour agents[38].

Further, as mutant p53 has been reported to confer drug resistance in different cancer therapies, its reactivation or neutralization can be beneficial in this context[33].

1.4. NEGATIVE REGULATORS OF p53

Protein-protein interactions (PPIs) have an important role in cancer because they regulate various cellular processes, particularly in cell cycle or cell signalling pathaways[41].

The small molecule inhibitors of protein-protein interactions have received considerable interest in the last years. In particular, the inhibitory interaction of p53 with regulatory proteins, MDM2 and MDMX, provided a focus of effort due to its importance in various types of cancer, and the prospect that inhibition of these interactions may provide new therapies[42].

The MDM´s proteins are present at high levels and inhibit activity p53 in many human cancers. Thus, interrupting the p53-MDM interaction to reactivate p53 is a valuable therapeutic strategy for the treatment of tumours[43].

Several studies currently focus on the design of small inhibitory molecules of both MDM´s (MDM2 and MDMX). Despite the efforts, there are no compounds in clinical stages for this purpose, since existing compounds for inhibiting MDM2 are inefficient in the inhibition of MDMX[44]. This problem derives, at least in part, from the "sub-pocket" Leu26 that represents the greatest challenge to design a dual inhibitor of MDM2/MDMX. The two proteins significantly differ in shape and in the properties of the residues surrounding the cavity[39,44–46].

Therefore, the development of specific inhibitors for MDMX must take into account their unique structural properties that go beyond this "simple" difference. The well-defined binding furrows in MDM´s suggest the feasibility of designing small-molecule inhibitors to block their interaction with p53[39].

1.5. p53-MDM2/MDMX PROTEIN-PROTEIN INTERACTION

The information of diverse proteins correlating their function in the tumour environment is emerging as an important aspect of studying protein function in cancer. The structural

changes of protein in the course of mutation with its altered cellular localization is a important point to understand better the progression of the disease[22].

MDM2 belongs to the family of E3 ubiquitin ligase that contains a RING (*r*eally *i*nteresting *n*ew *g*ene) domain and serves as the major ubiquitin ligase for p53 degradation[32,39,47].

The MDM2 protein binds directly to the *N*-terminal domain of p53, thus inhibiting its transcriptional activity through multiple mechanisms including, direct occlusion of p53 transactivation domain, induction of p53 nuclear export and target of p53 for proteasomal degradation[32,39]. However, recent research has demonstrated that MDM2 alone is insufficient to suppress p53 activity[32].

Under normal conditions, MDM2, which is itself a product of a p53 target gene, inhibits the activity of p53 by physical interaction[48]. This inhibition is accomplished through a negative autoregulatory feedback loop in which p53 activates the transcription of its own inhibitor, as mentioned above. Therefore, in non-stressed cells, the low level of MDM2 mediate multiple mono-ubiquitination of p53, promoting its nuclear export[29,37,49] (Figure 3).

When cells are challenged by a stress insult, p53 levels are rapidly up-regulated to enable repair. Meanwhile, the expression levels of MDM2 in cells under stress are also higher promoting the poly-ubiquitination and degradation of p53 after the repair has occurred. In the cytosol, mono-ubiquitinated p53 induces Bax oligomerization followed by mitochondrial translocation, eventually leading to the release of cytochrome *c* and other pro-apoptotic molecules into the cytosol. These mechanisms show that p53 ubiquitination by MDM2 is another layer of p53 activity regulation[31,37,49], further demonstrating the importance of p53-MDM2 binding as a therapeutic target in cancer.

MDM2 also interacts with its equivalent MDMX through the RING domain[31].

In the same way that MDM2, MDMX is an important negative regulator of p53. MDMX is a homologue of MDM2, in particular in the domain that binds to p53. Nevertheless, both proteins present enough differences to turn p53-Mdm2 inhibitors ineffective in inhibiting p53-MDMX interaction. It has been demonstrated that MDM2 regulates p53 mainly by protein degradation, whereas MDMX is a potent inhibitor of its transcriptional activity[50]. In fact, unlike MDM2, MDMX does not have appreciable ubiquitin ligase activity[44]. Another key difference between Mdm2 and MDMX is that MDMX is primarily located in the cytoplasm, while MDM2 is located in the nucleus. MDMX nuclear translocation may occur to form the complex MDM2/MDMX and inhibit p53[31]. The formation of MDM2/MDMX heterodimers through the RING domains participate in p53 poly-ubiquitination and proteasomal degradation. In response to DNA damage signals, MDM2/MDMX heterodimers are poly-ubiquitinated, resulting in degradation of the complex and consequent p53 stabilization and activation[45,49] (Figure 3).

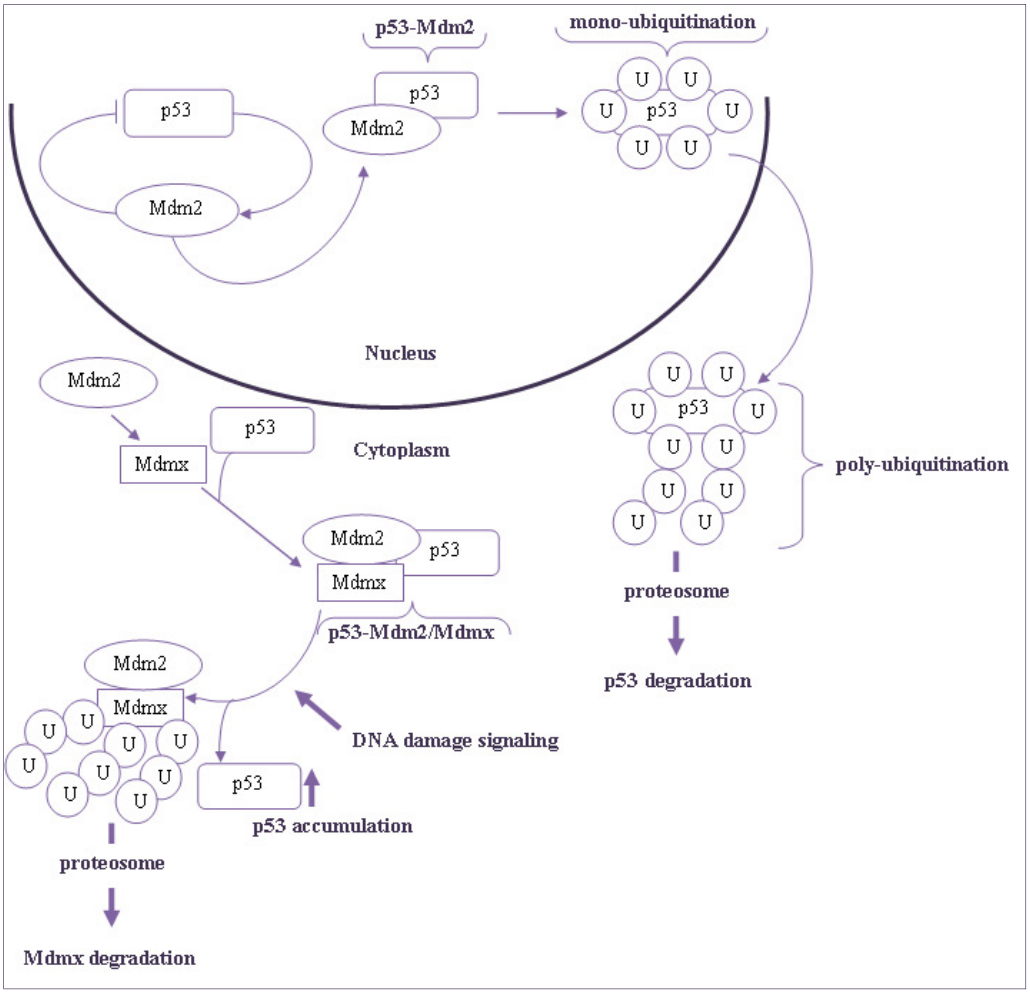

Figure 3 - Schematic diagram of p53 degradation regulated by MDM2 and MDMX. In unstressed conditions, p53 fails to accumulate due to constitutive degradation. Under genotoxic stress, cells activate an evolved response for MDMX degradation that stabilizes p53 and activity. U - ubiquitination.

In addition to having its own effects on p53, MDMX also plays an important role in stabilizing the MDM2 protein. Taking into account the role of MDMX in inhibiting p53, several molecules are being developed for MDMX inhibition.

In Table 1, are presented the main inhibitors developed for inhibition of the interactions between p53 and MDM´s proteins (Table 1).

Table 1 – Main MDM´s antagonists[51]**.**

Strategy	Compound
Interruption of p53 interaction with MDM2	Small molecules that bind the MDM2 N_ pocket: Nutlin-3a/RG7112, MI-219, MI-63, MI-319, MI-773, AM-8553, AMG-232, benzodiazepinediones, MK-8242 Small molecules that bind the p53 N-terminal domain: RITA
Interruption of p53 interaction with MDMX	Small molecules: WK 298, SJ-172550
Interruption of p53 interaction with both MDM2 and MDMX	Peptidic compounds: SAH-p53s, PMI peptide, pDI peptide Small molecules: RO-5963, CGM097

1.6. INHIBITORS OF p53-MDM2 INTERACTION

To date, there are over 20 different chemotypes that have been shown to antagonise the p53-MDM2 interaction, such as cis-imidazolines[52] (eg, RG-7112), benzodiazepinediones[53] (eg, TDP665759), spiropyrrolidine oxindoles[54] (eg, MI-77301), and piperidinones[55] (eg, AMG-232) (see Figure 4.2). Although these compounds share different scaffold structures, they all inhibit the p53-MDM2 interaction by mimicking the three hot spots residues of p53[39] (figure 4.1).

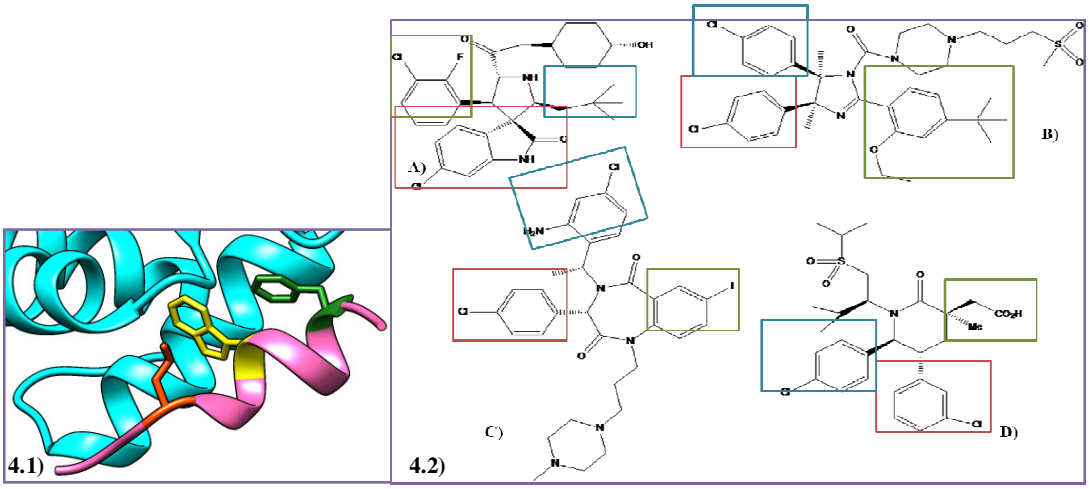

Figure 4 - 4.1) p53 structure (pink) with three hydrophobic residues Phe19 (Green), Trp23 (Yellow) and Leu26 (Orange). Image obtained using the UCSF Chimera software. **4.2)** Chemical structures of: A) MI-77301, B) RG-7112, C) TDP665759, D) AMG-232 mimic the three hydrophobic residues Phe19 (Green), Trp23 (Red) and Leu26 (Blue). Image obtained using the ChemDraw software.

1.6.1. Cis-Imidazolines (Nutlins)

The nutlins (cis-imidazolines) were identified as the first class of potent, non-peptide and specific small molecule MDM2 inhibitors, from a large chemical screen and chosen for their potency and selectivity for inhibition of the p53-MDM2 interaction[35,39]. Nutlin-3a, arrests proliferating cancer cells in the G1 and G2 cell cycle phases as well as induces apoptosis in

wild-type p53 dependent manner, in a number of different cancer cell lines expressing wt-p53 including colorectal, lung, breast, prostate, melanoma, osteosarcoma and renal cancer[35,56].

Further structure-based optimization of nutlin-3a led to compound RG-7112, the first MDM2 inhibitor advancing into clinical trials. In fact, RG-7112 presented enhanced binding affinity to MDM2 and more potency to inhibit wild-type p53 tumour growth[35,39,57].

1.6.2. Benzodiazepinediones

The Benzodiazepinediones disrupt the p53-MDM2 interaction in a similar manner to the nutlins, by mimicking the action of the key amino acids involved in the binding of the p53 peptide to MDM2[35]. One of these compounds is TDP665759[53], which binds to the binding cleft of MDM2, predominantly hydrophobic, and occupies the same pockets as the peptide side chains Phe_{19}, Trp_{23}, and Leu_{26} of p53. MDM2 interacts with the inhibitor through nonspecific Van Der Waals contacts[58].

1.6.3. Piperidinones

Compound AMG-232, was obtained by a structure-based design and wide optimization of a new class of MDM2 inhibitors containing a piperidinone scaffold. AMG-232 has entered in phase I clinical trials for human cancer treatment in 2012. In this compound the 3-chlorophenyl and 4-chlorophenyl groups are project into the Leu_{26} and Trp_{23} pockets, respectively. The Phe_{19} pocket is occupied by the ethyl group. The sulfonyl tert-butyl group resides in the small pocket around G_{58}, and the carboxylic acid forms a salt bridge with the His_{96} residue of MDM2, increasing the inhibitory effect of the compound on MDM2. Thus, AMG-232 not only mimics the three key p53 residues but captures additional interactions to achieve a very high binding affinity with MDM2[57,59].

1.6.4. Spiropyrrolidine oxindoles

In the past years, several classes of small molecule inhibitors that disrupt p53-MDM2 binding, such as MI-219, have been revealed. Extensive optimization of spiropyrrolidine oxindoles family has yielded SAR405838 (MI-77301). This compound is in phase I of clinical trials for neoplasm malignant[60]. Before going to clinical trials, its ability to inhibit cancer cell proliferation and to inhibit tumour growth in xenograft models was reported. A good tissue bioavailability in mice, a desirable pharmacokinetic profile and an orally activity, were also reported for MI-77310[54].

1.6.5. Dual Inhibitors

The need for a compound with a double ability for MDM2 and MDMX, led to the discovery of compound, RO-2443 that showed potent MDM2/MDMX inhibitory activity *in vitro*, but poor water solubility. Optimization of RO-2443 yielded RO-5963, a close analogue with slightly increased potency but substantially improved solubility. RO-5963 (figure 6) also showed p53-MDM2 inhibitory activity similar to that of nutlin-3a and p53-MDMX inhibitory activity was nearly equivalent to MDM2 activity but approximately 400-fold better than the MDMX potency of nutlin-3a[39,44].

Studies have shown that RO-5963, inhibits cell growth, stabilizes p53 in a dose-dependent manner, and elevates protein levels of its transcription targets (p21 and MDM2). The RO compounds binding method is really interesting because, sub-pocket Leu26 is not occupied by these compounds. They have a very high affinity to both MDM2 and MDMX proteins, through their chloro-indole and di-fluoro-phenyl moieties, which fill Phe and Trp sub-pockets, respectively. These compounds also show, a high activity in cellular line cancer cells lines with wt-p53[44].

A new class of molecules that mimic p53 α-helix, the pyrrolopyrimidines (Figure 5), and show effect on both MDM2 and MDMX proteins. These new molecules mimic α-helixes, secondary structures of most common proteins, which are involved in several protein-protein interactions (PPI). Pyrrolopyrimidines have several advantages over the majority of structures known as PPI inhibitors, such as improved aqueous solubility, excellent cell permeability and synergistic effect over MDM2 and MDMX[61].

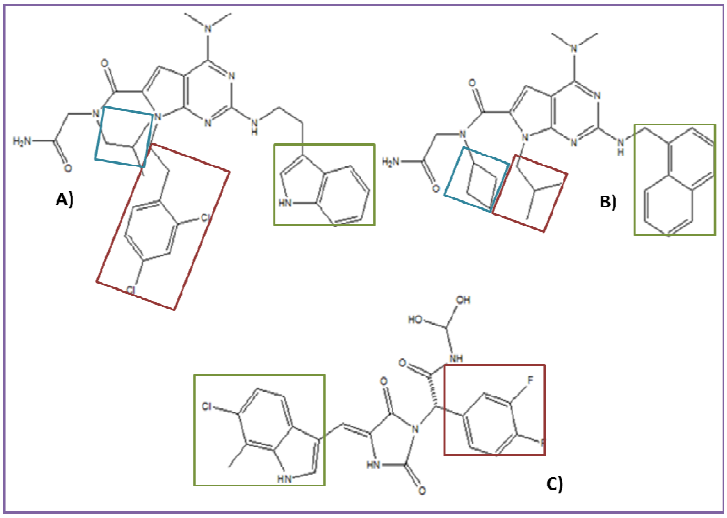

Figure 5 - Chemical struture of: A) and B) pyrrolopyrimidines; C) RO-5963 mimic the three hydrophobic residues Phe19 (Green), Trp23 (Red) and Leu26 (Blue). Image obtained using the ChemDraw software.

Chapter 2

GENERAL GOALS

The main objective of the studies presented in this thesis was the development and optimization of new anticancer agents that potentially target the molecular interaction between p53 tumour suppressor and its main negative regulators, MDM´s. Our strategy involved not only the chemical synthesis, but also the biological activity evaluation of the newly synthesized compounds, using several cellular models.

Primarily, we aimed at developing a novel spirooxindole scaffold containing a pyrazoline ring that functions as the rigid heterocyclic scaffold, from which the three lipophilic groups can be projected to mimic the p53 amino acids.

Secondly, we decided to study the biological effect of changing the CH-4´ (pyrazoline) by a *N*-4´ (tryazoline) on the five-member ring of the spirooxindole skeleton.

In parallel, we performed a broad range of molecular and biochemical studies to dissect the cellular mechanisms triggered by the most potent compounds. More specifically, our goals were to:

- Evaluate the antiproliferative capacity of the compounds in several cancer cell lines as well as in normal cells;
- Evaluate their ability to induce cell death, in particular apoptosis, and/or cell cycle arrest;
- Determine whether the compounds inhibit p53-MDM2 interaction;
- Evaluate the potential synergistic effect between the most potent molecule and a chemotherapeutic drug already in use;
- Assess compound stability in saline solution.

Chapter 3

SPIROPYRAZOLINE OXINDOLES: DESIGN AND EVALUATION

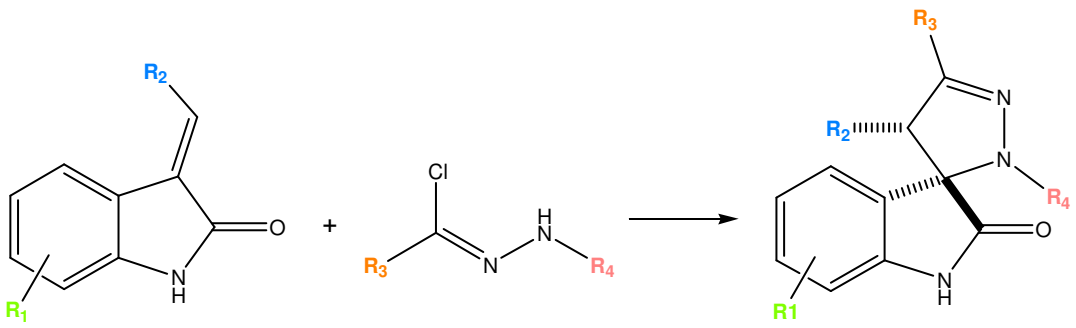

Spirooxindoles are reported as the core structure of a variety of medicinal agents with several applications, such as anticancer agents[62]. These molecules have a big potential because the oxindoles moiety can mimic the p53 Trp_{23} sub-pocket. Another advantage of spirooxindoles, is that some derivatives were described to have specificity against cancer cell lines and not against normal epithelial cells[35,57,63–66]. This chemical structure is considered an important heterocyclic molecule, which belongs to a large family of bioactive compounds, such as compounds MI-77301 and RO-5353[65,67].

Pyrazoline is also a privileged unit in medicinal chemistry, and is described to have anti-viral, anti-tumour, antibacterial, anti-inflammatory, and anti-fungal activities[68].

These two units are structural parts of our compounds, the spiropyrazoline oxindoles (Figure 6).

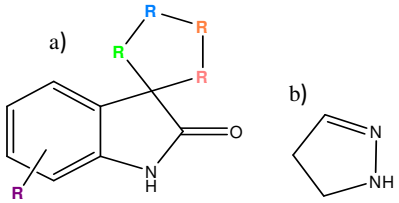

Figure 6 – a) Spirooxindole stucture; b) Pyrazoline structure.

In the last years, Santos's group (iMed.ULisboa) has been investigating the potential of several families of spirooxindoles with 5-membered rings as potential anti-cancer agents. Previous work from the research group shown that spiroisoxazoline oxindoles **1**[69] and spiropyrazoline oxindoles **2**[70] have *in vitro* anticancer properties.

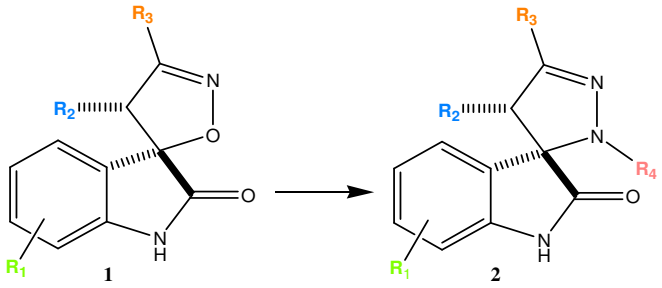

Scheme 1 - Optimization strategy: from spiroisoxazoline **1** to spiropyrazoline **2** oxindoles.

Spiroisoxazoline oxindoles **1** presented ability to disrupt the p53-MDM2 interaction, as determined by a Venus-based bimolecular fluorescence complementation assay (BiFC). However, the IC_{50} values were very high compared with other spirooxindoles described in the literature (around 40µM for the colorectal cancer cell line HCT-116). Computational studies showed that the optimal Trp_{23} mimicry by the oxindole was lost due to the spatial orientation of the groups: oxindole R2 and R_3. Instead, these molecules, the oxindole is projected into $Phe19_{(p53)}$ pocket, while aromatic substituent's R_2 and R_3 are projected into $Trp_{23(p53)}$ and $Leu26_{(p53)}$ pockets, respectively[71]. However, the inclusion of a fourth substituent to the main

scaffold and the substitution of the isoxazoline oxygen atom for a *N*-Ar group could allow a potential reorientation of the ligands in the MDM2 pocket (Scheme 1).

In this thesis, a family of spirooxindoles containing a five ring (pyrazoline) was synthesized and the antiproliferative activity evaluated. Previously, some spiropyrazoline oxindoles **2** were tested against the MCF7 and MDA-MB-231 breast cancer cell lines, and the most active compounds showed an IC_{50} value around 7µM, and were selective over MDA-MB-231 tumour cells and non-cytotoxic against Hek-293T non-tumour cells. Therefore, in this work, we developed and optimized the previously developed spiropyrazoline oxindoles and assessed their biological effects.

0.1. SYNTHESIS OF THE TARGET COMPOUNDS

p53 interacts with MDM2 through the residues Phe_{19}, Trp_{23} and Leu_{26} that occupy the hydrophobic cleft of the MDM2 protein. These three residues represent the critical ones for binding between these two proteins. Having this into account 2-indolinones **3a-h** and hydrazonyl chlorides **4a-e**, containing substituent's to mimic these important aminoacids, were synthesized (Tables 2 and 3). The R_1 in indole part of the compounds mostly presents halogens as the main choice. This choice was based on previous reports of potent MDM2 inhibitors (example MI-77301, SM13) that contain halogens in the indole moiety. The R_2, R_3 and R_4 were synthesized taking into account the ability of an halogenated 5-membered aromatic ring to insert into Phe_{19} pocket, and an often branched aliphatic moiety or an often halogenated 5-membered aromatic ring to occupy the Leu_{26} pocket[65,72].

Spiropyrazolines´ **2** have a basic molecular structure derived from the corresponding pyrazoline and are exemplified by a unique spiro junction at the C-5 position of a pyrazoline ring. The 1,3-dipolar cycloaddition is a very useful reaction for the synthesis of spirooxindole ring systems[62,66,73–75].

The synthetic strategy employed to synthesize spiropyrazolines oxindoles **2a-x** is depicted in scheme 2. The final spiropyrazoline oxindoles **2** were obtained by 1,3-dipolar cycloaddition between 2-indolinones **3a-h** and nitrile imines **5** (generated *in situ* by dehydrohalogenation of hydrazonyl chlorides **4a-e)** (Scheme 2).

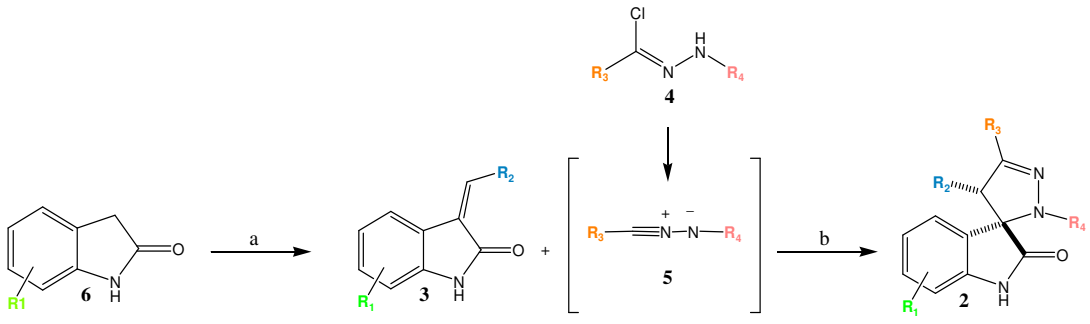

Scheme 2 - Synthesis of spiropyrazoline oxindoles **2a**-**x**. (a) aromatic aldehydes, piperidine, EtOH in reflux; (b) Et3N/DIPEA, CH_2Cl_2, r.t.

The 2-indolinones **3a-h** containing R_2 aromatic groups, were synthesized by aldolic condensation reaction of substituted indolin-2-ones **6** with different aromatic aldehydes in the presence of piperidine[70,76–79] with yields between 30 – 93% (Table 2). Additionally, indolin-2-one **3e** was generated using 5-bromo isatin in the presence of hydrazine monohydrate and ethylene glycerol, under reflux[80].

Table 2 - Synthesis of 2-indolinones **3a**-**3h**.

Compound	R_1	R_2	Yield (%)
3a	H	Ph	80
3b	5-Cl	Ph	72
3c	6-Cl	Ph	92
3d	7-Cl	Ph	74
3e	5-Br	Ph	46
3f	6-Br	Ph	82
3g	6-Cl, 5-F	Ph	30
3h	6-Cl	Ph-*m*-Cl	93

The dipole required for the synthesis of the final compounds, through a 1,3-dipolar cycloaddition, was obtained *in situ* from hydrazonyl chlorides **4b**, **4d** and **4e**[75]. These molecules were synthesized by Appel reaction, where hydrazone reacts with triphenylphosphine and carbon tetrachloride (Scheme 3.**b**). Hydrazonoyl **7** was obtained by reaction of phenylhydrazine with trimethylacetyl chloride (Scheme **3.a**)[75,81].

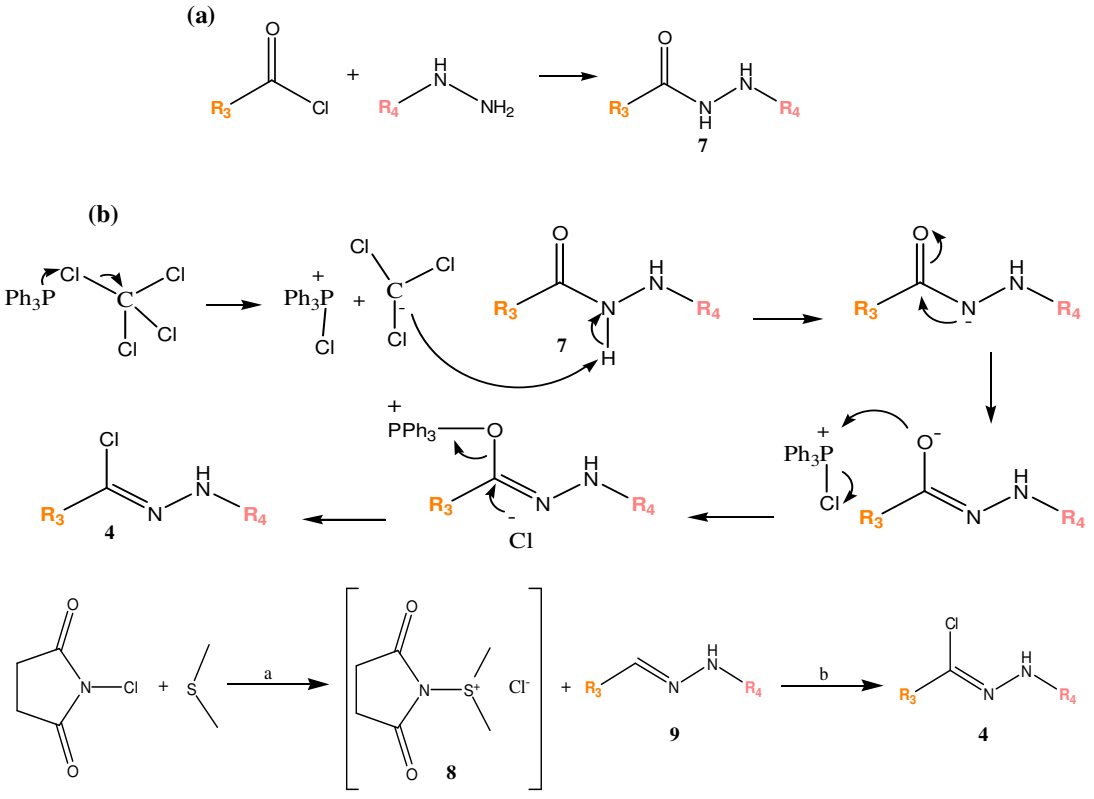

Scheme 3 - Synthesis of hydrazonoyl **7** and hydrazonyl chlorides **4**. (a) aqueous ethanol 20%, r.t., 2-3h, 81-99%; (b) NCS, $S(CH_3)_2$, 0ºC, 15 min; -78ºC, 1h, then allowed to warm up to r.t., 62-88%.

They can be, also, synthesized by reacting *N*-chlorosuccinimidedimethyl sulphide complex **8,** prepared *in situ* from the appropriate hydrazones **9** at -78 ºC[82], resulting in hydrazonyl chlorides **4a** and **4c** with yields between 33 - 96% (Table 3).

Table 3 - Synthesis of hydrazonyl chlorides **4**.

Compound	R_3	R_4	Yield (%)
4a	Ph	Ph	86
4b	Ph	Ph-*o*-Cl	80
4c	Ph-*p*-O-CH_3	Ph	33
4d	*t*-Bu	Ph	44
4e	*t*-Bu	Ph-*o*-Cl	52

Finally, spiropyrazoline oxindoles **2** were obtained with yields between (27.5 – 97.8 %) (Table 4).

Table 4 - Yields obtained in the synthesis of spiropyrazoline oxindoles **2a**-**2x**.

Compound	R_1	R_2	R_3	R_4	Yield (%)
2a	H	Ph	Ph	Ph	78
2b	5-Cl	Ph	Ph	Ph	82
2c	6-Cl	Ph	Ph	Ph	83
2d	7-Cl	Ph	Ph	Ph	92
2e	5-Br	Ph	Ph	Ph	82
2f	6-Br	Ph	Ph	Ph	84
2g	6-Cl, 5-F	Ph	Ph	Ph	40
2h	7-Cl	Ph	Ph	Ph-*o*-Cl	94
2i	H	Ph	Ph-*p*-O-CH_3	Ph	74
2j	5-Cl	Ph	Ph-*p*-O-CH_3	Ph	33
2k	7-Cl	Ph	Ph-*p*-O-CH_3	Ph	71
2l	6-Br	Ph	Ph-*p*-O-CH_3	Ph	92
2m	6-Cl	Ph-*m*-Cl	Ph-*p*-O-CH_3	Ph	98
2n	H	Ph	*t*-Bu	Ph	73
2o	5-Cl	Ph	*t*-Bu	Ph	80
2p	6-Cl	Ph	*t*-Bu	Ph	79
2q	7-Cl	Ph	*t*-Bu	Ph	87
2r	5-Br	Ph	*t*-Bu	Ph	42
2s	6-Br	Ph	*t*-Bu	Ph	92
2t	6-Cl	Ph-*m*-Cl	*t*-Bu	Ph	83
2u	H	Ph	*t*-Bu	Ph-*o*-Cl	62
2v	5-Cl	Ph	*t*-Bu	Ph-*o*-Cl	28
2x	7-Cl	Ph	*t*-Bu	Ph-*o*-Cl	71

The spiropyrazoline oxindoles **2a**-**x** were characterized by NMR. In general, in the ^{13}C-NMR, the spiro carbon appeared between 75.66 – 78.98 ppm and the C-4' between 61.02 - 63.22 ppm. Additionally, the pyrazoline C=N appeared between 148.13 – 164.32 ppm and the carbonyl C=O between 176.36 - 178.62 ppm.

^{13}C NMR spectra obtained for spiropyrazoline oxindole **2g**, shown the spiro carbon at 77.01 ppm, the signal of C-4' at 5.08 ppm, the signal of the pyrazoline C=N at 149.23 ppm and the signal of the carbonyl at 178.47 ppm (Figure 7).

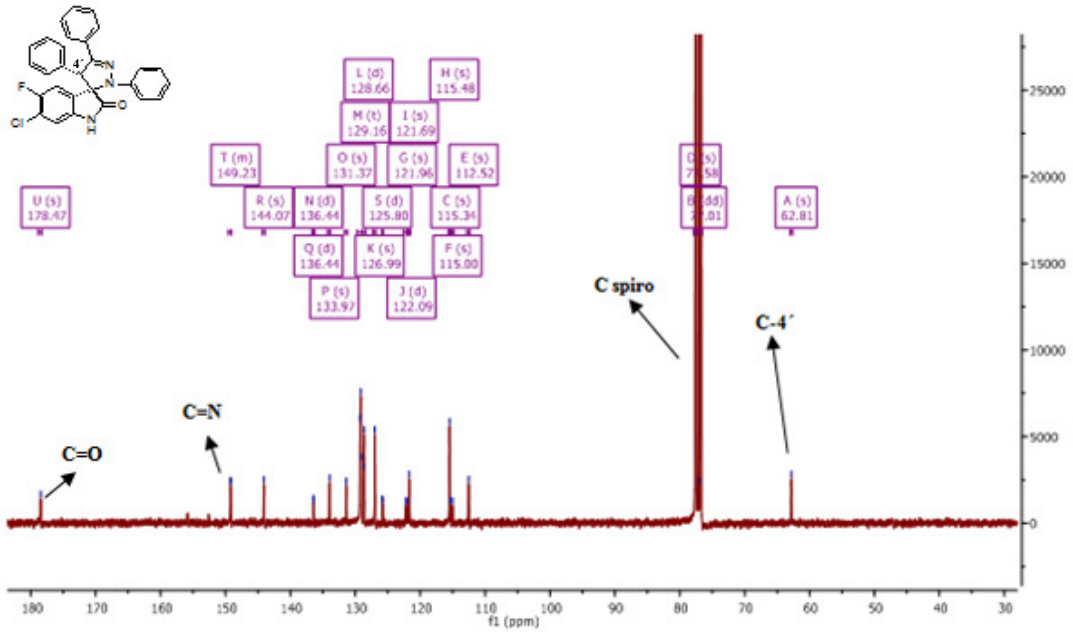

Figure 7 - ^{13}C NMR spectra of compound **2g**.

In the ^{1}H-NMR, the most characteristic signal was the one of H-4' , which appeared between 4.39 – 6.82 ppm[70,83]. Below it is presented the ^{1}H NMR spectra obtained for spiropyrazoline oxindole **2g**. The most characteristic proton is H-4' at 5.08 ppm (Figure 8).

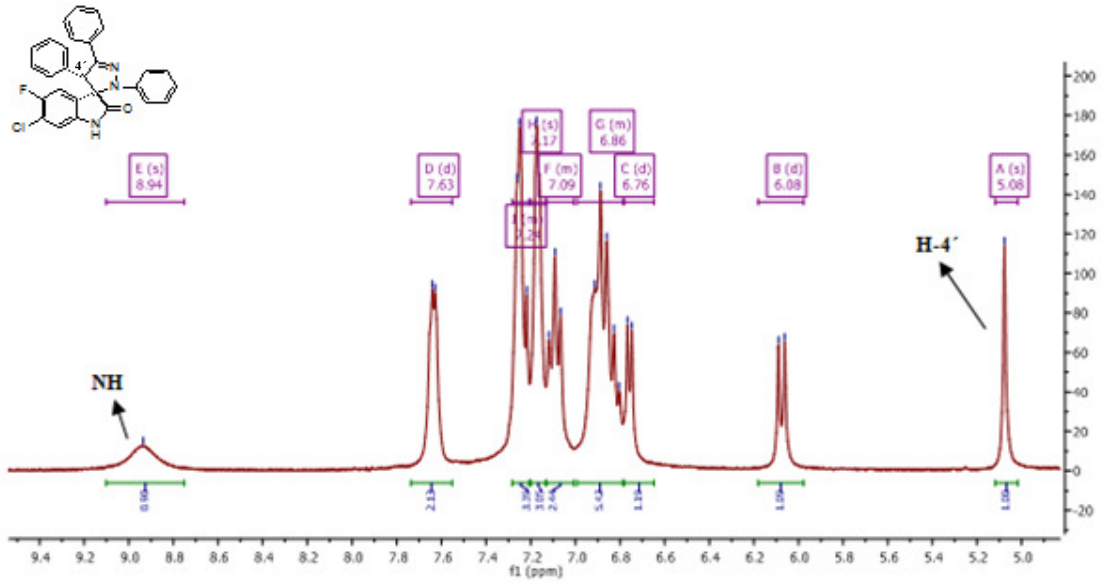

Figure 8 - ^{1}H NMR spectra of compound **2g**.

3.2. BIOLOGICAL EVALUATION - COLORECTAL AND BREAST CANCER CELL LINES

0.2.1. Antiproliferative Assays and SAR Studies

p53 mutations remain the most common genetic change identified in human neoplasia. The status of p53 mutation is closely related to the progression and outcome of colorectal cancer, and approximately half of all colorectal cancers have p53 gene mutations (*TP53*). In breast cancer, both the overall survival rate and the aggression level of the disease are closely related with mutations in p53 and nearly 30% of the patients have *TP53* mutated.

In order to evaluate the antiproliferative potential of spiropyrazoline oxindoles derivatives, we used different cancer cell lines with different *TP53* status. Taking into account the previous information about the importance of p53 in both colorectal and breast tumours, the cell lines selected for the antiproliferative assays were the HCT-116 human colorectal cell line harbouring wild-type p53 (HCT-116 $p53^{(+/+)}$) or lacking p53 (HCT-116 $p53^{(-/-)}$), and the MCF-7 and MDA-MB-23 human breast cancer cell lines expressing wild-type p53 or a mutated form, respectively.

The antiproliferative potential of compounds **2a**-**2x** was first evaluated in HCT-116 colorectal cancer cells, using the MTS metabolism assay. Taking into account that some compounds (**2a**-**2f**, **2j**-**2l**, **2p**, **2q** and **2s**) of this family had been previously tested in human breast cancer cell lines (MCF-7 and MDA-MB-231)[70], compounds **2g**-**i**, **2m**-**o**, **2r** and **2t**-**x** were also tested in these same cell lines. From the results obtained, we determined the relative IC_{50} values (Table 5), which prove themselves fundamental for the validation and characterization of the compounds.

Table 5 - *In vitro* antiproliferative activities of spiropyrazoline oxindoles **2a**-**x**.

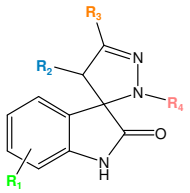

					Breast cancer cell lines		Colorectal cancer cell lines		"Normal" cell line	
Compound	R_1	R_2	R_3	R_4	**MCF-7 IC_{50}, µM[a]**	**MDA-MB-231 IC_{50}, µM[a]**	**HCT 116 *p53*$^{(+/+)}$ IC_{50}, µM[b]**	**HCT 116 *p53*$^{(-/-)}$ IC_{50}, µM[b]**	**Hek-293T IC_{50}, µM[a]**	**SI**
2a	H	Ph	Ph	Ph	>100	N.D.	>20	N.D.	N.D.	N.D.
2b	5-Cl	Ph	Ph	Ph	37.7±14.1	N.D.	11.0±0.3	14.3±3.1	N.D.	N.D.
2c	6-Cl	Ph	Ph	Ph	27.1±8.2	>50	16.7±0.9	17.0±0.9	>50	1.8
2d	7-Cl	Ph	Ph	Ph	22.4±3.5	16.9±1.2	16.6±1.5	17.1±1.4	>100	< 1.0
2e	5-Br	Ph	Ph	Ph	7.3±1.4	>100	13.1±1.0	14.2±0.8	>100	13.7
2f	6-Br	Ph	Ph	Ph	9.6±1.0	8.3±1.2	15.9±0.6	16.4±0.6	28.9±1.2	< 1.0
2g	6-Cl, 5-F	Ph	Ph	Ph	N.D.	N.D.	12.4±0.7	15.2±1.6	N.D.	N.D.
2h	7-Cl	Ph	Ph	Ph-*o*-Cl	N.D.	N.D.	>20	N.D.	N.D.	N.D.
2i	H	Ph	Ph-*p*-O-CH_3	Ph	>50	N.D.	11.7±0.3	14.7±0.3	N.D.	N.D.
2j	5-Cl	Ph	Ph-*p*-O-CH_3	Ph	33.9±15.4	N.D.	10.6±1.5	13.9±2.0	N.D.	N.D.
2k	7-Cl	Ph	Ph-*p*-O-CH_3	Ph	11.5±1.6	>100	15.6±0.9	16.4±0.8	>100	8.7
2l	6-Br	Ph	Ph-*p*-O-CH_3	Ph	7.0±1.1	28.7±1.1	12.8±0.7	10.0±0.6	>100	4.1
2m	6-Cl	Ph-*m*-Cl	Ph-*p*-O-CH_3	Ph	>50	N.D.	10.9±0.8	11.6±0.8	N.D.	N.D.
2n	H	Ph	t-Bu	Ph	16.9±3.7	13.9±2.9	>20	N.D.	10.9±1.7	< 1.0
2o	5-Cl	Ph	t-Bu	Ph	12.0±3.7	14.4±2.6	17.±1.3	16.6±1.5	16.4±1.9	1.2
2p	6-Cl	Ph	t-Bu	Ph	25.8±4.0	>50	>20	N.D.	>50	1.9
2q	7-Cl	Ph	t-Bu	Ph	8.6±3	6.4±1.2	13.3±1.4	9.7±1.6	17.8±1.2	< 1.0
2r	5-Br	Ph	t-Bu	Ph	N.D.	N.D.	>20	N.D.	N.D.	N.D.
2s	6-Br	Ph	t-Bu	Ph	8.5±1.8	15±1.2	>20	N.D.	20.9±1.2	1.7
2t	6-Cl	Ph-*m*-Cl	t-Bu	Ph	>50	N.D.	18.4±1.8	20.4±1.1	N.D.	N.D.
2u	H	Ph	t-Bu	Ph-*o*-Cl	N.D.	N.D.	>20	N.D.	N.D.	N.D.
2v	5-Cl	Ph	t-Bu	Ph-*o*-Cl	N.D.	N.D.	>20	N.D.	N.D.	N.D.
2x	7-Cl	Ph	t-Bu	Ph-*o*-Cl	16.2±2.0	11.3±1.6	17.3±0.2	15.3±0.8	18.8±2.7	< 1.0

[a] IC_{50} determined by the MTT method after 48h compound incubation. Each value is the mean (IC_{50} ± SD) of three independent experiments; [b] IC_{50} determined by the MTS method after 72h compound incubation. Each value is the mean (IC_{50} ± SD) of three independent experiments performed in duplicate. **N.D -** not determined. **SI** - Selectivity index towards MDA-MB-231 between cancer cell lines, expressed by the ratio MDA-MB-231 IC_{50}/MCF-7 IC_{50}.

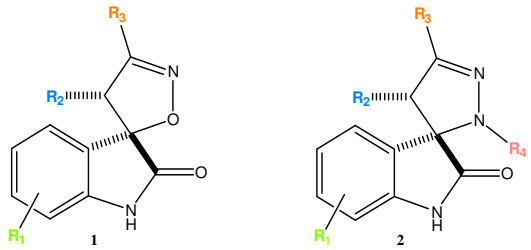

Table 6 – Chemical structure of spiroisoxazoline oxindoles **1** and spiropyrazoline oxindoles **2**.

Compound	R_1	R_2	R_3	R_4	HCT 116 *p53* $^{(+/+)}$ IC_{50}, µM	HCT 116 *p53* $^{(-/-)}$ IC_{50}, µM
2c	6-Cl	Ph	Ph	Ph	16.7±0.9	17.0±0.9
1a	6-Cl	Ph	Ph	-	39.8±1.1	48.2±1.1
2f	6-Br	Ph	Ph	Ph	15.9±0.6	16.4±0.6
1b	6-Br	Ph	Ph	-	35.0±1.1	40.6±1.1
2l	6-Br	Ph	Ph-*p*-O-CH_3	Ph	12.8±0.7	10.0±0.6
1c	6-Br	Ph	Ph-*p*-O-CH_3	-	33.4±1.1	39.0±1.2

As mentioned before, optimization of spirooxindole structure is an important part of this work. In a first glance, it can be noticed that the inclusion of a *N*-phenyl group in spiropyrazoline oxindoles **2c**, **2f** and **2l** increased the activity in HCT-116 *p53*$^{(+/+)}$ more than 2-fold comparing with the equivalent spiroisoxazoline oxindoles **1a**, **1b** and **1c** (Table 6). This reassures the importance of the inclusion an extra aryl group for the activity.

Our results showed that the most active compounds in HCT-116 *p53*$^{(+/+)}$ cancer cell line, i.e. compounds **2b**, **2e**, **2g**, **2i**, **2j**, **2l, 2m** and **2q,** have activities between 10µM - 13µM in HCT-116 *p53*$^{(+/+)}$ (Table 5). To investigate if cytotoxicity was in fact mediated by activation of p53, compounds with IC_{50} values lower than 20 µM were subsequently tested in HCT-116 cells lacking p53 (HCT-116 *p53*$^{(-/-)}$). However, none of them was selective for p53, revealing that p53 related effects may not be the main contributors to cytotoxicity.

The structure activity relationship studies (study SAR) for this family of compounds in HCT-116 *p53*$^{(+/+)}$ showed that change on the R_3 group of a *tert*-butyl by a *p*-methoxy group (compound **2s** versus compund **2l)** leads to an increase of activity in this cell line. Halogens as chloro, bromo and fluoro, in the indole part are normally described with ability to occupy the Trp_{23} pocket leading to better antiproliferative activities, as is possible observe in the table 5.

As a control of the cytotoxicity induced by the compounds towards cancer cells, we also analyzed the viability of CCD-18Co human normal colon fibroblasts after incubation with compounds **2e**, **2m** and **2q** at the IC_{50} and IC_{80} concentrations, as previously determined for HCT-116 *p53*$^{(+/+)}$ (Figure 9). Notably, at the IC_{50} concentration, compounds **2e** and **2m** induced no cytotoxicity in normal colon fibroblasts. When the same compounds were used at the IC_{80} concentration, a decrease of approximately 20% in cell viability was observed. In contrast, compound **2q** was cytotoxic at both equitoxic concentrations, in both cancer and

normal cell lines. These results suggest that compounds **2e** and **2m** are promising molecules to further develop as anti-tumoral agents probably with reduced off-target effects.

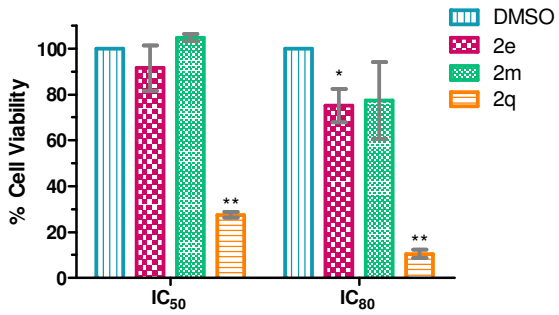

Figure 9 - Evaluation of cell viability in human normal colon fibroblasts (CCD-18co) following 72 h compound incubation **2e**, **2m** and **2q** at equitoxic (IC_{50} and IC_{80}) concentrations using the MTS metabolism assay. *p<0.05; **p<0.01 0.01 *vs* respective DMSO control. Data are mean ± S.D. of three independent experiments.

Regarding human breast cancer cell lines, the most active compounds in MCF-7 cells (ER+/HER2-) were compounds **2e**, **2f**, **2k**, **2l**, **2o**, **2q** and **2s** with IC_{50} values between 7 - 12µM (Table 5). Conversely, compounds **2f**, **2q** and **2x** were more active for MDA-MB-231 triple negative cells (ER-/HER2-) with activities between 6 – 11µM (Table 5). Although, triple negative breast tumours are the most aggressive and the most in need for innovative therapeutic options, none of the compounds tested was selective for MDA-MB-231 cells. Nonetheless, compounds **2e** (13.7 fold), **2k** (8.7 fold), **2l** (4.1 fold) and **2s** (1.8 fold) were more potent in MCF-7 cells in comparison with MDA-MB-231, suggesting selectivity for tumour cells expressing ER. Of note, compounds **2b** and **2m** appear to be tissue-specific, since their activities are markedly different between colorectal and breast cancer cell lines (Table 5).

Our SAR results have also revealed that further modification in R_1 at 5-bromo, 6- and 7-chloro positions of indole moiety may allow the development of spiropyrazoline compounds with better antiproliferative activities for breast cancer cell lines.

Finally, we tested spiropyrazoline oxindoles derivatives with IC_{50} values lower than 20µM in MCF-7 cells, in Hek-293T human embryonic kidney cells. As depicted in Table 5, compounds **2d** and **2l** showed higher potency (4.5 and 3.5 fold, respectively) towards cancer cells compared with Hek-293T non-tumoral cell line. Although, this cell line is of non-tumor origin, it is immortalized by transformation with adenovirus, which could have a significant impact on the results.

During this thesis, additional assays were carried out to better characterize the molecular mechanisms involved in compounds **2e** and **2m** mediated effects, which will be subsequently presented and discussed.

3.1.2. Evaluation of Cell Death

Considering the antiproliferative activity determined for compounds **2e** and **2m** in HCT-116 *p53*$^{(+/+)}$ cells, and in order to further explore the molecular mechanisms underlying the loss of cell viability, we decided to evaluate general cell death by lactate dehydrogenase (LDH) release, and apoptosis by flow cytometry and Western blot analysis.

LDH release

As depicted in Figure 10, incubation of HCT-116 *p53*$^{(+/+)}$ cells with compound **2m** and **2e** at 2xIC_{50} concentration, for 72h, resulted in an increase of approximately 1.5 fold in LDH release. Interestingly, when we incubated the compounds at the IC_{50} concentration, this induction no longer occurred, suggesting that pore formation at the cellular membrane and leakage of cytosolic cellular contents, such as LDH, may be a late-stage event. On the other hand, dysfunction of mitochondria, an organelle partially involved in MTS metabolism, appears to be the initial step in the death cascade.

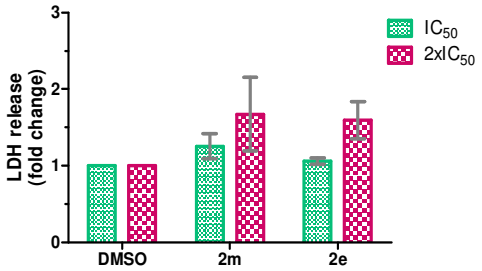

Figure 10 - Assessment of death cell induction in human colorectal cancer cell line (HCT116 *p53*$^{+/+}$) following 72 hours incubation with compounds **2e** and **2m** at equitoxic (IC_{50} and 2xIC_{50}) concentration, or DMSO (vehicle control). Data are mean ± S.D. of three independent experiments.

Flow Cytometry

To evaluate if incubation of HCT-116 *p53*$^{(+/+)}$ cells with compounds **2e** and **2m** triggers apoptosis, we performed a double staining method with Annexin V-FITC and 7-Aminoactinomycin D (7-AAD) followed by flow cytometry analysis. This assay allows to distinguish viable cells ($FITC^-/7\text{-}AAD^-$) from early ($FITC^+/7\text{-}AAD^-$) and late apoptotic cells ($FITC^+/7\text{-}AAD^+$).

The flow cytometry results of HCT-116 *p53* $^{(+/+)}$ cells exposed to compounds **2e** and **2m** are illustrated in Figure 11. Control cells exposed to DMSO showed intact cytoplasmic membrane as evidenced by the high percentage of viable cells (about 80%). When cells were exposed to compounds **2e** and **2m** at the IC_{50} concentration, the percentage of viable cells decreased to 72.9% and 71.1%, respectively. This decrease in cell viability was accompanied by an increase of cells in early-apoptosis. When HCT-116 *p53*$^{(+/+)}$ cells were exposed to compounds **2e** and **2m** at 2xIC_{50} concentration, the massive cell death observed was mainly

due to cells in late-apoptosis or necrosis, suggesting that at this concentration both compounds may be toxic *per se*.

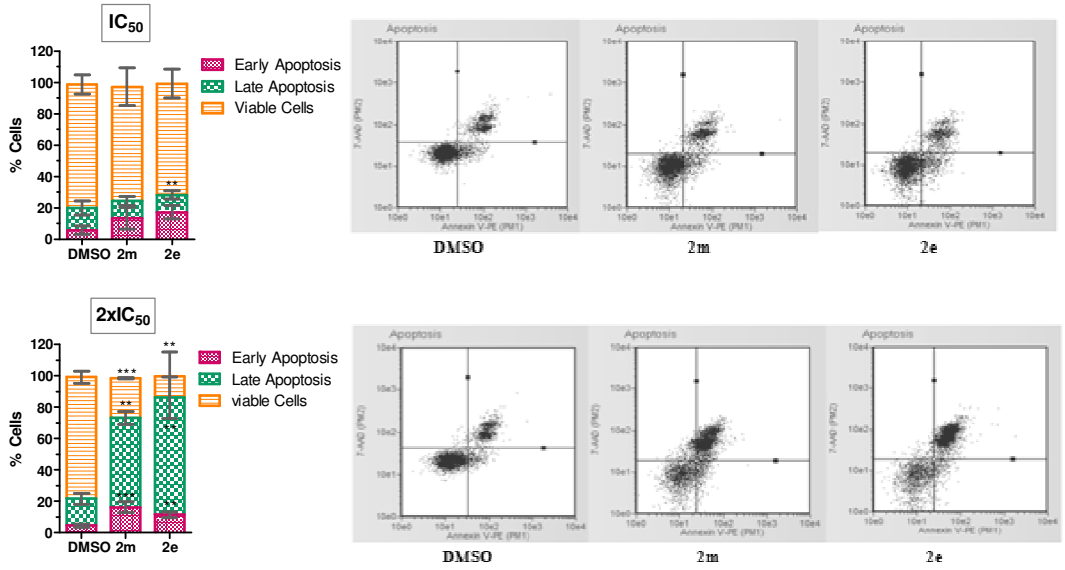

Figure 11 - Evaluation of apoptosis in human colorectal cancer cell line (HCT116 *p53*$^{(+/+)}$) following 72 h incubation with **2e** and **2m** at equitoxic concentrations (IC_{50} and $2xIC_{50}$), or DMSO (vehicle control). ***p*<0.01; ****p*<0.001*vs* DMSO. Data are mean ± S.D. of three independent experiments.

Western blot Analysis

To corroborate the flow cytometry results, we also analyzed apoptosis markers by Western blot.

In theory, inhibition of p53-MDMs protein-protein interaction results in p53 stabilization and activation, thus leading to transcription of p53 target genes. As depicted in Figure 12, incubation of HCT-116 *p53* $^{(+/+)}$ cells with compounds **2e** and **2m** at the IC_{50} concentration induced a mild increase in p53 total levels, and a tendency to decrease MDM2. Importantly, compound **2e** slightly increased caspase-3 activation which is in agreement with the flow cytometry results and indicates that apoptosis is playing a role in **2e**-mediated cytotoxic. Surprisingly, incubation with compound **2e** did not change the cleavage of PARP, a substrate of caspase-3. Compound **2m** did not induce caspase-3 activation or PARP cleavage. It is possible that 72h of compound incubation is too late to detect the differences in caspase-3 processing and PARP cleavage. To further clarify these results, we should evaluate the same markers at earlier time points.

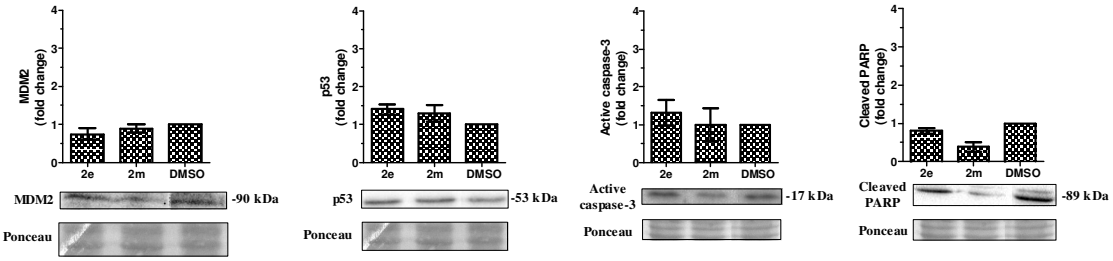

Figure 12 – Effect of compounds **2e** and **2m** in p53 and MDM2 protein levels, caspase-3 activation and PARP cleavage. Immunoblots analyzed in total cell extracts of HCT-116*p53*$^{(+/+)}$ cell line following 72 h incubation at equitoxic IC_{50} concentration, or DMSO (vehicle control). Blots were normalized with ponceau staining as control. Cropped blot to exclude two other compounds used from other spirooxindole family.Data are mean ± S.E.M. of two independent experiments.

3.2.3. Cell Cycle Analysis

As mentioned before, the delicate balance between cell proliferation and cell death is mainly orchestrated by tumour suppressors, such as p53. In fact, p53 activation is involved various cellular outcomes, in which apoptosis and growth arrest stand out as the most well-known (Chapter 1).

Since, cell death by apoptosis contributes only in part to **2e** and **2m** cytotoxic effects; we decided to further analyze cell cycle progression to better understand which mechanisms underlie these effects.

HCT-116 *p53*$^{(+/+)}$ cells were exposed to compounds **2e** and **2m** at the respective IC_{50} concentrations, for 24 h and 48 h. Cell cycle distribution was measured by flow cytometry using propidium iodide. As observed in Figure 13.a, 50% or 40% of cells were in the G0/G1 phase after 24 h exposure to compounds **2m** or **2e**, respectively, representing a significant increase of 51% (p<0.01) relative to control cells. In respect to the S phase, no significant changes were observed. Regarding the percentage of cells in the G2/M phase, incubation with compound **2m** resulted in a decrease of approximately 50% (p<0.01) comparing to control.

When we analyzed cell cycle progression after 48 hour of compound exposure (Figure 13b), the majority of cells were in G0/G1 phase, with a count of 51.6% for **2m** and of 62.2% for **2e** incubation, whereas only 42% of the control cells progressed into G0/G1 phase. Regarding compound **2m**, about 50% of G0/G1 phase cells remained in the G0/G1 phase of the cell cycle (from 24 to 48 hour), emphasizing the arrest of the cell cycle. This effect was also noted for compound **2e**. Importantly, the arrest of cells in G0/G1 was time-dependent for both compounds. Additionally, compound **2e** significantly decreased the arrest of cells in the G2/M phase (2.5-fold; p<0.01) and compound **2m** in the S phase (1.7-fold; p<0.01), in comparison to control.

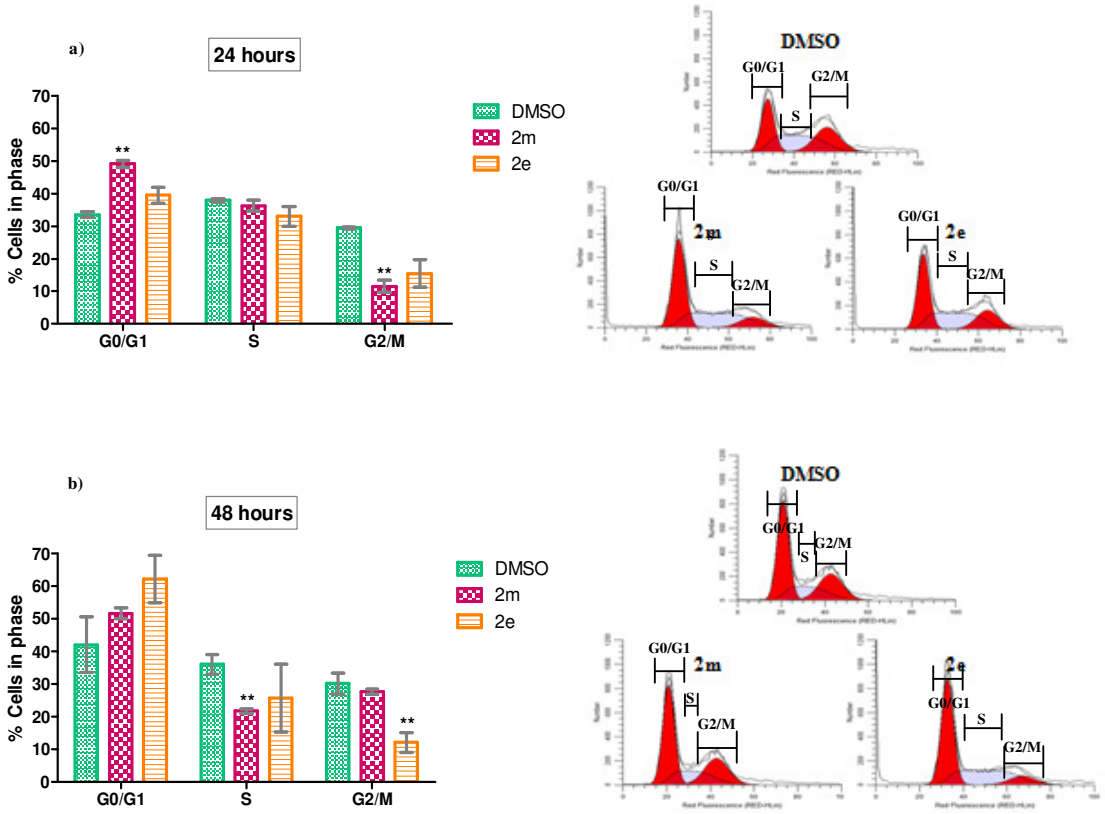

Figure 13 - Evaluation of cell cycle progression in human colorectal cancer cell line (HCT116 $p53^{+/+}$) following (a) 24 hours and (b) 48 hours incubation with compounds **2e** and **2m** at equitoxic (IC_{50}) concentration, or DMSO (vehicle control). $^{**}p<0.01$ *vs* respective DMSO control. Data are mean ± S.D. of three independent experiments.

The arrest of cells in the G0/G1 phase may be induced to allow the repair of damaged DNA, or to inhibit cell growth[84,85]. These results suggest that both induction of apoptosis and cell cycle arrest are important mechanisms underlying **2e** and **2m** effects in HCT-116 $p53^{(+/+)}$ cells.

3.2.4. Combination of Spiropyrazoline Oxindoles and Chemotherapeutic Drugs

Drug combination is widely used to achieve efficacy when treating several types of cancer. The main goal is to achieve a synergistic therapeutic effect accompanied by decreased toxicity, and reduced drug resistance. Taking this into account, studying the effect of a combination of drugs compared to the single agent is of particular interest[86,87].

We determined the IC_{50} values of commercial chemotherapeutic drug 5-FU prior to combined therapy assay. 5-FU acts as a thymidylate synthase inhibitor (blocking DNA replication) [88,89]. The compound in test has the ability to arrest cell cycle in the G0/G1 phase and in a less extent to induce apoptosis.

Cell viability of HCT-116 $p53^{(+/+)}$ subjected to combined therapies and coefficient drug interaction were calculated applying formula (3) of Chapter 6. As observed in Figure 14, combination of 5-FU at IC_{10} with **2e** at IC_{20} concentration, resulted in the best synergistic effect (CDI<1) (p<0.001). Nevertheless, when **2e** was used at IC_{10} (p<0.001) and IC_{50} (p<0.01) the synergism was still significant. In contrast, combination of 5-FU at IC_{50} concentration with compound **2e** at IC_{10} concentration resulted in an antagonic effect (CDI>1). Overall, the results suggest that by combining different drugs at concentrations below the IC_{50} we can achieve better results and possibly with less side effects. However, more studies should be performed to further address this question.

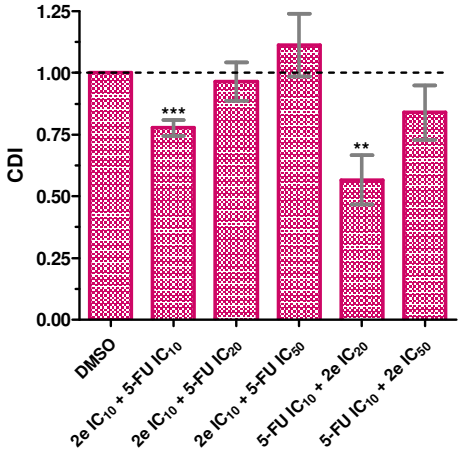

Figure 14 - Coefficient drug interaction (CDI) analysis of compound **2e** with 5-Fluorouracil. HCT-116 cells were exposed to compounds for 72h and cell viability was evaluated using the MTS metabolism assay. Threshold- CDI value threshold (CDI=1). **2e**IC_{10}=9.5µM; **2e**IC_{20}=10.7 µM; **2e**IC_{50}=13.0 µM and **5-FU**IC_{10}=1.7 µM; **5-FU**IC_{20}=2.2 µM; **5-FU**IC_{50}=3.2 µM. **p<0.01; ***p<0.001. Data are mean ± S.E.M. of five independent experiments.

3.2.5. Evaluation of Compounds' Ability to block the p53-MDM2 Interaction

To verify if this family of compounds can inhibit the p53–MDM2 interaction, a bimolecular fluorescence complementation assay (BiFC) was used. BiFC is a simple and robust assay that allows the direct visualization and quantification of p53–MDM2 interaction in live cells[71,90]. This assay is based on the reconstitution of an intact fluorescent protein when two complementary non-fluorescent fragments are brought together by a pair of interacting proteins (Figure 15).

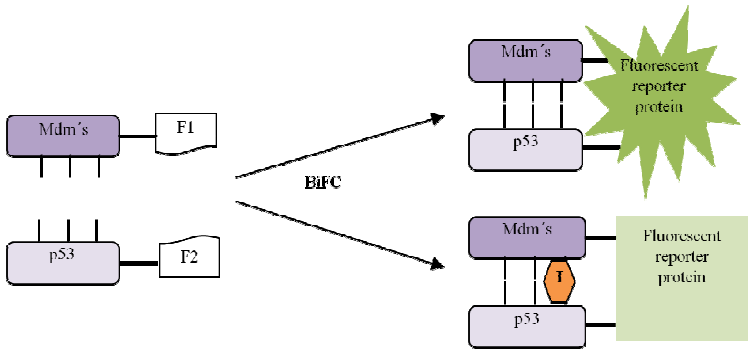

Figure 15 - The proteins of interest are fused to non-fluorescent fragments (F1 and F2) of a fluorescent reporter protein. When the proteins of interest interact, the non-fluorescent halves get close enough to fold together and reconstruct the functional fluorophore. When inhibition of p53-MMDM2 interaction exist by an inhibitor molecule (I), occurs a reduced signal.

By applying this methodology, it was demonstrated that compounds **2e** and **2m** at 20μM, can inhibit p53-MDM2 interaction in the same level as half concentration of nutlin-3a (10μM) (p<0.05 and p<0.01, respectively) (Figure 16). This assay, allows the quantification of p53-MDM2 interaction in live cells by flow cytometry, given that, the observed decrease of fluorescence represents the ability of the compounds to decrease p53-MDM2 interaction.

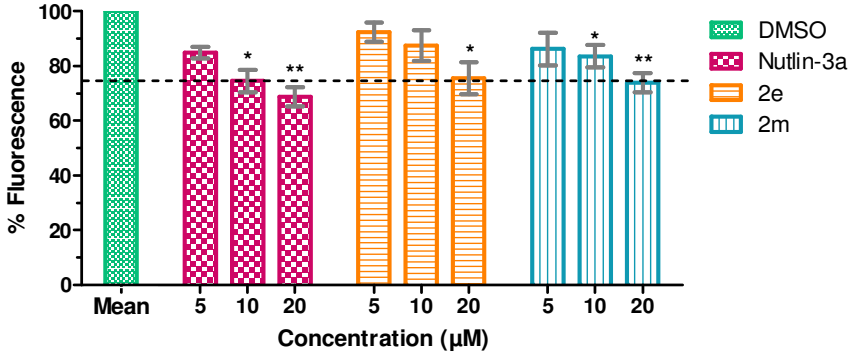

Figure 16 - Compound **2e** and **2m** decreases p53-MDM2 interaction by BiFC. HCT116 $p53^{(-/-)}$ cells were co-transfected for 24 hours. *p<0.05; **p<0.01. Data are mean ± S.D. of three independent experiments.

3.3. BIOLOGICAL EVALUATION - GLIOMA CANCER CELL LINE

Glioblastoma multiforme (GBM) is the most common primary malignancy in the brain. *TP53* mutation affects approximately 28% of primary glioblastoma cases and 65% of secondary glioblastomas, making it the most common molecular abnormality in glioma. Recent studies showed that alterations of p53 pathway in GBM included MDM2 amplification (11%), and MDM4 amplification (4 %), in addition to mutations of p53 itself. Taking into account the results using this library of spiropyrazoline oxindoles in two other types of cancer (breast and colorectal cancer), we decided to further test these molecules in a mouse glioma cell line (GL-261).

The library of spiropyrazolines was screened in GL-261 cells that present a *TP53* gene mutation[91,92]. Importantly, compound **2x** exhibited moderate antiproliferative activity with an IC_{50} value below 20µM. Therefore, to evaluate its effects in non-tumoral control cells, we further tested **2x** at IC_{50} and IC_{98} equitoxic concentrations in primary mouse astroglial cultures.

As observed in Figure 17, incubation of primary astroglial cells with compound **2x** reduced cell viability in approximately 20% at the IC_{50} concentration, and 50% at the IC_{98} concentration, suggesting that compound induced non-cytotoxicity in normal cells and is promising molecule to further develop as anti-tumoural agents with reduced off-target effects.

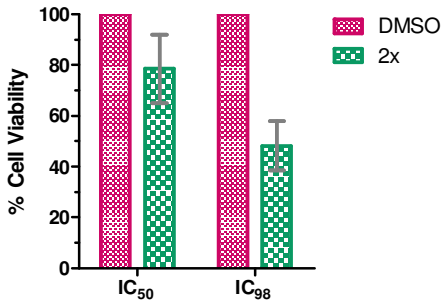

Figure 17 - Evaluation of cell viability in primary mouse astroglial cell culture following 72 h incubation with compound **2x** at equitoxic (IC_{50} and IC_{98}) concentrations using the MTS metabolism assay. Data are mean ± S.D. of three independent experiments.

During this thesis, additional assays were carried out to better characterize the molecular mechanisms involved in compound **2x** mediated effects, which will be subsequently presented and discussed.

3.3.1. Evaluation of Cell Death

Considering the antiproliferative activity determined for compound **2x** in GL-261 cells, and in order to further explore the molecular mechanisms underlying the loss of cell viability, we decided to evaluate apoptosis by flow cytometry.

Regarding GL-261 cells, the results demonstrate that apoptosis is not the death mechanism induced by compound **2x** (Figure 18), since no significant changes were observed in the 7-AAD/Annexin V assay. Therefore, alternative mechanisms, such as cell growth inhibition[93], should be investigated to better understand the mode of action of this compound.

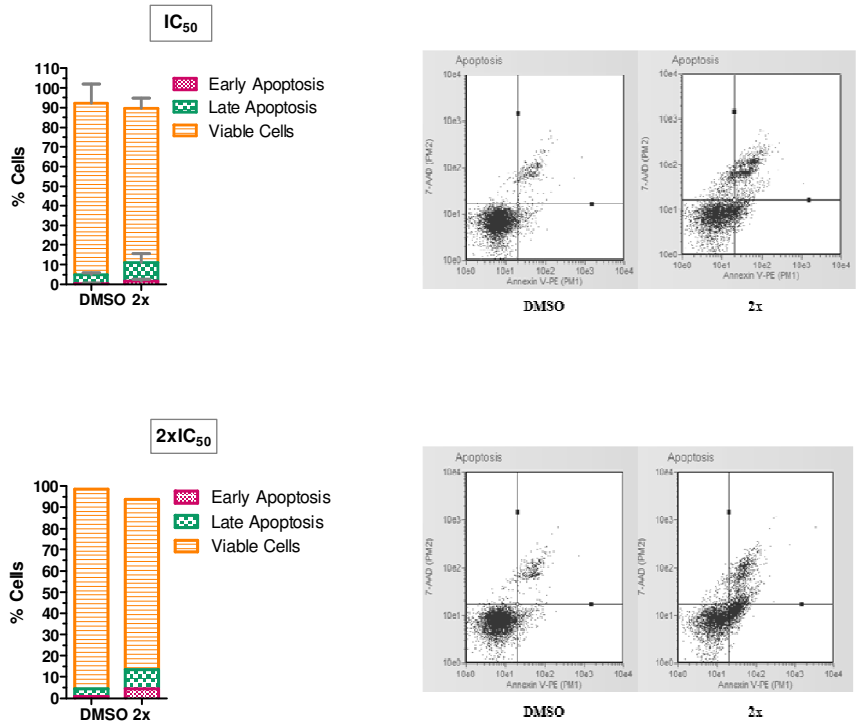

Figure 18 - Evaluation of apoptosis in GL261 cells, following 72 h incubation with compound **2x** at equitoxic (IC_{50} and twice of IC_{50}) concentration, or DMSO (vehicle control). Data are mean ± S.D. of two independent experiments.

3.3.2. Cell Cycle Analysis

GL-261 cells were exposed to compound **2x**, at the respective IC_{50} concentrations, for 24 h and 48 h. Cell cycle distribution was measured by flow cytometry using propidium iodide. As depicted in Figure 19, exposure of GL-261 cells to compound **2x** did not induce any changes in the cell cycle profile as compared with vehicle control. Therefore, we did not proceed the studies in this cell line.

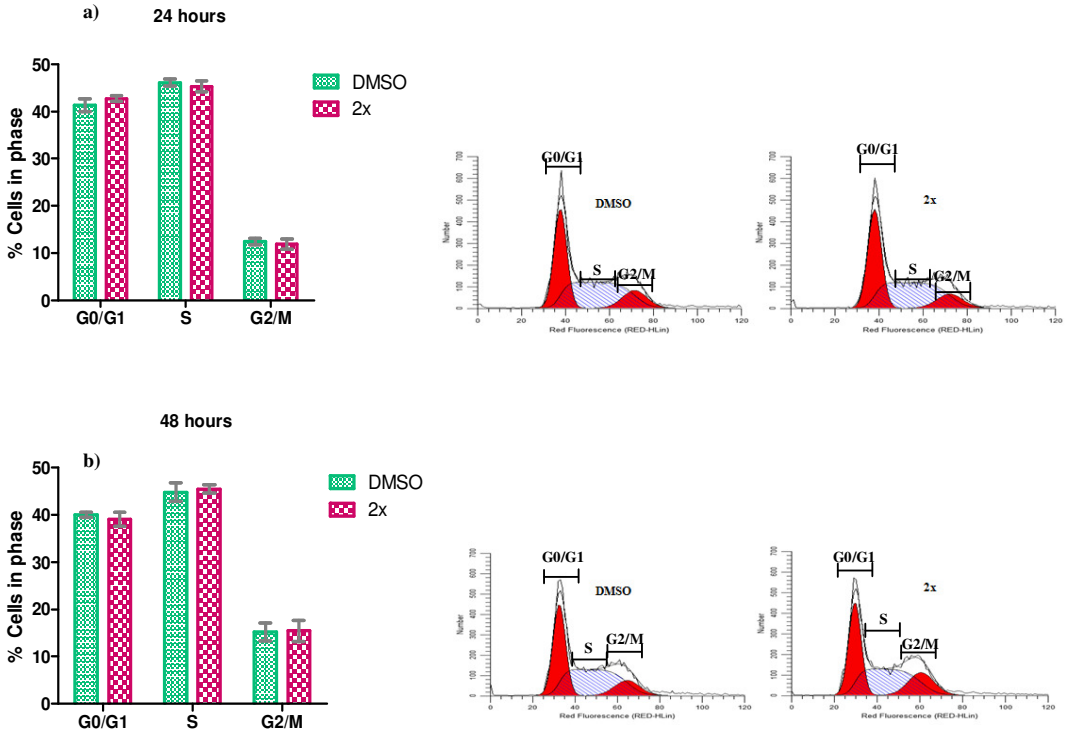

Figure 19 - Evaluation of cell cycle progression in GL261 cells, following (a) 24 hours and (b) 48 hours incubation with compound **2x** at equitoxic (IC_{50}) concentration, or DMSO (vehicle control). Data are mean ± S.D. of three independent experiments.

3.4. COMPOUND STABILITY STUDIES

The stability of a compound in PBS is an important parameter to assure that the compound effect is truly achieved by the molecule itself and not by subsequent derivatives of its degradation. Therefore, the chemical stability of compounds **2e, 2m** and **2x** was evaluated in pH 7.4 phosphate buffer (PBS) at 37 ºC. Importantly, compounds **2e** and **2m** were stable in PBS for 72 h (Table 7). This property is still significant for future therapeutic applications.

Table 5 - Stability of spiropyrazoline oxindole compounds (**2e**, **2m** and **2x**) in PBS. Data of three independent experiments.

Compounds	Incubation time (hours)	Original peak		Degraded peak	
		%	abs	%	abs
2m	0	100,0	12,783	0,0	-
	72	89,44	12,947	10,56	5,671
2e	0	100,0	12,083	0,0	-
	72	59,39	11,907	40,61	5,240
2x	0	100,0	12,083	0,0	-
	72	59,39	11,907	40,61	5,240

3.5. FINAL CONSIDERATIONS

A library of twenty-three spiropyrazoline oxindoles was designed and synthesized. Compound screening in HCT-116 $p53^{(+/+)}$ cell line revealed that seven derivatives displayed potency below 13μM. However, a lack of selectivity between the isogenic pair of cell lines HCT-116 $p53^{(+/+)}$ and $p53^{(-/-)}$ was observed for all compounds. Nevertheless, we demonstrated that spiropyrazolines oxindoles **2e** and **2m** were capable of disrupting the p53-MDM2 interaction. Compounds **2e** and **2m** also promoted induction of apoptosis and cell cycle arrest in G0/G1 phase, and increased p53 expression levels in HCT-116 $p53^{(+/+)}$ cell line. Importantly, no cytotoxic effects were detected in human normal colon fibroblasts (CCD-18-Co cell line). In addition, four spiropyrazoline oxindoles (**2e**, **2k**, **2l** and **2s**) showed selectivity for tumour cells expressing ER, more specifically for MCF-7 breast cancer cell lines.

All compounds were also screened in GL-261 glioma cell line, with only one compound presenting potency below 20 μM. However, this compound failed in inducing both apoptosis and cell cycle arrest.

Finally, three compounds of this library were stable in PBS (pH 7.4) for 72 h.

Chapter 4

SPIROTRYAZOLINE OXINDOLES: MECHANISM OF ACTION

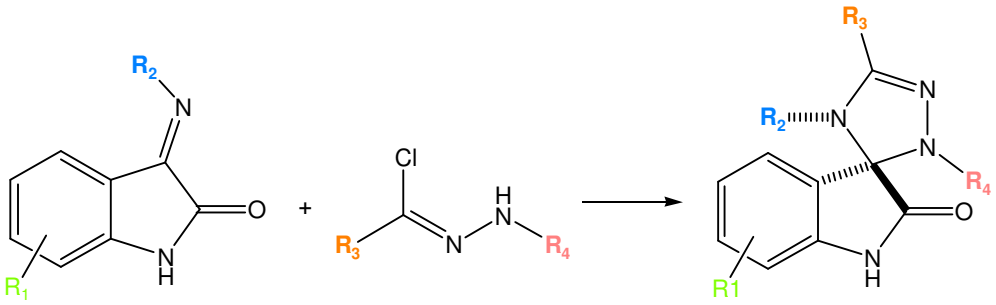

A library of spirotryazoline oxindoles was previously studied in our research group as potential anti-cancer agents. This family presented good antiproliferative activity for the MCF-7 breast cancer cell line, with some compounds showing selectivity towards the MDA-MB-231 triple negative breast cancer cell line. In addition, these compounds were capable of disrupting the p53-MDM2 interaction as observed using a live-cell bimolecular fluorescence complementation assay in a human colorectal cancer cell line, and were also selective toward tumoural cell lines *versus* non-tumoural Hek-293T cells. These compounds also induced cell death by apoptosis as observed by the dose-dependent increase of caspase-3 and -7 and PARP cleavage. Finally, good stability in plasma and susceptibility towards NADPH-dependent rat microsomal enzymes were observed[94].

Now, we further explored the molecular mechanisms of action of the most promising spirotryazoline oxindoles developed, compounds **7f**, **7h**, **7z**, to be used as potential anti-tumoural agents.

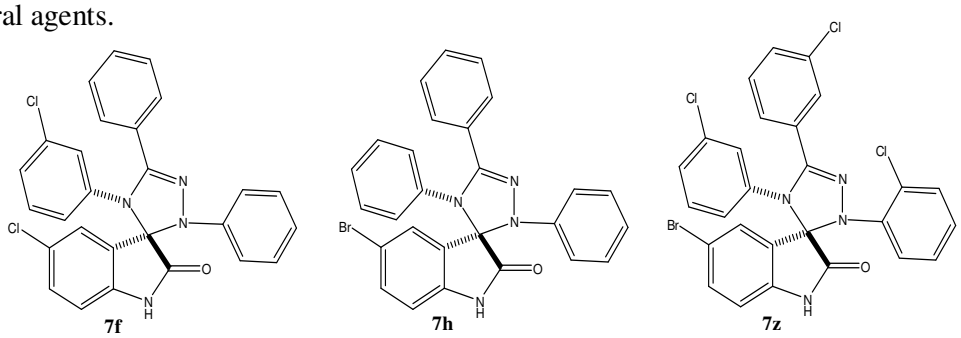

Scheme 4 - Chemical structure of spirotryazoline oxindoles **7f**, **7h** and **7z**.

4.1. BIOLOGICAL STUDIES – COLORECTAL CANCER CELL LINE

4.1.1. Evaluation of Cell Death

Flow Cytometry

Among the library of spirotryazoline oxindoles previously described (manuscript in preparation), compounds **7f** and **7z** were the most promising as potential antitumoral agents and therefore they were selected to further explore their mechanism of action.

Cell death by apoptosis was evaluated by flow cytometry using a biparametric analysis with 7-AAD and Annexin-V-FITC in HCT-116 $p53^{(+/+)}$ cells.

As depicted in Figure 20, approximately 80% of control cells exposed to DMSO were viable. Incubation of cells with compounds **7f** and **7z** at the IC_{50} concentration slightly induced cell death in approximately 7%. However, if we look at the subpopulation of cells exhibiting hallmarks of early apoptosis (FITC+/7-AAD-), a significant increase of 3.1-fold (p<0.01) and 2.8-fold (p<0.05) was observed for compounds **7f** and **7z**, respectively. These results become more interesting when we incubated the same compounds at $2xIC_{50}$

concentration. Here, we observed a robust dose-dependent response. When we incubated the same compounds at 2xIC_{50} concentration, the percentage of viable cells significantly decreased from 77.5% to 65.8% and 43.9% after incubation with **7f** and **7z**, respectively, corresponding to a 1.2-fold (p<0.05) and 1.8-fold (p<0.01) decrease, respectively. More importantly, this decrease of cell viability was accompanied by a significant increase of cells dying exclusively by apoptosis (FITC+/7-AAD+) (**7f,** 2.5-fold, p<0.01 and **7z,** 4.4-fold, p<0.001) in comparison with DMSO vehicle control.

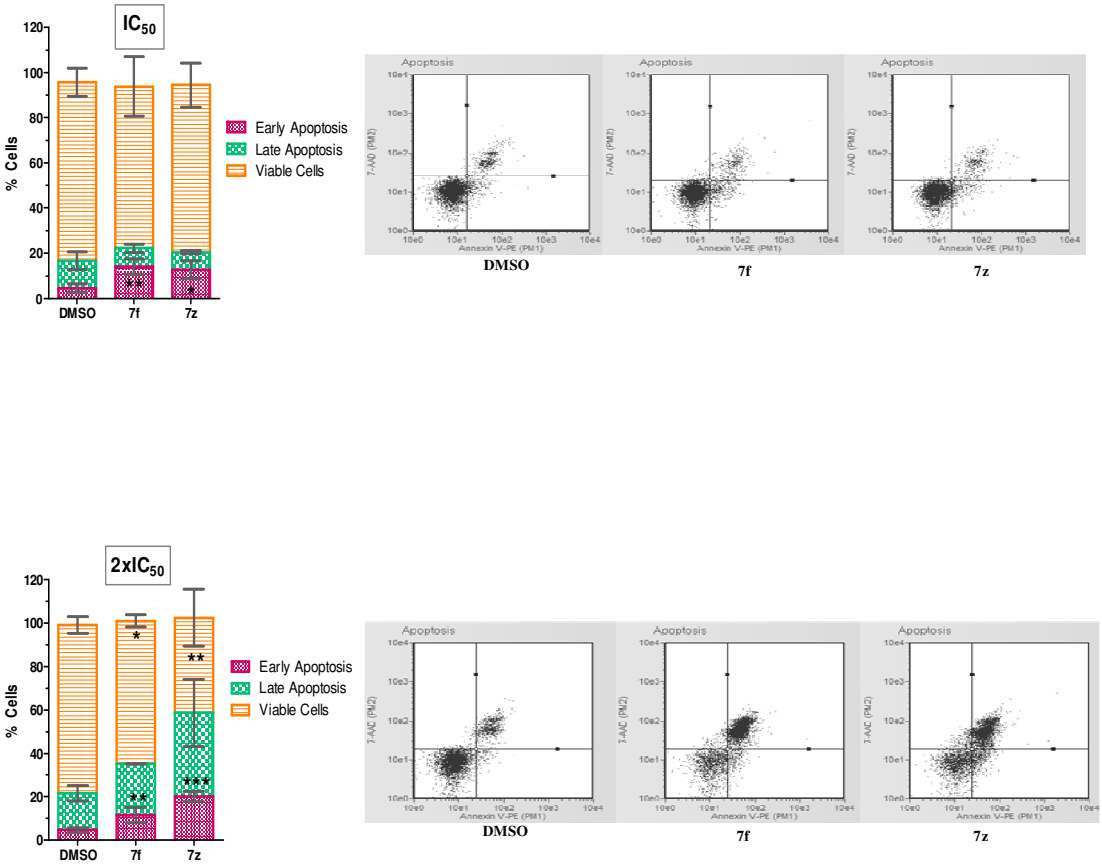

Figure 20 - Evaluation of apoptosis in human colorectal cancer cell line (HCT-116 $p53^{+/+}$) following 72 h incubation with compounds **7f** and **7z** at equitoxic (IC_{50} and 2xIC_{50}) concentrations, or DMSO (vehicle control). *p<0.05; **p<0.01; ***p<0.001 *vs* DMSO. Data are mean ± S.D. of three independent experiments.

Western blot Analysis

To corroborate the flow cytometry results, we further analyzed apoptosis markers by Western blot using total extracts of HCT-116 $p53^{(+/+)}$ cells treated with compounds **7f** and **7z**.

As shown in Figure 21, compounds **7f** and **7z** significantly decreased MDM2 protein expression levels (p<0.05), while a tendency to increase p53 was observed for both compounds. Regarding caspase-3 activation and PARP cleavage, the results were somehow contradictory, since we could not detect an increase of caspase-3 activation with both compounds, but we still detected an increase of PARP cleavage, at least for compound **7f**.

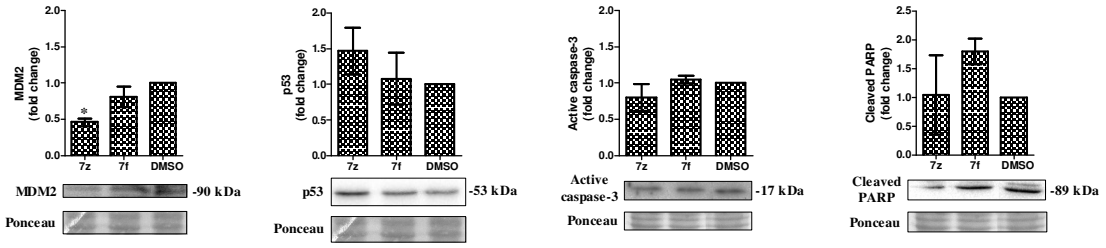

Figure 21 - Effect of compounds **7f** and **7z** in p53 and MDM2 protein levels, caspase-3 activation and PARP cleavage. Immunoblots analyzed in total cell extracts of HCT-116 cell line following 72 h incubation at equitoxic IC_{50} concentration, or DMSO (vehicle control). Blots were normalized with ponceau staining as control. Cropped blot to exclude two other compounds used from other spirooxindole family. *p<0.05 *vs* DMSO. Data are mean ± S.E.M. of two independent experiments.

4.1.2. Cell Cycle Analysis

In addition to cell death, growth inhibition may also play an important role in the loss of cell viability. In fact, several cytostatic agents show a marked growth inhibitory effect on a variety of tumors where growth arrest is followed by the activation of apoptotic pathways and cell death. In this regard, cell cycle analysis may help to understand whether the loss of viability observed upon cell treatment with compounds **7f** and **7z** is also mediated by changes in the cell cycle progression.

HCT-116 $p53^{(+/+)}$ cells were exposed to compounds **7f** and **7z** at the IC_{50} concentration for 24 and 48 hours.

At 24 hours of exposure, compound **7f** increased the number of cells in the G0/G1 phase in about 50% (p<0.01) (Figure 22). Both **7f** and **7z** induced a significant decrease of approximately 10% (p<0.05) and 22% (p<0.01) of cells in the G2/M phase, respectively.

After 48 hours, approximately 54% of the cells treated with both **7f** and 7**z** were in the G0/G1 phase whereas only 42% of the control cells progressed into this phase. Moreover, compounds **7f** and **7z** decreased the percentage of cells in G2/M phase in about 15% and 10%, respectively (p<0.05).

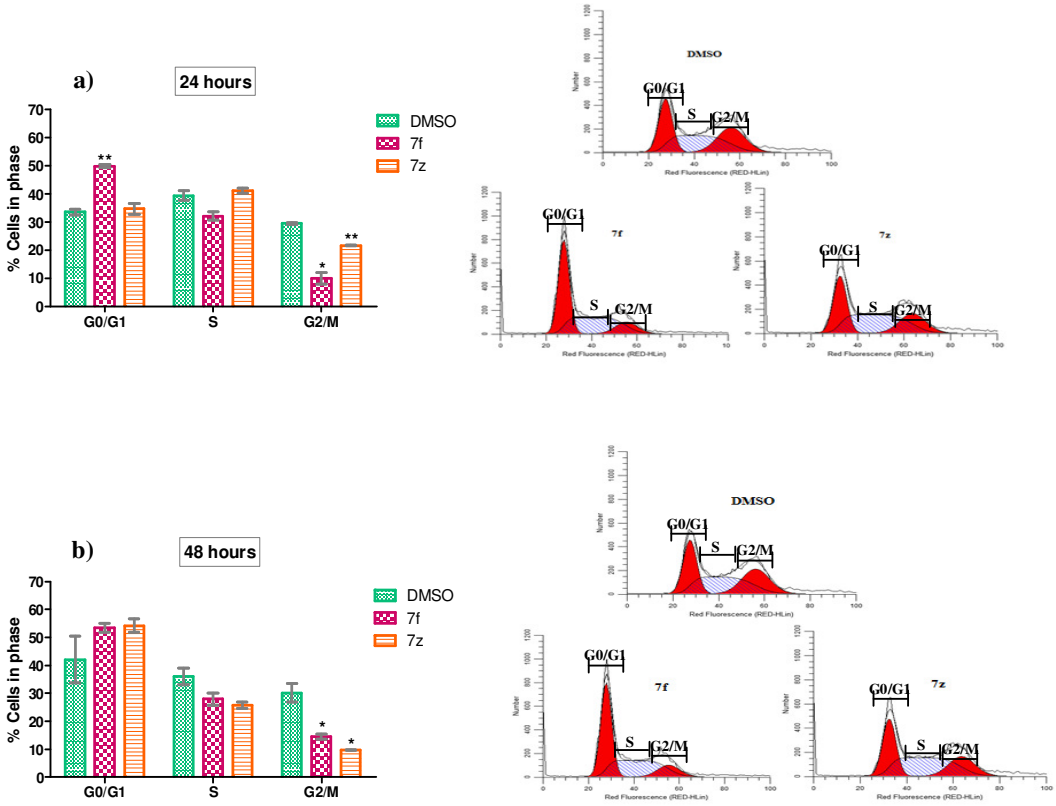

Figure 22 - Evaluation of cell cycle progression in human colorectal cancer cell line (HCT116 $p53^{+/+}$) following (a) 24 hours and (b) 48 hours incubation with compounds **7f** and **7z** at equitoxic (IC_{50}) concentration, or DMSO (vehicle control). *p<0.05; **p<0.01 *vs* respective DMSO (control). Data are mean ± S.D. of three independent experiments.

4.1.3. Cytotoxicity evaluation in human normal colon fibroblasts

To discard the potential cytotoxic effects of compounds **7f** and **7z** in non-tumoral cells, we analyzed the viability of human normal colon fibroblasts after treatment with the two compounds, at the IC_{50} and IC_{80} equitoxic concentrations**,** previously determined for HCT-116 $p53^{(+/+)}$ cells. As observed in Figure 23, treatment with **7f** and **7z** at the IC_{50} concentration did not affect cell viability. When we used higher concentrations, we could detect a reduction of approximately 40% in cell viability, which is still far below of the values obtained for the HCT-116 $p53^{(+/+)}$ cell line.

The absence of cytotoxic effects induced by compounds **7f** and **7z** in human normal colon fibroblast cells is an advantage for using these compounds as potential therapeutic agents.

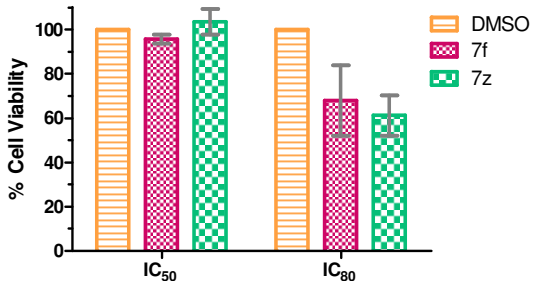

Figure 22 – Evaluation of cell viability in human normal colon fibroblasts (CCD-18co) following 72 hours incubation with compounds **7f** and **7z** at equitoxic (IC_{50} and IC_{80}) concentrations using the MTS metabolism assay. Data are mean ± S.D. of two independent experiments.

4.2. BIOLOGICAL STUDIES – BREAST CANCER CELL LINE

4.2.1. Evaluation of Cell Death

Flow Cytometry

MDA-MB-231 cell line represents the triple negative cancer, one of the most aggressive and most in need of innovative therapeutic. One compound of the library in study, showed the best antiproliferative activity toward MDA-MB-231 breast cancer cell line in comparison with other cancer cells lines[94] (HCT-116 *p53*$^{(+/+)}$ and MCF-7).

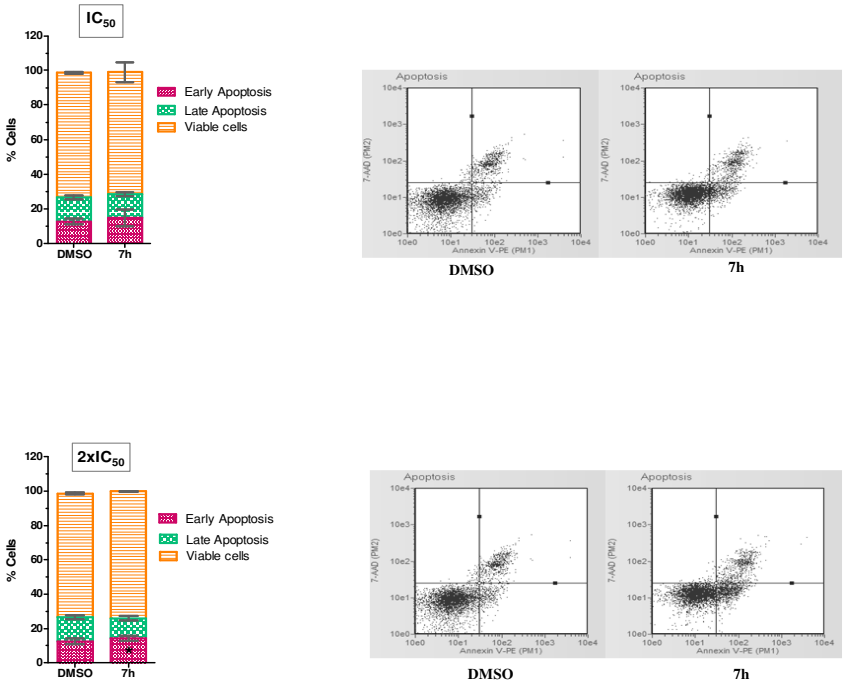

Figure 23 - Evaluation of apoptosis in human breast cancer cell line (MDA-MB-231) following 72 h incubation with compound **7h** at equitoxic (IC_{50} and 2x IC_{50}) concentrations, or DMSO (vehicle control). **p*<0.05; ***p*<0.01 *vs* respective DMSO (control) Data are mean ± S.D. of three independent experiments.

These results shown in Figure 24 reveal that compound **7h** does not induce apoptosis in this cell line, thus suggesting that the antiproliferative activity observed for this compound should be dependent of other mechanisms rather than apoptosis. The cytostatic mechanism[93] that lead to a cell growth/proliferation inhibition can be one of these mechanisms.

Caspase-3/7Activity Analysis

To corroborate the flow cytometry results, we also analyzed caspase-3/7 activity in MDA-MB-231 cells using a luminescent assay. In contrast to what we observed by flow cytometry, here we could detect a significant increase of caspase-3/7 activity (p<0.01) after incubation of cells with compound **7h** (Figure 25). Therefore, other experiments should be performed to better clarify the role of apoptosis in **7h**-mediated effects in this cell line.

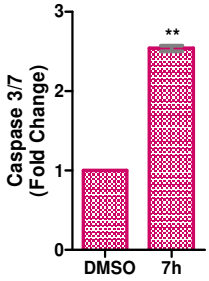

Figure 24 - Compound **7h** induces activation of caspase-3 and -7 after 48 hours of exposition. Caspase-3/7 activity was measured using the Caspase-Glo 3/7 assay (Promega) in total cell extracts of MDA-MB-231 cell line. **p<0.01 *vs* DMSO. Data are mean ± S.D. of two independent experiments.

4.2.2. Cell Cycle Analysis

The cell cycle study allows understanding whether the loss of viability through the compound **7h** could be preceded by changes in the cell cycle progression.

MDA-MB-231 cell line was exposed to the IC_{50} of compounds over 24 hours and 48 hours.

The results observed in Figure 26, show a small cell cycle arrest in G2/M, when we compare the MDA-MB-231 cells exposed to compound **7h** with the control group DMSO, over the exposure time (24 to 48 hours of exposure).

Thus, the cell cycle arrest in G2/M may indicate a growth inhibition in cells but it is not necessary to happen an induction of cell death, and this can happen through the mechanisms associated with p53 in cell homeostasis[84,85].

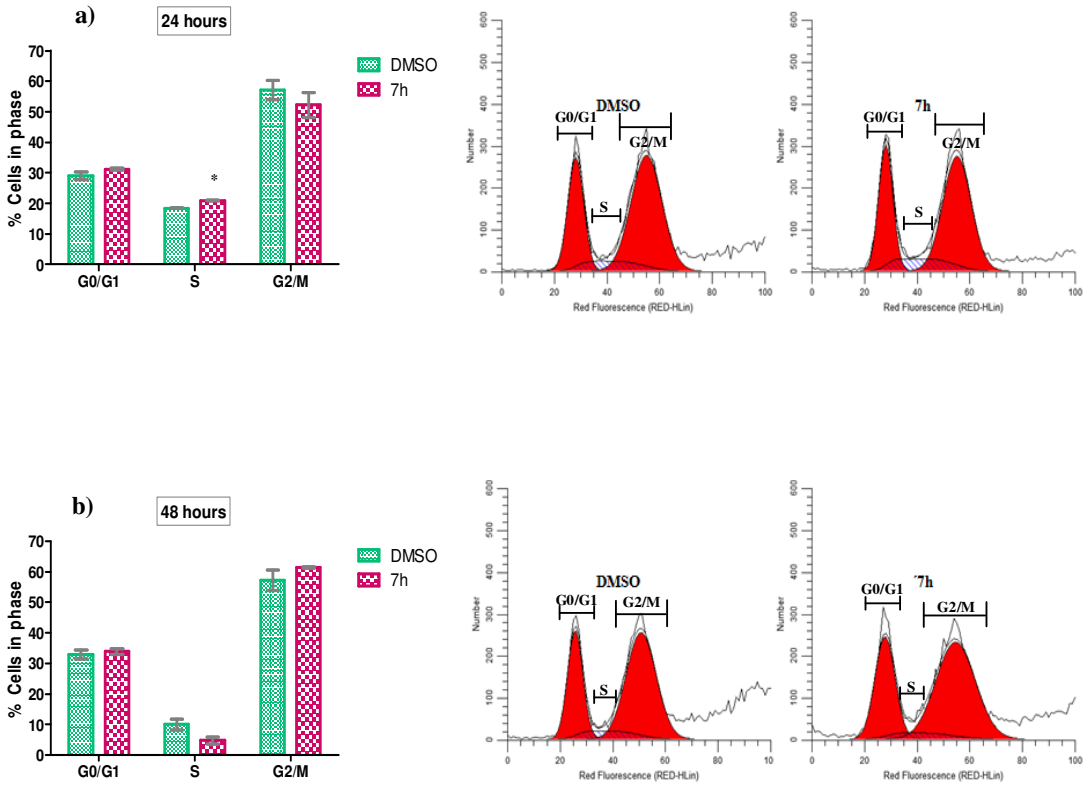

Figure 25 - Evaluation of cell cycle progression in human breast cancer cell line (MDA-MB-231 following (a) 24 hours and (b) 48 hours incubation with compound **7h** at equitoxic (IC_{50}) concentration, or DMSO (vehicle control). *p<0.05 *vs* respective DMSO control. Data are mean ± S.D. of two independent experiments.

4.3. FINAL CONSIDERATIONS

The mechanism of action of three spirotryazoline oxindoles as potential anti-cancer agents was studied in more detail. Compounds **7f** and **7z** were not cytotoxic in normal cells, while induced apoptosis and cell cycle arrest in G0/G1 phase in the HCT-116 colorectal cell line. Additionally, **7f** and **7z** slightly induced p53 and decreased MDM2 expression. These changes in p53 and MDM2 expression levels, confirm the ability of spirotryazoline oxindoles to modulate p53-MDM2 interaction. Moreover, 48 hours of cell exposure to compound **7h** also promoted cell cycle arrest in G2/M and a significant increase of caspase-3 and -7 activities, which may indicate that 72 hours was too late to observe other apoptosis-related changes, such as caspase-3 processing and PARP cleavage.

Chapter 5

CONCLUSIONS AND FUTURE PERSPECTIVES

The main goal of this master thesis was the development and optimization of spirooxindoles with different 5-membered rings as new anticancer agents. This thesis was divided into two major goals.

The first, presented in chapter three, includes the development and optimization of a library of spiropyrazoline oxindoles (synthesized by 1,3-dipolar cycloaddition reaction), and the biological evaluation of these compounds as potential anticancer agents.

More specifically, chapter three focused on the synthesis of twenty three spiropyrazoline oxindoles, their biological evaluation and stability assessment. In this chapter, spiropyrazoline oxindoles containing different phenyl groups at position 4', presented an increase in the antiproliferative activity, compared with the ones obtained for the equivalent spiroisoxazoline oxindoles.

Compounds **2b**, **2e**, **2g**, **2i**, **2j**, **2l**, **2m** and **2q** showed antiproliferative activities between 10 μM and 13 μM for HCT-116 $p53^{(+/+)}$ cell line, but for all compounds no significant differences were observed when using the isogenic cell line lacking p53. Subsequently, seven other compounds (**2e**, **2f**, **2k**, **2l**, **2o**, **2q** and **2s**) showed antiproliferative activities between 7μM and 12μM for MCF-7 breast cancer cell line, and three compounds (**2f**, **2q** and **2x**) showed antiproliferative activities between 6μM and 11μM for MDA-MB-231 cell line. MDA-MB-231 cell line represents the triple negative cancer, one of the most aggressive and the most in need of innovative therapeutic. In addition, six compounds showed selectivity toward cancer cell lines over Hek-293T with non-tumoral origin. Despite the lack of selectivity for p53 observed in the majority of compounds tested in HCT-116 cell lines, they were more active for breast cancer cell lines comparing with colorectal cancer cell lines.

Moreover, two compounds (**2e** and **2m**) revealed to be potentially non-cytotoxic to the normal human colon fibroblasts, which further show the therapeutic potential of these compounds. For these same compounds, a dose-response and an increase of late apoptosis hallmarks were found in HCT-116 cell line. The relevance of such noteworthy evidence comes from the fact that a higher proportion of cells in latter stages of apoptosis are indicative of the compound's ability to induce apoptosis faster and to induce a quicker mechanism of action. These compounds also exhibit a dose response to an increase of time exposure and the arrest of the cells in G0/G1. This arrest can be evidence of a potential p53's action. Thus, the cell cycle arrest in G0/G1 may indicate either a stop for the repair of the damaged DNA or a growth in the inhibition of cells. Additionally, the ability to induce cell death in HCT-116 cells by the compounds was confirmed by LDH assay. The apparent inhibition of p53-MDM´ proteins interaction was shown by p53 activation in cancer cell lines. This can thus lead an induction of target proteins of p53, such as activation of caspase-3 and a block of MDM2 function with a decrease of proteins expression levels. Additionally, the bimolecular fluorescence complementation (BiFC) assay corroborated the potential inhibition of the MDM2-p53 complex by spiropyrazoline oxindoles. Moreover, combined therapy studies were performed demonstrating a synergistic effect with a chemotherapeutic agent and potentiating the use of this family of compounds to a better therapy with possible minor side effects associated.

This family of compounds was also assessed in GL-261 cell line where it has not showed a dose-response effect and no apparent induction of apoptosis. Moreover, it has not showed an arrestment of the cell cycle. This can be explained through a cell growth/proliferation inhibition, known as cytostatic mechanism. These compounds exhibit a good stability in PBS.

Spiropyrazoline oxindoles compounds have different characteristics indicative of apoptosis induction for different cancer types. Advantageous characteristics are presented such as the non cytotoxicity in human normal cells; the inhibition of the MDM2-p53 complex and the potential use of these compounds in a combined therapy strategy with currently used chemotherapeutic agent (5-Fluorouracil).

Additionally, further testing should be performed, as the study of combination therapy with other chemotherapeutic agents (Oxaliplatin and Irinotecan) and subsequent verification of these compounds in normal cells. Moreover, for the best molecules should be made studies about cyclin expression involved in the cell cycle arrest, in order to better understand the effects of this family of compounds, should be performed.

The other main goal of this master thesis was to study the effect on biological activity of replacing, in the spirooxindole structure, a carbon at position 4´ (pyrazoline ring) by nitrogen (tryazoline ring).

Three compounds were evaluated as potential anticancer agents. Two were non-cytotoxic in normal human colon fibroblasts. This can be a potential favourable point, for further development of these compounds as therapeutic drugs. For these same compounds, a dose-response and an increase of late apoptosis hallmarks were found in HCT-116 $p53^{(+/+)}$ cell line. The relevance of such noteworthy evidence comes from the fact that a higher proportion of cells in latter stages of apoptosis are indicative of the compound's ability to induce apoptosis faster and to induce a quicker mechanism of action. Compound 7**f** presents a dose-response depending on the exposure time and presents the arrest of the cells in G0/G1 phase. This arrest can evidence a potential action of p53. However, compound 7**z** presents a progression on the cell cycle followed by an increase of the compound's concentration. The ability to inhibit p53-MDM´ proteins interaction was shown by an increase of p53 and MDM2 expression levels.

This family of compounds was also assessed in MDA-MB-231 cell line. Compound **7h** did not show a dose-response effect and no apparent induction of apoptosis. Moreover, cell cycle arrest in G2/M may indicates induction of growth cells inhibition. Activation of caspase 3/7 by compound **7h** was observed. This can indicate that the compound can be involved in an apoptotic process, since caspase-3 and -7 are reliable markers of apoptosis.

These data indicates that spirotryazoline oxindoles have different characteristics indicative of apoptosis induction for different cancer types. Advantageous characteristics are presented such as non cytotoxicity in human normal cells.

As all, the results were obtained *in vitro*. As pharmacokinetics and pharmacodynamics properties of compounds can be intricately different *in vivo*, it is now required to study the most promising compounds *in vivo*.

In conclusion, the potential of two spirooxindoles libraries as anticancer agents and inhibitors of the p53-MDM2 interaction was demonstrated. In particular, it was shown that these new molecules have different abilities, resulting from the inhibition of p53-MDM2 interaction, such as the ability to induction of apoptosis and cell cycle arrest, possible activation of caspase-3, increase of p53 and MDM2 expression levels in HCT-116 $p53^{(+/+)}$ cell line. Moreover, it was shown that they are non-cytotoxic to cells health, being selective for cancer cells over normal cells.

Chapter 6

MATERIALS AND METHODS

6.1. CHEMISTRY

All chemical and solvents were obtained from commercial suppliers and were used without further purification. When used as reaction solvents, CH_2Cl_2 was dried over $CaCl_2$ and distilled; THF was distilled from sodiumbenzophenone system. Et_3N was dried over KOH, distilled and stored with molecular sieves. Thin layer chromatography was performed using Merck Silica Gel 60 F254 aluminium plates and visualized by UV light. Flash column chromatography was performed on Merck Silica Gel (200-400 mesh ASTM). Preparative TLC was performed on Merck Silica Gel 60 GF254 over glass plates.

^1H and ^{13}C NMR spectra were recorded on a Bruker 400 Ultra-Shield at 400 MHz (^1H NMR) and 101 MHz (^{13}C NMR) or on a Bruker 300 Ultra-Shield at 300 MHz (^1H NMR) and 75 MHz (^{13}C NMR). ^1H and ^{13}C chemical shifts (δ) are expressed in parts per million (ppm) using the solvent as internal reference, and proton coupling constants (J) in hertz (Hz). ^1H spectral data are reported as follows: chemical shift, multiplicity (s, singlet; d, doublet; t, triplet; q, quartet; m, multiplet; dd, doublet of doublets; dt, doublet of triplets, and br, broadened), coupling constant, and integration.

The infrared spectra were collected on a Shimadzu FTIR Affinity-1 spectrophotometer. The spectra were determined using KBr disks. Only the most significant absorption bands are reported.

Spirotriazoline oxindoles were obtained by 1,3-dipolar cycloaddition between 3-imino-indolin-2-ones and nitrile imines generated *in situ* by dehydrohalogenation of hydrazonyl chlorides. They were synthesized in good yields (60-95 %), as reported[94].

Elemental analysis (C, H, and N) were performed in a Liquid Chromatography and Mass Spectrometry Laboratory, Faculty of Pharmacy of Lisbon University.

6.1.1. General Procedure for the Synthesis of 2-Indolinones

A reaction mixture of the proper substituted indolin-2-ones **6**, aldehyde, and piperidine in ethanol was refluxed for 3-5 hours, under nitrogen atmosphere. After, the mixture was cooled and put on ice, where the product precipitated. The product was filtered in vacuum with cold ethanol[70,76–79]. Finally, the product was placed in the vacuum desiccators to give the expected compound. The indolin-2-ones **3** were sometimes generated through substituted isatin in the presence of hydrazine monohydrate and ethylene glycerol, under reflux[80].

6.1.2. General Procedure for the Synthesis of Hydrazonyl Chlorides

Method A:

Triethylamine was added to a mix of phenylhydrazine derivative in dry THF at 0°C, under inert atmosphere. After stirring for 10 minutes, trimethylacetyl chloride was added dropwise.

The mixtures were then left to stir under inert atmosphere at room temperature. The reactions mixtures were quenched with water (H_2O) (1x of solvent volume). The phases were separated and the aqueous phase was extracted twice (2x of solvent volume) with Ethyl Acetate (EtOAc). All organic phases were extracted thrice with Sodium Bicarbonate ($NaHCO_3$) (2x of solvent volume) and dried over with Sodium Sulfate (Na_2SO_4). The product was dried on the rotary evaporator to afford the corresponding hydrazone. Then, triphenylphosphine dissolved in Acetonitrile was added to the corresponding hydrazone. After stirring for 30 minutes of the addition of triphenylphosphine, carbon tetrachloride was added to the reaction, at room temperature under inert atmosphere. The solvent was removed in rotary evaporator. Then, the crude was purified by flash chromatography on silica gel using an indicated gradient of eluent (n-hexane/EtOAc) for each compound, to afford the final hydrazonyl chloride (**4b**, **4d** and **4e**)[75,81].

Method B:

A mixture of phenylhydrazine derivative, and benzaldehyde derivative in aqueous ethanol 20% was stirred at room temperature in the dark for 2-3 hours. The precipitate formed was filtered and washed with aqueous ethanol 20%. Then, to NCS in CH_2Cl_2 at 0°C was added dropwise dimethyl sulfide over 5 minutes. After stirring for 15 minutes, the reaction was further cooled to –78°C. Subsequently, resulting hydrazone dissolved in CH_2Cl_2, was added. The reaction was stirred at –78°C for 1h, and then slowly allowed to warm to room temperature over 3 hours. The reaction was quenched by addition of cold water. The organic layer was then washed with brine (1x), saturated sodium sulfite aqueous solution (2x), and water. The organic layer was dried over anhydrous Na_2SO_4, filtered, and concentrated to afford the corresponding hydrazonyl chloride (**4a** and **4c**) [82].

6.1.3. General Procedure for the Synthesis of 2',4'-Dihydrospiro[Indoline-3,3'-[Pyrazol]-2-ones

Triethylamine/*N*,*N*- diisopropylethylamine was added dropwise to a mixture of indolin-2-one **3** derivative and hydrazonyl chloride **4** derivative in dry CH_2Cl_2 under nitrogen atmosphere. The reaction mixture was quenched with water (H_2O). The phases were separated and the aqueous phase was extracted with Ethyl Acetate (3xEtOAc). The combined organic extracts were dried over anhydrous Na_2SO_4 and the product was dried on the rotary evaporator. The residue was purified by flash chromatography on silica to afford the final spiropyrazoline oxindole compound **2**[70].

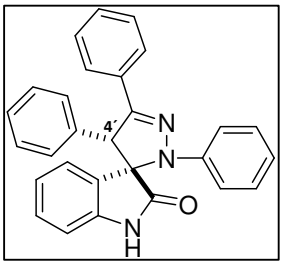

2',4',5'-triphenyl-2',4'-dihydrospiro[indoline-3,3'-pyrazol]-2-one (2a)

Following the general procedure, to a solution of **3a** (0.075g, 0.34mmol) in CH_2Cl_2 (2ml) was added **4a** (0.12g, 0.51mmol, 1.5 eq) and triethylamine (0.14 ml, 1.02 mmol, 3 eq). Reaction time: 22h. The compound was purified by flash chromatography (eluent: EtOAc/*n*-Hexane 1:3) and then recrystallized in diethyl ether to afford compound **2a** as a light yellow solid (0.1g, 0.3mmol, 78.0%).

IR (KBr): 3198 (NH), 1719 (C=O), 1618 (C=N) cm^{-1}.

^{1}H NMR (400 MHz, $CDCl_3$) δ 8.97 (s, 1H, NH), 7.71 – 7.65 (m, 2H, H), 7.31 – 7.24 (m, 3H, H), 7.16 – 7.06 (m, 5H, H), 7.03 (t, J = 7.7 Hz, 1H, H), 6.94 (d, J = 7.9 Hz, 4H, H), 6.81 (t, J = 7.3 Hz, 1H, H), 6.76 (d, J = 7.8 Hz, 1H, H), 6.55 (t, J = 7.6 Hz, 1H, H), 6.35 (d, J = 7.5 Hz, 1H, H), 5.16 (s, 1H, H-4).

^{13}C NMR (101 MHz, $CDCl_3$) δ 178.50 (C=O), 148.93 (C=N), 144.33 (Cq), 140.25 (Cq), 134.78 (Cq), 131.81 (Cq), 129.48 (CH), 129.29 (CH), 129.03 (CH), 128.76 (CH), 128.66 (CH), 128.47 (CH), 128.02 (CH), 126.95 (CH), 126.54 (CH), 125.65 (Cq), 122.40 (CH), 121.08 (CH), 115.43 (CH), 110.63 (CH), 76.84 (Cspiro), 62.67 (CH-4). Anal. Calc. for $C_{28}H_{21}N_3O$: C 80.94, H 5.09, N 10.11, Found: C 80.88, H 5.34, N 9.95.

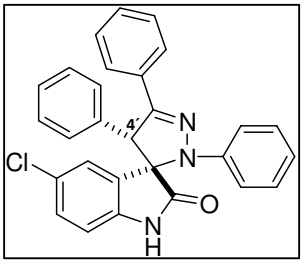

5-chloro-2',4',5'-triphenyl-2',4'-dihydrospiro[indoline-3,3'-pyrazol]-2-one (2b)

Following the general procedure, to a solution of **3b** (0.075g, 0.29mmol) in CH_2Cl_2 (2ml) was added **4a** (0.10g, 0.44mmol, 1.5 eq) and triethylamine (0.12 ml, 0.87 mmol, 3 eq). Reaction time: 16h30min. The compound was purified by flash chromatography (eluent: EtOAc/*n*-Hexane 1:4) and then recrystallized in dichloromethane to afford compound **2b** as a light yellow solid (0.1g, 0.2mmol, 81.8%).

IR (KBr): 3171 (NH), 1730 (C=O), 1595 (C=N) cm^{-1}.

^{1}H NMR (400 MHz, DMSO.d_6) δ 10.11 (s, 1H, NH), 7.63 – 7.53 (m, 2H, H), 7.19 (d, J = 5.2 Hz, 3H, H), 7.15 – 7.07 (m, 3H, H), 7.03 (t, J = 8.0 Hz, 2H, H), 6.94 (dd, J = 8.3, 2.0 Hz, 1H, H), 6.86 (dd, J = 13.3, 5.6 Hz, 4H, H), 6.74 (t, J = 7.3 Hz, 1H, H), 6.68 (d, J = 8.3 Hz, 1H, H), 6.18 (d, J = 1.6 Hz, 1H, H), 5.06 (s, 1H, H-4).

^{13}C NMR (101 MHz, DMSO.d_6) δ 177.03 (C=O), 148.17 (C=N), 143.57 (Cq), 139.06 (Cq), 133.81 (Cq), 130.98 (Cq), 128.68 (C-Cl), 128.43 (CH), 128.17 (CH), 127.84 (CH), 127.65 (CH), 126.83 (CH), 126.67 (CH), 126.26 (CH), 125.99 (Cq), 120.46 (CH), 114.65 (CH), 110.84 (CH), 76.35 (Cspiro), 62.08 (CH-4). Anal. Calc. for $C_{28}H_{20}ClN_3O.0.5CH_2Cl_2$: C 69.63, H 4.31, N 8.55, Found: C 69.19, H 4.31, N 8.55.

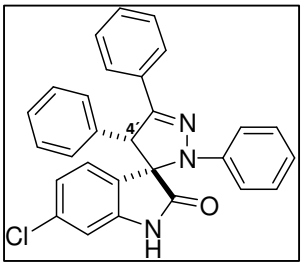

6-chloro-2',4',5'-triphenyl-2',4'-dihydrospiro[indoline-3,3'-pyrazol]-2-one (2c)

Following the general procedure, to a solution of **3c** (0.075g, 0.29mmol) in CH_2Cl_2 (2ml) was added **4a** (0.098g, 0.41mmol, 1.5 eq) and triethylamine (0.12 ml, 0.87 mmol, 3 eq). Reaction time: 21h. The compound was purified by flash chromatography (eluent: EtOAc/*n*-Hexane 1:4) and then recrystallized in dichloromethane to afford compound **2c** as a light yellow solid (0.1g, 0.2mmol, 83.1%).

IR (KBr): 3171 (NH), 1722 (C=O), 1611 (C=N) cm^{-1}.

^{1}H NMR (400 MHz, $CDCl_3$) δ 8.95 (s, 1H, NH), 7.68 (d, J = 5.4 Hz, 2H), 7.29 (d, J = 5.1 Hz, 3H), 7.18 (s, 3H), 7.12 (t, *J* = 7.7 Hz, 2H), 6.94 (t, J = 8.5 Hz, 4H), 6.85 (t, J = 7.0 Hz, 1H), 6.78 (s, 1H), 6.55 (d, J = 8.1 Hz, 1H, H), 6.23 (d, J = 8.1 Hz, 1H, H), 5.11 (s, 1H, H-4).

^{13}C NMR (101 MHz, $CDCl_3$) δ 178.62 (C=O), 149.19 (C=N), 144.22 (Cq), 141.12 (Cq), 135.39 (C-Cl), 134.44 (Cq), 131.56 (Cq), 129.17 (CH), 128.99 (CH), 128.93 (CH), 128.56 (CH), 128.34 (CH), 127.39 (CH), 126.97 (CH), 124.09 (Cq), 122.65 (CH), 121.48 (CH), 115.52 (CH), 111.48 (CH), 76.84 (Cspiro), 62.60 (CH-4). Anal. Calc. for $C_{28}H_{20}ClN_3O.0.5H_2O$: C 74.29, H 4.53, N 9.29, Found: C 73.96, H 4.34, N 9.09.

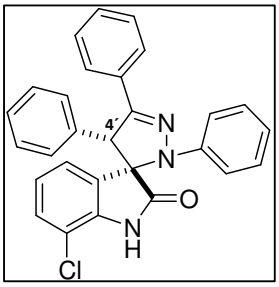

7-chloro-2',4',5'-triphenyl-2',4'-dihydrospiro[indoline-3,3'-pyrazol]-2-one (2d)

Following the general procedure, to a solution of **3d** (0.075g, 0.29mmol) in CH_2Cl_2 (2ml) was added **4a** (0.075g, 0.32mmol, 1.1 eq) and triethylamine (0.12 ml, 0.87 mmol, 3 eq). Reaction time: 10h. The compound was purified by flash chromatography (eluent: EtOAc/*n*-Hexane 1:3) and then recrystallized in diethyl ether to afford compound **2d** as a white solid (0.1g, 0.3mmol, 90.9%).

^{1}H NMR (400 MHz, DMSO) δ 9.29 (d, *J* = 4.9 Hz, 2H, H), 9.22 (s, 1H, NH), 8.90 (s, 3H, H), 8.86 – 8.71 (m, 6H, H), 8.62 (s, 2H, H), 8.56 (d, *J* = 8.3 Hz, 2H, H), 8.50 (t, *J* = 7.3 Hz, 1H, H), 8.21 (t, *J* = 7.9 Hz, 1H, H), 7.96 (d, *J* = 7.5 Hz, 1H, H), 6.82 (s, 1H, H-4).

^{13}C NMR (101 MHz, DMSO) δ 176.62 (C=O), 148.31 (C=N), 143.59 (Cq), 137.96 (Cq), 133.87 (Cq), 130.96 (Cq), 128.85 (CH), 128.57 (CH), 128.41 (CH), 128.19 (CH), 128.15 (CH), 127.81 (Cq), 127.52 (CH), 126.69 (CH), 126.26 (CH), 124.08 (CH), 122.21 (CH), 120.61 (CH), 114.90 (CH), 114.79 (C-Cl), 77.07 (Cspiro), 62.22 (CH-4). Anal. Calc. for $C_{28}H_{20}ClN_3O$: C 74.74, H 4.48, N 9.34, Found: C 74.4, H 4.69, N 8.86.

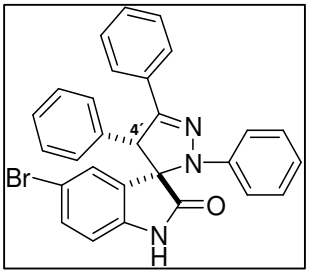

5-bromo-2',4',5'-triphenyl-2',4'-dihydrospiro[indoline-3,3'-pyrazol]-2-one (2e)

Following the general procedure, to a solution of 3**e** (0.075g, 0.25mmol) in CH_2Cl_2 (2ml) was added **4a** (0.07g, 0.28mmol, 1.1 eq) and triethylamine (0.10 ml, 0.75 mmol, 3 eq). Reaction time: 11h30min. The compound was purified by flash chromatography (eluent: EtOAc/*n*-Hexane 1:3) and then recrystallized in diethyl ether to afford compound **2e** as a white solid (0.1g, 0.2mmol, 81.8%).

IR (KBr): 3180 (NH), 1718 (C=O), 1618 (C=N) cm^{-1}.

^{1}H NMR (400 MHz, DMSO.d_6) δ 10.21 (s, 1H, NH), 7.86 – 7.69 (m, 2H, H), 7.41 (dd, *J* = 22.4, 3.3 Hz, 3H, H, H), 7.34 – 7.25 (m, 4H, H), 7.23 (t, *J* = 7.2 Hz, 2H, H), 7.04 (d, *J* = 7.9 Hz, 4H, H), 6.94 (t, *J* = 7.2 Hz, 1H, H), 6.82 (d, *J* = 8.2 Hz, 1H, H), 6.50 (s, 1H, H), 5.24 (s, 1H, H-4).

^{13}C NMR (101 MHz, DMSO.d_6) δ 176.86 (C=O), 148.13 (C=N), 143.56 (Cq), 139.42 (Cq), 133.79 (Cq), 131.50 (CH), 130.96 (Cq), 128.78 (CH), 128.42 (CH), 128.16 (CH), 127.74 (Cq), 127.13 (CH), 126.25 (CH), 120.46 (CH), 114.64 (CH), 113.99 (C-Br), 111.27 (CH), 62.10 (CH-4). Anal. Calc. for $C_{28}H_{20}BrN_3O.0.55H_2O$: C 66.68, H 4.23, N 8.33, Found: C 66.29, H 4.09, N 8.18.

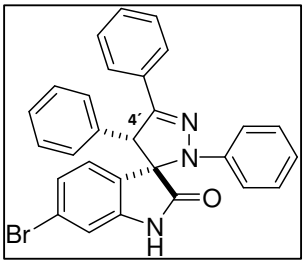

6-bromo-2',4',5'-triphenyl-2',4'-dihydrospiro[indoline-3,3'-pyrazol]-2-one (2f)

Following the general procedure, to a solution of **3f** (0.075g, 0.25mmol) in CH_2Cl_2 (2ml) was added **4a** (0.07g, 0.3mmol, 1.2 eq) and triethylamine (0.10 ml, 0.75 mmol, 3 eq). Reaction time: 5h. The compound was purified by flash chromatography (eluent: EtOAc/*n*-Hexane 1:3) and then recrystallized in dichloromethane to afford compound **2f** as a white solid (0.07g, 0.14mmol, 83.9%).

IR (KBr): 3172 (NH), 1720 (C=O), 1609 (C=N) cm^{-1}.

^{1}H NMR (400 MHz, DMSO.d_6) δ 9.90 (s, 1H, NH), 9.32 (d, *J* = 3.8 Hz, 2H, H), 8.95 – 8.90 (m, 3H, H), 8.84 (s, 3H, H, H), 8.78 (t, *J* = 7.8 Hz, 2H, H), 8.67 – 8.55 (m, *J* = 14.9, 7.9 Hz, 5H, H), 8.52 (t, *J* = 7.3 Hz, 1H, H), 8.39 (d, *J* = 8.1 Hz, 1H, H), 7.87 (d, *J* = 8.1 Hz, 1H, H), 6.78 (s, 1H, H-4).

^{13}C NMR (101 MHz, DMSO.d_6) δ 177.12 (C=O), 148.45 (C=N), 143.72 (Cq), 141.90 (Cq), 133.99 (Cq), 131.01 (Cq), 128.56 (CH), 128.29 (Cq), 127.81 (CH), 127.55 (CH), 126.97 (CH), 126.26 (CH), 124.23 (CH), 124.06 (C-Br), 122.56 (CH), 120.60 (CH), 114.96 (CH),

113.33 (CH), 76.19 (Cspiro), 61.79 (CH-4). Anal. Calc. for $C_{28}H_{20}BrN_3O$: C 68.02, H 4.048, N 8.50, Found: C 67.61, H 4.13, N 8.25.

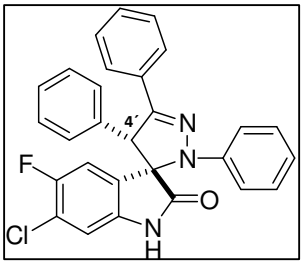

6-chloro-5-fluoro-2',4',5'-triphenyl-2',4'-dihydrospiro[indoline-3,3'-pyrazol]-2-one (2g)

Following the general procedure, to a solution of **3g** (0.0175g, 0.06mmol) in CH_2Cl_2 (2ml) was added **4a** (0.04g, 0.16mmol, 2.5 eq) and triethylamine (0.023 ml, 0.15 mmol, 2.5 eq). Reaction time: 46h30min. The compound was purified by flash chromatography (eluent: EtOAc/*n*-Hexane 1:3) to afford compound **2g** as a white solid (0.01g, 0.03mmol, 40.0%).

IR (KBr): 3419 (NH), 1730 (C=O), 1597 (C=N) cm^{-1}.

^{1}H NMR (300 MHz, $CDCl_3$) δ 8.94 (s, 1H, NH), 7.63 (d, *J* = 3.6 Hz, 2H, H), 7.28 – 7.21 (m, 3H, H), 7.17 (s, 3H, H), 7.13 – 7.01 (m, 2H, H), 6.99 – 6.79 (m, 5H, H), 6.76 (d, *J* = 5.8 Hz, 1H, H), 6.08 (d, *J* = 8.4 Hz, 1H, H), 5.08 (s, 1H, H-4).

^{13}C NMR (75 MHz, $CDCl_3$) δ 178.47 (C=O), 149.23 (C=N), 144.07 (Cq), 136.44 (d, J = 2.7 Hz, C-F), 133.97 (Cq), 131.37 (Cq), 129.16 (CH), 128.66 (CH), 126.99 (CH), 125.80 (d, J = 7.2 Hz, C-Cl), 122.22 (Cq), 121.96 (Cq), 121.69 (CH), 115.48 (CH), 115.34 (CH), 115.00 (CH), 112.52 (CH), 77.00 (Cspiro), 62.81 (CH-4). Anal. Mass for $C_{28}H_{19}ClFN_3O$: 467.1, Found: 468.3.

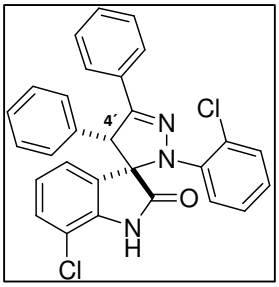

7-chloro-2'-(2-chlorophenyl)-4',5'-diphenyl-2',4'-dihydrospiro[indoline-3,3'-pyrazol]-2-one (2h)

Following the general procedure, to a solution of **3d** (0.05g, 0.20mmol) in CH_2Cl_2 (1.5ml) was added **4b** (0.08g, 0.29mmol, 1.5 eq) and N,N-Diisopropylethylamine (0.10 mL, 0.59 mmol, 3 eq.). Reaction time: 23h. The compound was purified by flash chromatography (eluent: EtOAc/*n*-Hexane 1:4) to afford compound **2h** as a white solid (0.09g, 0.18mmol, 93.9%).

IR (KBr): 3412 (NH), 1720 (C=O), 1620 (C=N) cm^{-1}.

^{1}H NMR (300 MHz, $CDCl_3$) δ 7.79 (s, 1H, NH), 7.71 – 7.63 (m, 2H, H), 7.44 (dd, *J* = 8.4, 1.3 Hz, 1H, H), 7.28 (d, *J* = 3.3 Hz, 2H, H), 7.23 – 7.13 (m, 6H, H), 7.09 – 7.01 (m, 3H, H), 6.98 (dd, *J* = 7.2, 2.3 Hz, 2H, H), 6.34 (t, *J* = 7.9 Hz, 1H, H), 5.89 (d, *J* = 7.5 Hz, 1H, H), 5.07 (s, 1H, H-4).

^{13}C NMR (75 MHz, $CDCl_3$) δ 177.61 (C=O), 151.84 (C=N), 141.18 (Cq), 138.50 (Cq), 134.80 (Cq), 131.51 (Cq), 130.37 (CH), 129.72 (CH), 129.22 (CH), 129.11 (CH), 128.95

(CH), 128.55 (CH), 128.24 (CH), 127.27 (CH), 127.12 (Cq), 126.55 (CH), 126.00 (CH), 125.88 (Cq), 125.50 (CH), 122.42 (CH), 114.65 (C-Cl), 78.98 (Cspiro), 62.59 (CH-4). Anal. Calc. for $C_{28}H_{19}Cl_2N_3O$: C 69.42, H 3.96, N 8.68, Found: C 69.04, H 3.78, N 9.30.

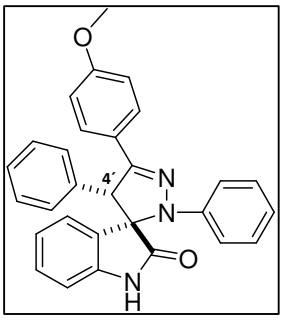

5'-(4-methoxyphenyl)-2',4'-diphenyl-2',4'-dihydrospiro[indoline-3,3'-pyrazol]-2-one (2i)

Following the general procedure, to a solution of **3a** (0.075g, 0.34mmol) in CH_2Cl_2 (2ml) was added **4c** (0.13g, 0.51mmol, 1.5 eq) and triethylamine (0.14 ml, 1.02 mmol, 3 eq). Reaction time: 17h. The compound was purified by flash chromatography (eluent: EtOAc/*n*-Hexane 1:3) to afford compound **2i** as a white solid (0.1g, 0.3mmol, 73.5%).

IR (KBr): 3362 (NH), 1741 (C=O), 1600 (C=N) cm^{-1}.

^{1}H NMR (400 MHz, $CDCl_3$) δ 8.63 (s, 1H, NH), 7.62 (d, *J* = 8.8 Hz, 2H, H), 7.16 – 7.00 (m, 6H, H), 6.94 (t, *J* = 8.3 Hz, 4H, H), 6.80 (t, *J* = 9.0 Hz, 3H, H, H), 6.74 (d, *J* = 7.8 Hz, 1H, H), 6.57 (t, *J* = 7.5 Hz, 1H, H), 6.36 (d, *J* = 7.4 Hz, 1H, H), 5.13 (s, 1H, H-4), 3.78 (s, 3H, CH_3).

^{13}C NMR (101 MHz, $CDCl_3$) δ 178.52 (C=O), 160.08 (C=N), 148.81 (C-O), 144.48 (Cq), 139.89 (Cq), 134.75 (Cq), 129.31 (CH), 129.21 (CH), 128.91 (CH), 128.53 (CH), 128.36 (CH), 127.88 (CH), 126.47 (CH), 125.72 (Cq), 124.41 (Cq), 122.36 (CH), 120.78 (CH), 115.25 (CH), 113.86 (CH), 110.44 (CH), 77.23 (Cspiro), 62.78 (CH-4), 55.26 (O-CH_3). Anal. Calc. for $C_{29}H_{23}N_3O_2$: C 78.18, H 5.20, N 9.43, Found: C 77.96, H 5.19, N 9.34.

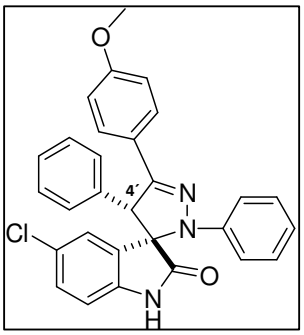

5-chloro-5'-(4-methoxyphenyl)-2',4'-diphenyl-2',4'-dihydrospiro[indoline-3,3'-pyrazol]-2-one (2j)

Following the general procedure, to a solution of **3b** (0.075g, 0.29mmol) in CH_2Cl_2 (2ml) was added **4c** (0.12g, 0.44mmol, 1.5 eq) and triethylamine (0.12 ml, 0.87 mmol, 3 eq). Reaction time: 18h30min. The compound was purified by flash chromatography (eluent: EtOAc/*n*-Hexane 1:3) and then recrystallized in diethyl ether to afford compound **2j** as a white solid (0.05g, 0.1mmol, 33.4%).

IR (KBr): 1740 (NH), 1711 (C=O), 1599 (C=N) cm^{-1}.

^{1}H NMR (400 MHz, DMSO.d_6) δ 10.97 (s, 1H, NH), 7.61 (d, *J* = 8.5 Hz, 2H, H), 7.27 – 7.15 (m, 4H, H), 7.12 (t, *J* = 7.7 Hz, 2H, H), 7.00 (d, *J* = 6.7 Hz, 2H, H), 6.92 (d, *J* = 8.5 Hz, 2H, H), 6.87 (d, *J* = 8.3 Hz, 1H, H), 6.78 (dd, *J* = 12.6, 7.8 Hz, 3H, H, H), 6.12 (s, 1H, H), 5.41 (s, 1H, H-4), 3.74 (s, 3H, CH_3).

^{13}C NMR (101 MHz, DMSO.d_6) δ 176.36 (C=O), 159.90 (C=N), 149.44 (C-O), 144.20 (Cq), 140.31 (Cq), 134.71 (Cq), 129.30 (CH), 128.95 (CH), 128.50 (CH), 128.16 (CH), 127.88 (CH), 127.26 (C-Cl), 125.52 (Cq), 125.45 (CH), 123.65 (Cq), 120.30 (CH), 114.23 (CH), 114.08 (CH), 111.58 (CH), 75.66 (Cspiro), 61.02 (CH-4), 55.20 (O-CH_3). Anal. Calc. for $C_{29}H_{22}ClN_3O_2.1.25H_2O$: C 69.43, H 4.93, N 8.38, Found: C 69.42, H 4.92, N 8.56.

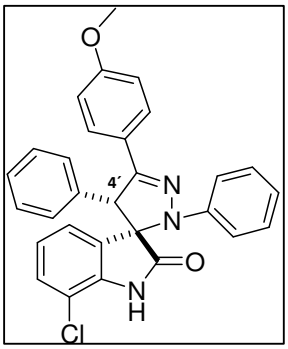

7-chloro-5'-(4-methoxyphenyl)-2',4'-diphenyl-2',4'-dihydrospiro[indoline-3,3'-pyrazol]-2-one (2k)

Following the general procedure, to a solution of **3d** (0.075g, 0.29mmol) in CH_2Cl_2 (2ml) was added **4c** (0.08g, 0.32mmol, 1.1 eq) and triethylamine (0.12 ml, 0.87 mmol, 3 eq). Reaction time: 24 hours. The compound was purified by flash chromatography (eluent: EtOAc/*n*-Hexane 1:4) and then recrystallized in diethyl ether to afford compound **2k** as a white solid (0.10g, 0.2mmol, 71.1%).

IR (KBr): 3204 (NH), 1732 (C=O), 1608 (C=N) cm^{-1}.

^{1}H NMR (400 MHz, $CDCl_3$) δ 7.78 (s, 1H, NH), 7.59 (d, J = 8.8 Hz, 2H, H), 7.16 (dd, J = 7.6, 4.5 Hz, 3H, H), 7.13 – 7.05 (m, 3H, H), 6.98 (s, 2H, H), 6.91 (d, J = 7.9 Hz, 2H, H), 6.85 (d, J = 7.3 Hz, 1H, H), 6.80 (d, J = 8.9 Hz, 2H, H), 6.55 (t, J = 7.9 Hz, 1H, H), 6.30 (d, J = 7.5 Hz, 1H, H), 5.14 (s, 1H, H-4), 3.77 (s, 3H, CH_3).

^{13}C NMR (101 MHz, $CDCl_3$) δ 176.78 (C=O), 160.30 (C=N), 149.06 (C-O), 144.49 (Cq), 137.57 (Cq), 134.51 (Cq), 129.35 (CH), 129.29 (CH), 129.13 (CH), 128.80 (CH), 128.51 (CH), 128.24 (CH), 127.51 (Cq), 124.99 (CH), 124.23 (Cq), 123.30 (CH), 121.39 (CH), 115.70 (CH), 115.22 (C-Cl), 114.00 (CH), 77.90 (Cspiro), 63.22 (CH-4), 55.39 (O-CH_3). Anal. Calcd for $C_{29}H_{22}ClN_3O_2$: C 72.57, H 4.63, N 8.76, Found: C 72.34, H 4.56, N 8.66.

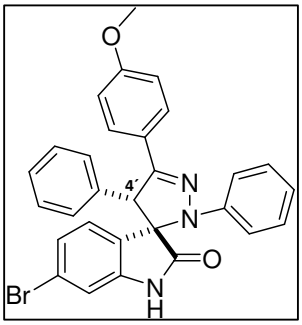

6-bromo-5'-(4-methoxyphenyl)-2',4'-diphenyl-2',4'-dihydrospiro[indoline-3,3'-pyrazol]-2-one (2l)

Following the general procedure, to a solution of **3f** (0.075g, 0.25mmol) in CH_2Cl_2 (2ml) was added **4c** (0.08g, 0.3mmol, 1.2 eq) and triethylamine (0.10 ml, 0.75 mmol, 3 eq). Reaction time: 3h10min. The compound was purified by flash chromatography (eluent: EtOAc/*n*-Hexane 1:3) and then recrystallized in diethyl ether to afford compound **2l** as a white solid (0.12g, 0.28mmol, 91.6%).

IR (KBr): 3220 (NH), 1747 (C=O), 1608 (C=N) cm^{-1}.

^{1}H NMR (400 MHz, $CDCl_3$) δ 8.76 (s, 1H, NH), 7.61 (d, *J* = 8.5 Hz, 2H, H), 7.17 (d, *J* = 3.0 Hz, 3H, H), 7.11 (t, *J* = 7.8 Hz, 2H, H), 6.96 (s, 2H, H, H), 6.91 (d, *J* = 9.4 Hz, 3H, H),

6.83 (dd, *J* = 11.7, 8.2 Hz, 3H, H), 6.71 (d, *J* = 8.1 Hz, 1H, H), 6.17 (d, *J* = 8.1 Hz, 1H, H), 5.07 (s, 1H, H-4), 3.78 (s, 3H, CH_3).

^{13}C NMR (101 MHz, $CDCl_3$) δ 178.46 (C=O), 160.33 (C=N), 149.20 (C-O), 144.54 (Cq), 141.24 (Cq), 134.54 (Cq), 129.23 (CH), 129.15 (CH), 128.92 (CH), 128.52 (CH), 128.32 (CH), 127.74 (CH), 125.54 (CH), 124.86 (Cq), 124.25 (C-Br), 123.28 (Cq), 121.31 (CH), 115.51 (CH), 114.12 (CH), 114.04 (CH), 77.26 (Cspiro), 62.75 (CH-4), 55.41 (O-CH_3). Anal. Calcd for $C_{29}H_{22}BrN_3O_2.0.2H_2O$: C 65.96, H 4.28, N 7.96, Found: C 65.60, H 4.39, N 7.70.

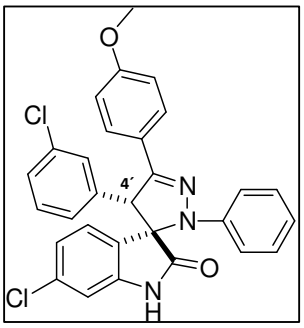

6-chloro-4'-(3-chlorophenyl)-5'-(4-methoxyphenyl)-2'-phenyl-2',4'-dihydrospiro[indoline-3,3'-pyrazol]-2-one (2m)

Following the general procedure, to a solution of **3h** (0.075g, 0.26mmol) in CH_2Cl_2 (2ml) was added **4c** (0.14g, 0.52mmol, 2 eq) and triethylamine (0.11 ml, 0.78 mmol, 3 eq). Reaction time: 22 hours. The compound was purified by flash chromatography (eluent: EtOAc/*n*-Hexane 1:3) and then recrystallized in diethyl ether to afford compound **2m** as a white solid (0.13g, 0.25mmol, 97.8%).

IR (KBr): 3406 (NH), 1703 (C=O), 1597 (C=N) cm^{-1}.

^{1}H NMR (400 MHz, $CDCl_3$) δ 8.81 (s, 1H, NH), 7.59 (d, *J* = 8.8 Hz, 2H, H), 7.17 (d, *J* = 8.3 Hz, 1H, H), 7.11 (t, *J* = 7.8 Hz, 3H, H), 6.97 (s, 1H, H), 6.90 (d, *J* = 7.9 Hz, 2H, H), 6.84 (t, *J* = 8.3 Hz, 4H, H), 6.78 (d, *J* = 1.5 Hz, 1H, H), 6.62 (dd, *J* = 8.1, 1.7 Hz, 1H, H), 6.28 (d, *J* = 8.1 Hz, 1H, H), 5.02 (s, 1H, H-4), 3.79 (s, 3H, CH_3).

^{13}C NMR (101 MHz, $CDCl_3$) δ 178.29 (C=O), 160.49 (C=N), 148.59 (C-O), 144.34 (Cq), 141.13 (Cq), 136.73 (C-Cl), 135.65 (Cq), 134.87 (C-Cl), 130.18 (CH), 129.18 (CH), 128.58 (CH), 128.46 (CH), 127.48 (CH), 127.29 (Cq), 123.88 (Cq), 122.77 (CH), 121.51 (CH), 115.59 (CH), 114.17 (CH), 111.62 (CH), 76.66 (Cspiro), 62.20 (CH-4), 55.43 (O-CH_3). Anal. Calcd for $C_{29}H_{21}Cl_2N_3O_2$: C 67.71, H 4.11, N 8.17, Found: C 67.19, H 4.15, N 7.98.

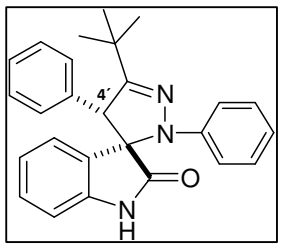

5'-(tert-butyl)-2',4'-diphenyl-2',4'-dihydrospiro[indoline-3,3'-pyrazol]-2-one (2n)

Following the general procedure, to a solution of **3a** (0.05g, 0.26mmol) in CH_2Cl_2 (2ml) was added **4d** (0.1g, 0.47mmol, 2 eq) and triethylamine (0.11 ml, 0.78 mmol, 3 eq). Reaction time: 5h30min. The compound was purified by flash chromatography (eluent: EtOAc/*n*-Hexane 1:3) and then recrystallized in dichloromethane:*n*-hexane to afford compound **2n** as a white solid (0.07g, 0.16mmol, 72.7%).

IR (KBr): 3236 (NH), 1709 (C=O), 1599 (C=N) cm^{-1}.

^{1}H NMR (300 MHz, $CDCl_3$) δ 7.65 (s, 1H, NH), 7.35 (s, 2H, H), 7.12 (dd, *J* = 7.7, 1.2 Hz, 2H, H), 7.09 – 6.99 (m, 3H, H), 6.83 (dd, *J* = 8.8, 1.0 Hz, 3H, H), 6.80 – 6.74 (m, 2H, H), 6.57 (td, *J* = 7.6, 1.0 Hz, 1H, H), 6.24 (d, *J* = 7.2 Hz, 1H, H), 4.46 (s, 1H, H-4), 1.19 (s, 9H, CH_3).

^{13}C NMR (75 MHz, $CDCl_3$) δ 178.37 (C=O), 161.70 (C=N), 145.79 (Cq), 140.40 (Cq), 135.29 (Cq), 129.28 (CH), 128.90 (CH), 128.12 (CH), 126.41 (CH), 125.74 (Cq), 122.24 (CH), 120.92 (CH), 115.96 (CH), 110.46 (CH), 77.28 (Cspiro), 62.32 (CH-4), 34.87 ($\underline{C}(CH_3)_3$), 29.49 ($C(\underline{C}H_3)_3$). Anal. Calc. for $C_{26}H_{25}N_3O.0.05H_2O$: C 78.77, H 6.40, N 10.60, Found: C 77.70, H 6.47, N 10.18.

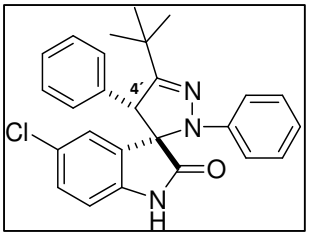

5'-(tert-butyl)-5-chloro-2',4'-diphenyl-2',4'-dihydrospiro[indoline-3,3'-pyrazol]-2-one (2o)

Following the general procedure, to a solution of **3b** (0.05g, 0.27mmol) in CH_2Cl_2 (2ml) was added **4d** (0.09g, 0.47mmol, 2 eq) and triethylamine (0.09 ml, 0.68 mmol, 3 eq). Reaction time: 4h50min. The compound was purified by flash chromatography (eluent: EtOAc/*n*-Hexane 1:2) to afford compound **2o** as a white solid (0.08g, 0.19mmol, 80.2%).

IR (KBr): 3254 (NH), 1718 (C=O), 1691 (C=N) cm^{-1}.

^{1}H NMR (300 MHz, $CDCl_3$) δ 7.62 (s, 1H, NH), 7.47 – 7.39 (m, 1H, H), 7.31 (d, *J* = 7.8 Hz, 1H, H), 7.20 (dd, *J* = 10.8, 8.7 Hz, 1H, H), 7.12 – 7.03 (m, 1H, H), 6.84 (s, 2H, H, H), 6.82 – 6.78 (m, 2H, H), 6.69 (d, *J* = 8.3 Hz, 1H, H), 6.15 (d, *J* = 2.1 Hz, 1H, H), 4.46 (s, 1H, H-4), 1.19 (s, 9H, CH_3).

^{13}C NMR (75 MHz, $CDCl_3$) δ 177.60 (C=O), 161.51 (C=N), 145.42 (Cq), 138.52 (Cq), 134.53 (Cq), 129.18 (CH), 129.09 (CH), 128.87 (CH), 128.39 (Cq), 127.71 (C-Cl), 127.46 (CH), 126.64 (CH), 121.13 (CH), 115.87 (CH), 113.52 (CH), 111.06 (CH), 77.16 (Cspiro), 62.39 (CH-4), 34.74 ($\underline{C}(CH_3)_3$), 29.33 ($C(\underline{C}H_3)_3$). Anal. Calc. for $C_{26}H_{24}ClN_3O.0.05AcOEt$: C 72.45, H 5.67, N 9.68, Found: C 72.47, H 5.74, N 9.52.

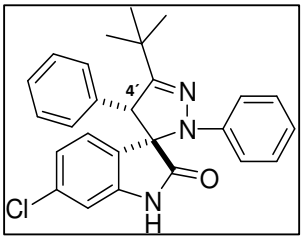

5'-(tert-butyl)-6-chloro-2',4'-diphenyl-2',4'-dihydrospiro[indoline-3,3'-pyrazol]-2-one (2p)

Following the general procedure, to a solution of **3c** (0.075g, 0.29mmol) in CH_2Cl_2 (2ml) was added **4d** (0.13g, 0.59mmol, 2 eq) and triethylamine (0.12 ml, 0.87 mmol, 3 eq). Reaction time: 15h30min. The compound was purified by flash chromatography (eluent: EtOAc/*n*-Hexane 1:3) to afford compound **2p** as a white solid (0.1g, 0.23mmol, 79.1%).

IR (KBr): 3213 (NH), 1724 (C=O), 1608 (C=N) cm^{-1}.

^{1}H NMR (400 MHz, $CDCl_3$) δ 8.37 (s, 1H, NH), 7.35 (s, 2H, H), 7.26 (q, *J* = 6.9 Hz, 1H, H), 7.15 (s, 1H, H), 7.06 (t, *J* = 7.9 Hz, 2H, H), 6.81 (t, *J* = 8.3 Hz, 3H, H), 6.74 (d, *J* = 1.5 Hz, 1H, H), 6.66 (s, 1H, H), 6.55 (dd, *J* = 8.2, 1.7 Hz, 1H, H), 6.12 (d, *J* = 8.2 Hz, 1H, H), 4.43 (s, 1H, H-4, H), 1.19 (s, 9H, CH_3).

^{13}C NMR (101 MHz, $CDCl_3$) δ 177.91 (C=O), 161.88 (C=N), 145.72 (Cq), 141.38 (Cq), 135.18 (Cq), 134.99 (C-Cl), 128.99 (CH), 128.37 (CH), 127.39 (CH), 124.32 (Cq), 122.43 (CH), 121.41 (CH), 116.29 (CH), 111.05 (CH), 77.05 (Cspiro), 62.36 (CH-4), 34.91 ($\underline{C}(CH_3)_3$), 29.49 ($C(\underline{C}H_3)_3$). Anal. Calc. for $C_{26}H_{24}ClN_3O.0.5CH_2Cl_2$: C 67.37, H 5.34, N 8.90, Found: C 67.14, H 5.39, N 8.84.

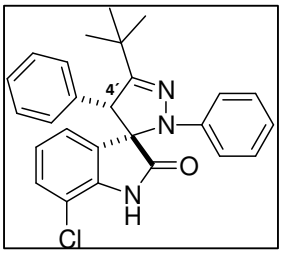

5'-(tert-butyl)-7-chloro-2',4'-diphenyl-2',4'-dihydrospiro[indoline-3,3'-pyrazol]-2-one (2q)

Following the general procedure, to a solution of **3d** (0.075g, 0.29mmol) in CH_2Cl_2 (2ml) was added **4d** (0.075g, 0.35mmol, 1.2 eq) and triethylamine (0.12 ml, 0.87 mmol, 3 eq). Reaction time: 3 hours. The compound was purified by flash chromatography (eluent: EtOAc/*n*-Hexane 1:3) and then recrystallized in diethyl ether to afford compound **2q** as a white solid (0.11g, 0.26mmol, 87.2%).

IR (KBr): 3177 (NH), 1752 (C=O), 1712 (C=N) cm^{-1}.

^{1}H NMR (400 MHz, $CDCl_3$) δ 7.89 (s, 1H, NH), 7.36 (s, 2H, H), 7.27 – 7.23 (m, 1H, H), 7.09 (dd, *J* = 15.8, 8.1 Hz, 4H, H), 6.88 – 6.78 (m, 3H, CH, H), 6.68 (s, 1H, H), 6.53 (t, *J* = 7.9 Hz, 1H, H), 6.15 (d, *J* = 7.6 Hz, 1H, H), 4.49 (s, 1H, H-4), 1.19 (s, 9H, CH_3).

^{13}C NMR (101 MHz, $CDCl_3$) δ 176.50 (C=O), 161.89 (C=N), 145.63 (Cq), 137.96 (Cq), 134.94 (Cq), 129.24 (CH), 129.01 (CH), 128.34 (CH), 127.46 (Cq), 124.85 (CH), 123.06 (CH), 121.55 (CH), 116.54 (CH), 115.12 (C-Cl), 78.17 (Cspiro), 62.59 (CH-4), 34.90 ($\underline{C}(CH_3)_3$), 29.48 ($C(\underline{C}H_3)_3$). Anal. Calcd for $C_{26}H_{24}ClN_3O.0.4H_2O$: C 71.43, H 5.73, N 9.61, Found: C 71.11, H 5.70, N 9.30.

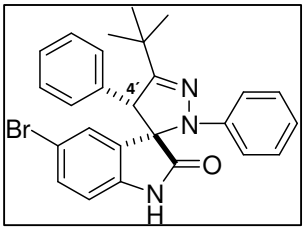

5-bromo-5'-(tert-butyl)-2',4'-diphenyl-2',4'-dihydrospiro[indoline-3,3'-pyrazol]-2-one (2r)

Following the general procedure, to a solution of **3e** (0.05g, 0.18mmol) in CH_2Cl_2 (2ml) was added **4d** (0.09g, 0.43mmol, 2.5 eq) and triethylamine (0.06 ml, 0.43 mmol, 2.5 eq). Reaction time: 5h30min. The compound was purified by flash chromatography (eluent: EtOAc/*n*-Hexane 1:1) to afford compound **2r** as a white solid (0.03, 0.06mmol, 41.5%).

IR (KBr): 3254 (NH), 1726 (C=O), 1695 (C=N) cm^{-1}.

^{1}H NMR (300 MHz, CDCl3) δ 7.69 (s, 1H, NH), 7.42 (s, 1H, H), 7.31 (t, *J* = 7.2 Hz, 2H, H), 7.24 (d, *J* = 2.0 Hz, 1H, H), 7.22 (d, *J* = 2.0 Hz, 1H, H), 7.07 (dd, *J* = 8.6, 7.4 Hz, 2H, H), 6.86 – 6.80 (m, 3H, H), 6.64 (d, *J* = 8.3 Hz, 2H, H), 6.27 (d, *J* = 1.9 Hz, 1H, H), 4.45 (s, 1H, H-4), 1.19 (s, 9H, CH_3).

^{13}C NMR (75 MHz, CDCl3) δ 177.17 (C=O), 161.68 (C=N), 145.62 (Cq), 139.06 (Cq), 134.71 (Cq), 132.11 (CH), 132.11 (CH), 129.73 (CH), 129.73 (CH), 129.04 (CH), 129.04 (CH), 128.59 (CH), 127.97 (Cq), 121.42 (CH), 116.21 (CH), 115.20 (C-Br), 111.45 (CH), 77.36 (Cspiro), 62.63 (CH-4), 34.91 ($\underline{C}(CH_3)_3$), 29.50 ($C(\underline{C}H_3)_3$). Anal. Mass for $C_{26}H_{24}BrN_3O$: 475.1, Found: 476.3.

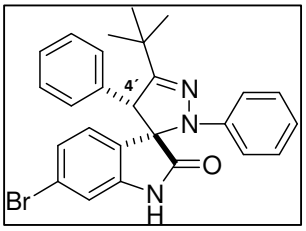

6-bromo-5'-(tert-butyl)-2',4'-diphenyl-2',4'-dihydrospiro[indoline-3,3'-pyrazol]-2-one (2s)

Following the general procedure, to a solution of **3f** (0.075g, 0.25mmol) in CH_2Cl_2 (2ml) was added **4d** (0.06g, 0.3mmol, 1.2 eq) and triethylamine (0.10 ml, 0.75 mmol, 3 eq). Reaction time: 1h30min. The compound was purified by flash chromatography (eluent: EtOAc/*n*-Hexane 1:3) and then recrystallized in diethyl ether to afford compound **2s** as a white solid (0.11, 0.23mmol, 92.1%).

IR (KBr): 3218 (NH), 1723 (C=O), 1610 (C=N) cm^{-1}.

^{1}H NMR (400 MHz, $CDCl_3$) δ 8.48 (s, 1H, NH), 7.34 (s, 2H, H), 7.26 (q, *J* = 7.1 Hz, 1H, H), 7.15 (s, 1H, H), 7.07 (t, *J* = 7.9 Hz, 2H, H), 6.90 (s, 1H, H), 6.81 (t, *J* = 7.5 Hz, 3H, H), 6.73 – 6.58 (m, 2H, H, H), 6.05 (d, *J* = 8.1 Hz, 1H, H), 4.43 (s, 1H, H-4), 1.18 (s, 9H, CH_3).

^{13}C NMR (101 MHz, $CDCl_3$) δ 177.88 (C=O), 161.89 (C=N), 145.70 (Cq), 141.50 (Cq), 134.93 (Cq), 129.01 (CH), 128.38 (CH), 127.65 (Cq), 125.35 (CH), 124.86 (CH), 123.15 (C-Br), 121.39 (CH), 116.21 (CH), 113.87 (CH), 77.09 (Cspiro), 62.29 (CH-4), 34.90 ($\underline{C}(CH_3)_3$), 29.49 ($C(\underline{C}H_3)_3$). Anal. Calcd for $C_{26}H_{24}BrN_3O.0.05H_2O$: C 65.70, H 5.12, N 8.84, Found: C 65.32, H 5.02, N 8.64.

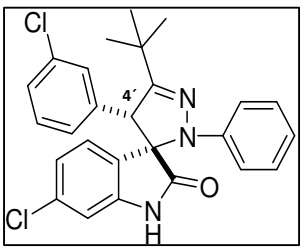

5'-(tert-butyl)-6-chloro-4'-(3-chlorophenyl)-2'-phenyl-2',4'-dihydrospiro[indoline-3,3'-pyrazol]-2-one (2t)

Following the general procedure, to a solution of **3h** (0.075g, 0.26mmol) in CH_2Cl_2 (2ml) was added **4d** (0.11g, 0.52mmol, 2 eq) and triethylamine (0.11 ml, 0.78 mmol, 3 eq). Reaction time: 18h30min. The compound was purified by flash chromatography (eluent: EtOAc/*n*-Hexane 1:3) and then recrystallized in diethyl ether to afford compound **2t** as a white solid (0.10, 0.23mmol, 82.7%).

IR (KBr): 3419 (NH), 1720 (C=O), 1616 (C=N) cm^{-1}.

^{1}H NMR (400 MHz, $CDCl_3$) δ 8.40 (s, 1H, NH), 7.31 (s, 1H, H), 7.28 – 7.20 (m, 2H, H), 7.07 (t, *J* = 7.8 Hz, 2H, H), 6.83 (t, *J* = 7.1 Hz, 3H, H), 6.76 (s, 1H, H), 6.73 – 6.50 (m, 2H, H), 6.18 (s, 1H, H), 4.40 (s, 1H, H-4), 1.19 (s, 9H, CH_3).

^{13}C NMR (101 MHz, $CDCl_3$) δ 177.60 (C=O), 161.34 (C=N), 145.48 (Cq), 141.42 (Cq), 137.17 (Cq), 135.52 (C-Cl), 134.81 (C-Cl), 129.72 (CH), 129.04 (CH), 128.62 (CH), 127.27 (CH), 123.88 (Cq), 122.62 (CH), 121.67 (CH), 116.41 (CH), 111.30 (CH), 76.97 (Cspiro), 61.75 (CH-4), 34.96 ($\underline{C}(CH_3)_3$), 29.47 ($C(\underline{C}H_3)_3$). Anal. Calcd for $C_{26}H_{23}Cl_2N_3O.0.6CH_2Cl_2$: C 67.25, H 4.99, N 9.05, Found: C 66.61, H 5.14, N 8.82.

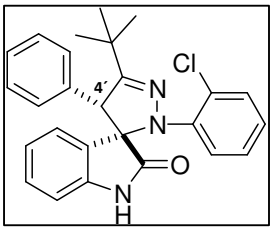

5'-(tert-butyl)-2'-(2-chlorophenyl)-4'-phenyl-2',4'-dihydrospiro[indoline-3,3'-pyrazol]-2-one (2u)

Following the general procedure, to a solution of **3a** (0.05g, 0.26mmol) in CH_2Cl_2 (2ml) was added **4e** (0.08g, 0.33mmol, 1.5 eq) and triethylamine (0.115 mL, 0.083 mmol, 3 eq.). Reaction time: 26h50min. The compound was purified by flash chromatography (eluent: EtOAc/*n*-Hexane 1:4) to afford compound **2u** as a white solid (0.06, 0.14mmol, 61.8%).

IR (KBr): 3419 (NH), 1716 (C=O), 1618 (C=N) cm^{-1}.

^{1}H NMR (300 MHz, $CDCl_3$) δ 7.91 (s, 1H, NH), 7.31 – 7.26 (m, 2H, H), 7.22 (d, *J* = 6.3 Hz, 1H, H), 7.14 (d, *J* = 9.2 Hz, 2H, H), 7.08 (d, 1H, H), 6.99 (t, *J* = 7.8 Hz, 1H, H), 6.93 (t, *J* = 7.8 Hz, 1H, H), 6.67 (d, *J* = 7.8 Hz, 1H, H), 6.38 (t, *J* = 7.8 Hz, 1H, H), 5.89 (d, *J* = 7.6 Hz, 1H, H), 4.40 (s, 1H, H-4), 1.20 (s, 9H,CH_3).

^{13}C NMR (75 MHz, $CDCl_3$) δ 178.55 (C=O), 164.14 (C=N), 141.65 (Cq), 140.88 (Cq), 135.54 (Cq), 130.27 (CH), 129.85 (C-Cl), 129.17 (CH), 128.62 (CH), 128.06 (CH), 127.60 (CH), 127.03 (CH), 125.72 (CH), 124.79 (CH), 123.70 (Cq), 121.52 (CH), 109.49 (CH), 77.95 (Cspiro), 61.79 (CH-4), 34.93 ($\underline{C}(CH_3)_3$), 29.51 ($C(\underline{C}H_3)_3$). Anal. Mass for C26H23ClN3O: 429.2, Found: 430.3.

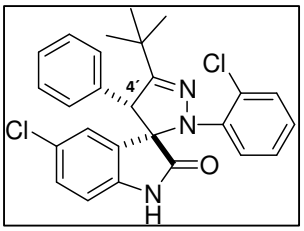

5'-(tert-butyl)-5-chloro-2'-(2-chlorophenyl)-4'-phenyl-2',4'-dihydrospiro[indoline-3,3'-pyrazol]-2-one (2v)

Following the general procedure, to a solution of **3b** (0.05g, 0.02mmol) in CH_2Cl_2 (2ml) was added **4e** (0.12g, 0.41mmol, 3 eq) and N,N-Diisopropylethylamine (0.118 mL, 0.068 mmol, 3 eq.). Reaction time: 21 hours. The compound was purified by flash chromatography (eluent: EtOAc/*n*-Hexane 1:4) to afford compound **2v** as a white solid (0.03, 0.05mmol, 27.5%).

IR (KBr): 3383 (NH), 1722 (C=O), 1620 (C=N) cm^{-1}.

^{1}H NMR (300 MHz, $CDCl_3$) δ 8.56 (s, 1H, NH), 7.57 – 7.38 (m, 2H, H, H), 7.33 – 7.22 (m, 3H, H), 7.20 – 7.06 (m, 3H, H), 6.95 (d, *J* = 5.5 Hz, 2H, H), 6.61 (d, *J* = 7.1 Hz, 1H, H), 5.78 (s, 1H, H), 4.39 (s, 1H, H-4), 1.20 (s, 9H, CH_3).

^{13}C NMR (75 MHz, $CDCl_3$) δ 178.34 (C=O), 164.16 (C=N), 141.42 (Cq), 139.48 (Cq), 134.91 (Cq), 130.39 (CH), 129.81 (C-Cl), 129.10 (CH), 128.42 (CH), 127.91 (CH), 127.16 (C-Cl), 126.93 (CH), 126.11 (CH), 125.45 (Cq), 124.95 (CH), 110.47 (CH), 78.18 (Cspiro), 61.93 (CH-4), 34.94 ($\underline{C}(CH_3)_3$), 29.48 ($C(\underline{C}H_3)_3$). Anal. Mass for C26H23Cl2N3O: 463.1, Found: 464.3.

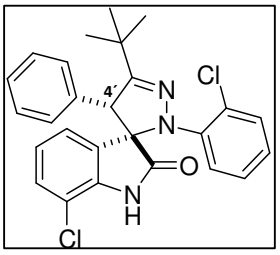

5'-(tert-butyl)-7-chloro-2'-(2-chlorophenyl)-4'-phenyl-2',4'-dihydrospiro[indoline-3,3'-pyrazol]-2-one (2x)

Following the general procedure, to a solution of **3d** (0.07g, 0.27mmol) in CH_2Cl_2 (2ml) was added **4e** (0.11g, 0.45mmol, 1.5 eq) and N,N-Diisopropylethylamine (0.13 mL, 0.82 mmol, 3 eq.). Reaction time: 22h20min. The compound was purified by flash chromatography (eluent: EtOAc/*n*-Hexane 1:4) to afford compound **2x** as a white solid (0.09, 0.2mmol, 70.8%).

IR (KBr): 3407 (NH), 1712 (C=O), 1620 (C=N) cm^{-1}.

^{1}H NMR (300 MHz, $CDCl_3$) δ 7.51 (s, 1H, NH), 7.35 (dd, *J* = 8.6, 1.6 Hz, 1H, H), 7.26 (m, 3H, H), 7.20 – 7.10 (m, 3H, H), 7.01 – 6.93 (m, 2H, H), 6.68 (s, 1H, H), 6.40 – 6.29 (m, 1H, H), 5.83 (d, *J* = 7.6 Hz, 1H, H), 4.42 (s, 1H, H-4), 1.19 (s, 9H, CH_3).

^{13}C NMR (75 MHz, $CDCl_3$) δ 177.63 (C=O), 164.32 (C=N), 141.50 (Cq), 138.70 (Cq), 135.14 (Cq), 130.16 (C-Cl), 129.14 (CH), 128.24 (CH), 127.19 (CH), 126.22 (CH), 125.94 (CH), 125.53 (CH), 125.18 (Cq), 122.22 (CH), 114.54 (C-Cl), 78.97 (Cspiro), 61.97 (CH-4), 34.92 ($\underline{C}(CH_3)_3$), 29.46 ($C(\underline{C}H_3)_3$). Anal. Calc. for $C_{26}H_{23}Cl_2N_3O.0.05H_2O$: C 67.24, H 5.00, N 9.05, Found: C 69.62, H 5.12, N 9.19.

6.2. STABILITY

6.2.1. HPLC Analysis

High-performance liquid chromatography (HPLC) measurements were carried out using a VWR HITACHI assembly equipped with a UV detector L-2400, a column oven L-2300, and a pump L-2130. An injection valve equipped with 20µL sample loop was used. The separation was performed on a LichroCART® RP-18 (5µm, 250-4 mm) analytical column (Merck). Acetonitrile: H2O (95:5, v:v) was used as eluent system for compounds. Elution was performed at a solvent flow rate of 1 mL/min. Chromatograms were monitored by UV

detection at 263 nm. All analyses were performed at 35 ºC. Acquisition and treatment of data were done using Ezchrom Elite software.

6.2.2. Stability in pH 7.4 Phosphate Buffer

For this part of the project, 250µL of a 10^{-3}M stock solution of tested compounds in DMSO were added to 2.5mL of potassium phosphate buffer solution (pH 7.4, 0.5M) at 37ºC. At appropriate intervals, samples (100µL) and analyzed by HPLC using the methodology previously described. The stability was assessed for a period of 72 hours.

6.3. BIOLOGY

6.3.1. Cell lines: tissue types, handling and maintenance

The cell lines used in this work are summarized in Table 8. Further, primary cultures of mouse mixed glial cells were also used.

Table 6 - Cell line general characterization.

Cell Line Designation	Disease	Organism	Morphology	Culture properties	Growth media % in (v/v)
HCT-116 $^{+/+}$	Colorectal carcinoma	Human	Epithelial	Adherent	McCoy´s; 10 % FBS; 1% Pen/Strep
HCT-116 $^{-/-}$	Colorectal carcinoma	Human	Epithelial	Adherent	McCoy´s; 10% FBS; 1% Pen/Strep
GL-261	Glioma	Mouse	-	Adherent	DMEM; 10% FBS; 1% Pen/Strep
MCF-7	Brest adenocarcinoma	Human	Epithelial	Adherent	RPMI 1640; 10% FBS; 1% Pen/Strep 2mM L-glutamine
MDA-MB-231	Brest adenocarcinoma	Human	Epithelial	Adherent	RPMI 1640; 10% FBS; 1% Pen/Strep 2mM L-glutamine
Hek-293T	Normal	Human	Epithelial	Adherent	RPMI 1640; 10% FBS; 1% Pen/Strep 2mM L-glutamine
CCD-18Co	Normal	Human	Fibroblast	Adherent	DMEM; 10% FBS 1% Pen/Strep 1% Glutamax; 1% NEAA; 0.025% TNF-α Human

All cell lines were cultivated and maintained in 75 cm^2 BD vented cell culture flasks (BD Biosciences, New Jersey, EUA) in a CO_2 incubator at 37ºC and humidified atmosphere of 5% CO_2.

Culture cell renewal was performed when cells reached approximately 80% confluence, which represents the critical point when cells start to detach and degenerate due to lack of

nutrients and contact inhibition. Briefly, cells were detached by adding TrypLE reagent (Gibco, Thermo Fisher Scientific, Waltham, USA) and incubate for 5 min in the CO_2 incubator. After that, cell suspension was transferred into 15 mL tubes and centrifuged at 500 *g* for 5 min at room temperature. Cell pellet was then resuspended in fresh medium and subsequently incubated at 37ºC and 5% (v/v) CO_2 for further usage.

Primary mouse mixed glial cultures were performed and kindly provided by Pedro Dionísio from Prof. Cecília Rodrigues' group within iMed.ULisboa. Briefly, the cerebral hemispheres of 2-day-old mice were isolated and the meninges and blood vessels were removed, as described previously[95]. Cells were collected by passing the tissue, in DMEM F12 containing antibiotics and fungicide, through a series of nylon screens with decreasing pore sizes. Cells were then centrifuged (300 *g*, 10 min) and resuspended in DMEM F12 containing 10% FBS. The cell suspension was distributed into 96-well plates and incubated at 37°C in a humidified atmosphere of 5% CO_2. Medium was replaced every 3 days. Confluent cultures (21 days) were used for compound testing.

6.3.2. Evaluation of cell death and viability

HCT-116 and GL-261 cells were plated in 96-well plates at $5x10^3$ cells/well, while CCD18-co colon fibroblasts and primary mouse mixed glial cells at $4x10^3$ cells/well. Hek-293T, MCF-7 and MDA-MB-231 cells were cultured and maintained by Prof. Lídia Gonçalves from iMed.ULisboa. These cells were plated in 96-well plates at $1x10^4$ cells/well.

Viable cells were counted by the Trypan blue exclusion method in a hemocytometer from a mixture of 9:1 of Trypan blue at 0.4% (v/v) (Sigma, St. Louis, United States of America) and cellular suspension, using equation (1)

(1) $$Cells/mL = \frac{Total\ cell\ count\ from\ quadrant}{4} \times 10\ (Dilution\ Factor) \times 10^4\ (Chamber\ Volume)$$

Compounds were dissolved in DMSO and diluted in culture medium to appropriate in range concentrations of µM.

Twenty-four hours after cell plating, media was removed and replaced with fresh medium containing each compound in the appropriate concentration for additional 48 h/72 h (Scheme 5). The same amount of DMSO was added to control cells. Cell viability and cell death were analyzed by standard methods as detailed below.

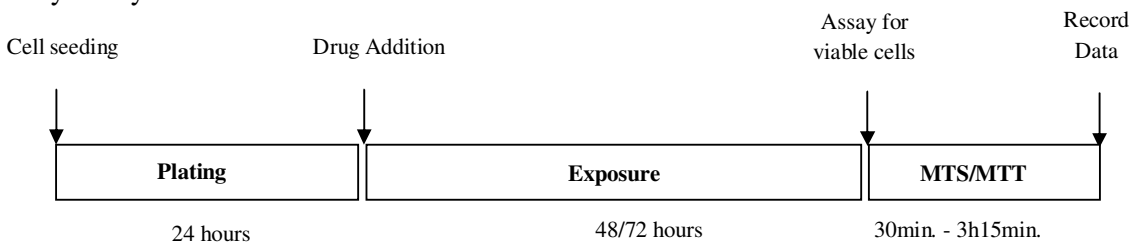

Scheme 5 - Schematic diagram of compound incubation.

Cell viability was evaluated using the CellTiter 96® AQueous Non-Radioactive Cell Proliferation Assay (Promega, Madison, USA), according to the manufacturer's instructions. This homogenous, colorimetric method determines the number of viable cells in cytotoxicity assays. The assay is composed of 3-(4,5-dimethylthiazol-2-yl)-5-(3-carboxymethoxyphenyl)-2-(4-sulfophenyl)-2H-tetrazolium (MTS) and an electron coupling reagent phenazine methosulfate (PMS). MTS is bioreduced by cells into a formazan product that can be measured spectrophotometrically at 490 nm in a plate reader. The conversion of MTS into the formazan product is accomplished by dehydrogenase enzymes found in metabolically active cells, and is directly proportional to the number of viable cells in culture[96]. In brief, cell culture supernatants were replaced by 100 µL of MTS/PMS (19:1) solution prepared in fresh RPMI/ITSF, and cells incubated at 37°C for 30 min. Changes in absorbance were measured at 490 nm using GloMax® Multi Detection System (Sunnyvale, CA, USA).

For Hek-293T, MCF-7 and MDA-MB-231 cell lines, cell viability was assessed by Prof. Lídia Gonçalves using 3-(4,5-dimethyl-2-thiazolyl)-2,5-diphenyl-2H-tetrazolium bromide (MTT), a yellow, water-soluble tetrazolium dye that is converted by mitochondrial dehydrogenases in viable cells to a water-insoluble, purple formazan. The procedure is similar to the MTS assay. The main difference is that cell media was removed and replaced with fresh medium, the MTT dye solution was added to each well (5 mg/mL in 10mM phosphate buffer solution at pH 7.4). After an incubation period of 3h the media was removed and intracellular formazan crystals were solubilized and extracted with DMSO. After 15 min at room temperature absorbance was measured at 570nm in a microplate reader (FLUOstar Omega, BMG Labtech, Germany)[96].

Cell viability results for each concentration were normalized regarding the control samples and obtained accordingly to the following equation (2):

(2) $$Cell\ Viability\ (\%) = \frac{Sample\ Absorbance\ (490\ nm)}{Control\ Absorbance\ (490\ nm)} \times 100$$

General cell death was evaluated using the lactate dehydrogenase (LDH) Cytotoxicity Detection Kit^{PLUS} (Roche Diagnostics GmbH, Manheim, Germany), according to the manufacturer's instructions. The LDH assay measures membrane integrity as a function of the amount of cytoplasmic LDH released into the medium that can be quantified by a coupled enzymatic reaction. In the first step, LDH catalyzes the conversion of lactate to pyruvate via reduction of NAD^+ to NADH. In the second step, diaphorase uses NADH to reduce a tetrazolium salt (INT) to a red formazan product. Thus, the level of formazan is directly proportional to the amount of LDH released, which is indicative of cytotoxicity. Hence, 50 µL of supernatant from treated cells was transferred into a new 96-well plate and then incubated with 50 µL of assay substrate for 10 to 30 min, at room temperature, protected from light.

Absorbance readings were measured at 490 nm, with 620 nm reference wavelength using a Bio-Rad Model 680 microplate reader.

The percentage of cellular death induced by compounds incubation was determined using Excel and a non-linear regression in GraphPad PRISM software.

6.3.3. IC_{50} determination

To determine the dose-response curves and the concentration that inhibited cell growth by 50% (IC_{50}) of the lead compounds, we used GraphPad Prism v.5.00 (GraphPad Software, San Diego, CA, USA) with the log (inhibitor) *versus* response function. In all cases, DMSO was used as control.

6.3.4. Evaluation of Apoptosis by Flow Cytometry (Guava Nexin assay)

Annexin V-FITC (Fluorescein Isothiocyanate) and and 7-Aminoactinomycin D (7-AAD) double staining is a common procedure to discriminate viable cells, early apoptotic and late apoptotic cells. Loss of plasma membrane asymmetry is one of the earliest features of apoptosis. In apoptotic cells, the membrane phospholipid phosphatidylserine (PS) is translocated from the inner to the outer leaflet of the plasma membrane, thereby exposing PS to the external cellular environment. Annexin V is a protein with high affinity for PS, and binds to exposed apoptotic cell surface PS. Annexin V can be conjugated to fluorochromes while retaining its high affinity for PS and thus serves as a sensitive probe for flow cytometric analysis of cells undergoing apoptosis. PS translocation precedes the loss of membrane integrity, which accompanies the later stages of cell death. Therefore, staining with Annexin V is typically used in conjunction with a vital dye such as and 7-Aminoactinomycin D (7-AAD) for identification of early and late apoptotic cells. Viable cells with intact membranes exclude 7-AAD, whereas the membranes of dead and damaged cells are permeable to 7-AAD[97–99].

HCT-116 $p53^{(+/+)}$ and MDA-MB-231 cells were plated in 24-well plates at $5x10^4$ and $2.5x10^4$ cells/well, respectively. Twenty-four hours after plating, cells were exposed to: 1) compounds in test at IC_{50} concentration; 2) compounds in test at $2xIC_{50}$ concentration, and 3) DMSO (control group), for 72 h. After that, the culture medium was collected and cells dettached with Accutase. Cells were collected and centrifuged at 500 *g* for 5 minutes at 4°C. The cell pellet was resuspended in PBS/2% FBS. Subsequently, 50 µL of cell suspension were mixed with 50 µL of Guava Nexin reagent and incubated for 20 minutes, at room temperature in the absence of light. Following the staining procedure, sample acquisition and data analysis of at least 5000 events per sample were performed using the Guava easyCyte™ Flow Cytometer (Merck Millipore) and Nexin software module.

6.3.5. Cell Cycle Analysis

The effects of compounds on cell cycle progression were verified using a standard propidium iodide staining procedure followed by flow cytometry analysis. Propidium iodide is a fluorescent intercalating agent that has high affinity to nucleic acids[100,101].

HCT116 *p53*$^{+/+}$and MCF-7 cells were plated in 6-well plates at 1.5×10^5 cells/well. Twenty-four hours after plating, cells were treated with the compounds in test at the IC_{50} concentration, or DMSO, for additional 24 or 48 h. After that, cells were detached with Tryple reagent and collected by centrifuged at 800 *g* for 5 min, at 4ºC. Cell pellets were resuspended in cold PBS and added an equal volume of 80% ice-cold ethanol (-20ºC) drop by drop, while vortexing gently. Samples were stored at -4ºC until data acquisition. For cell cycle analysis, cells were centrifuged again at 850*g* for 5 minutes, at 4ºC, and cell pellets were resuspended in 25µg/mL propidium iodide (PI) (Fluka, Sigma-Aldrich) and 50µg/mL RNase A (Sigma-Aldric) and further incubated for 30 min. Sample acquisition and data analysis were performed using the Guava easyCyte^{TM} Flow Cytometer (Merck Millipore) and Guava analysis software, with the acquisition of at least 10000 events per sample[102,103].

6.3.6. Total protein extraction

HCT-116 *p53*$^{(+/+)}$ and MDA-MB-231 cells were plated in 60 mm dishes at $8\text{x}10^5$ and $5\text{x}10^5$ cells/dish. Twenty-four hours after plating, cells were exposed to the compounds in test at the IC_{50} and $2\text{x}IC_{50}$ concentration, or vehicle control (DMSO), for additional 72 h. After that, floating and adherent cells were collected directly in nonyl phenoxypolyethoxylethanol (NP-40) lysis buffer (1% NP-40, 20 mM Tris-HCl pH 7.4, 150 mM NaCl, 5 mM EDTA, 10% Glycerol, 1 mM dithiothreitol (DTT), and 1X proteases and phosphatases inhibitors), followed by sonication and centrifugation at 3200 *g* for 10 min at 4°C. Total protein extracts were recovered and stored at - 80 ºC.

Protein concentration was determined by the colorimetric Bradford method using the Bio-Rad Protein Assay reagent (Bio-Rad), according to the manufacturer's instructions. BSA (Sigma-Aldrich) was used as standard, and absorbance measurements were performed at 595 nm using GloMax-Multi+ Detection System (Promega). Protein concentrations were interpolated from the BSA standard curve using Excel Software.

6.3.7. Western blot analysis and densitometric analysis

Steady-state protein production was determined by Western blot analysis. Briefly, total protein extracts were separated on 8% and 14% (w/v) sodium dodecyl sulfate (SDS) - polyacrylamide gel electrophoresis and transferred onto nitrocellulose membranes using the Trans-blot Turbo Transfer System (Biorad). Uniform protein loading and transfer was confirmed by transient staining with 0.2% Ponceau S (Merck, Darmstadt, Germany). Next,

nonspecific binding sites were blocked with a 5% milk solution in Tris-buffered saline (TBS) for 1 h. Membranes were then incubated overnight at 4°C with a mouse monoclonal anti-p53 (Pab-240, sc-99, 1:200), anti-MDM2 (SMP-14, sc-965, 1:200), anti-caspase-3 (H-277, sc-7148, 1:100) and anti-Parp-1/2 (H-250, sc-7150, 1:2000) (Santa Cruz Biotechnology, Santa Cruz, CA). Membranes were then washed three times with TBS containing 0.2% Tween 20 (TBS-T), and incubated with anti-rabbit or anti-mouse secondary antibodies conjugated with horseradish peroxidase (Bio-Rad) for 2 h at room temperature. After rinsing three times with TBS-T, the immunoreactive complexes were visualized by chemiluminescence with Immobilon™ Western (Milipore) or SuperSignal West Femto substrate (Thermo Fisher Scientific, Inc.). Ponceau was used as loading control. Densitometric analysis was performed with the Image Lab software Version 5.1 Beta (Bio-Rad).

6.3.8. Evaluation of caspase-3/7 activity

Caspase-3 and -7 activities were measured using the Caspase-Glo 3/7 Assay (Promega). This assay is based on the cleavage of a pro-luminescent substrate containing the specific DEVD sequence recognized by caspase-3 and -7 to release aminoluciferin in cell lysates. The subsequent luciferase cleavage of the unconjugated aminoluciferin generates a luminescent signal directly proportional to the amount of caspase activity present in the sample. In a 96-well plate were incubated 15µg of total protein extracts from HCT-116 and MDA-MB-231 cells, in 50µL of total volume and 50µL of caspase-Glo 3/7 reagent. Subsequently the mixture was incubated at room temperature for 30 min, leading to stabilization of substrate cleavage by caspases, and accumulation of luminescent signal[104,105]. The resulting luminescence was measured using the GloMax-Multi+ Detection System (Promega).

The data were analyzed using Excel and GraphPad PRISM software.

6.3.9. Combined Therapy Strategies

The objective of drug combination therapies is to achieve improved therapeutic results.

In this project, the commercial chemotherapeutic drug used is described in Table 9 and it was kindly provided by the laboratory of Prof. Cecilia Rodrigues in collaboration with the hospital pharmacy of Hospital Santa Maria in Lisboa.

Table 7 - Main feature of commercial chemotherapeutic drug used in the course of this project described as drug denomination, molecular weight, solvent, manufacturing company and molecular target.

Drug Denomination	Molecular weight (gmol-1)	Solvent	Manufacturing company	Molecular target
5-Fluorouracil	130.08	PBS	Accord	Inhibitor of thymidylate synthetase[88,89]

6.3.9.1. Cytotoxic potential evaluation

HCT116 $p53^{(+/+)}$ cells were plated as mentioned above. However, instead of incubating cells with compounds at IC_{50} concentration for 72 hours, the following combined strategies were applied:

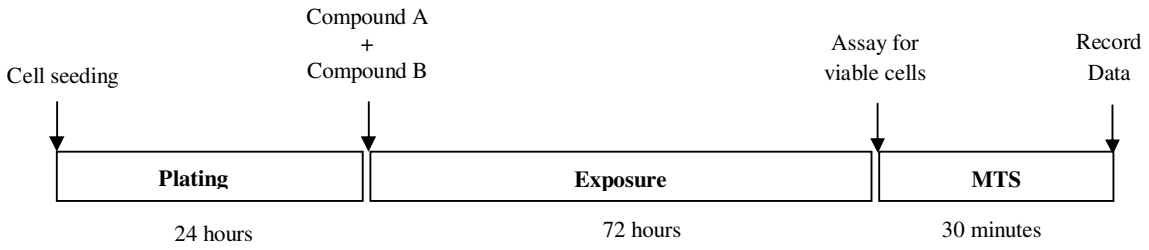

Scheme 6 - Cytotoxic potential evaluation. The cells per well were seeded in 96-well plate at 37ºC, humidified atmosphere of 99% and 5% (v/v) CO2, and 24 hours later the cells were exposed to compounds A and B for more 72 hours in the same conditions. Then, each well was aspirated and 100 µL of a solution mixture of complete culture medium, MTS and PMS (100:19:1) were pipetted to each well. After 30 minutes of incubation the absorbance at 490nm was read in a microplate reader.

Where A is the spiropyrazoline oxindole compound tested and B is the commercial drug. The strategy combines both A and B drugs at appropriate concentrations. In the control groups equivalent amounts of DMSO were added.

The data were analyzed using Excel and GraphPad PRISM software using the following equation:

(3) $$CDI = \frac{AB}{AxB}$$

Where CDI is coefficient drug interaction, AB is the cell viability ratio of combinatory strategy, A is the cell viability ratio of single agent A and B is the cell viability ratio of single agent B. Coefficient drug interaction (CDI) is a tool to analyze interaction between drugs allowing distinguishing synergistic, additive and antagonistic effects. For CDI values < 1, drugs have a synergistic effect, for CDI = 1, drugs have an additive effect and for CDI values > 1, drugs have an antagonistic effect[86,106–115].

6.3.10. Bimolecular Fluorescence Complementation (BiFC) Assay

To evaluate p53-MDM2 protein-protein interaction, HCT116 $p53^{(-/-)}$ cells were co-transfected using 1 µg of each BiFC pair plasmid and Lipofectamine 2000 (Invitrogen), following the manufacturer's instructions. 4–6 h after transfection, the medium was replaced with fresh medium, and the compounds in test were added to a final concentration of 5µM,

10μM and 20μM. Nutlin-3 at the same concentrations was used as positive control. Equal amounts of vehicle (DMSO) were used as control. Cells were washed twice with Ca^{2+} and Mg^{2+} free PBS (Invitrogen Corp.), treated with accutase and harvested with culture medium. Cell suspensions were centrifuged, supernatants discarded, and cell pellets resuspended in PBS. Fluorescence was measured using a Guava easyCyte™ Flow Cytometer[71,90].

6.3.11. Statistical analysis

Data were analyzed statistically using the GraphPad software. All data are presented as mean ± standard error of the mean (SEM) or mean ± standard deviation (SD) of at least three independent experiments. Differences between means were tested for significance using the Student's t-test (*$p < 0.05$; **$p < 0.01$; ***$p < 0.001$).

Chapter 7

REFERENCES

1. Jin, Z. & El-Deiry, W. S. Overview of cell death signaling pathways. *Cancer Biol. Ther.* **4,** 147–171 (2005).

2. Hanahan, D. & Weinberg, R. A. Hallmarks of Cancer: The Next Generation. *Cell* **144,** 646–674 (2011).

3. Bai, L. & Wang, S. Targeting Apoptosis Pathways for New Cancer Therapeutics. *Annu. Rev. Med.* **65,** 139–155 (2014).

4. International Agency for Research on Cancer & Cancer Research UK. World Cancer Factsheet. *Cancer Research UK* (2014). Available at: http://www.cancerresearchuk.org. (Accessed: 4th August 2016)

5. Torre, L. A., Siegel, R. L., Ward, E. M. & Jemal, A. Global Cancer Incidence and Mortality Rates and Trends--An Update. *Cancer Epidemiol. Biomarkers Prev.* **25,** 16–27 (2016).

6. World Health Organization (WHO). Cancer. *Media Center* (2015). Available at: http://www.who.int/mediacentre/factsheets/fs297/en/. (Accessed: 4th August 2016)

7. American Cancer Society. Treatment Types. *American Cancer Society, Inc.* (2016). Available at: http://www.cancer.org/treatment/treatmentsandsideeffects/treatmenttypes/. (Accessed: 8th August 2016)

8. Baskar, R., Lee, K. A., Yeo, R. & Yeoh, K.-W. Cancer and Radiation Therapy: Current Advances and Future Directions. *Int. J. Med. Sci.* **9,** 193–199 (2012).

9. Urruticoechea, a *et al.* Recent Advances in Cancer Therapy: An Overview. *Curr. Pharm. Des.* **16,** 3–10 (2010).

10. International Agency for Research on Cancer (IARC). Globocan 2012: Estimated Cancer Incidence, Mortality and Precalence Worldwide in 2012. (2016). Available at: http://globocan.iarc.fr. (Accessed: 9th August 2016)

11. Ferlay, J. *et al.* Cancer incidence and mortality patterns in Europe: Estimates for 40 countries in 2012. *Eur. J. Cancer* **49,** 1374–1403 (2013).

12. American Cancer Society. Colorectal Cancer - Facts & Figures 2014-2016. (2014).

13. American Cancer Society. Colorectal Cancer Treatment. *American Cancer Society, Inc.* (2015). Available at: http://www.cancer.org/cancer/colonandrectumcancer/detailedguide/colorectal-cancer-treating-general-info. (Accessed: 9th August 2016)

14. American Cancer Society. Breast Cancer in Men. *American Cancer Society, Inc* (2016). Available at: http://www.cancer.org/cancer/breastcancerinmen/detailedguide/breast-cancer-in-men-what-is-breast-cancer-in-men. (Accessed: 10th August 2016)

15. Polyak, K. Heterogeneity in breast cancer. *J. Clin. Invest.* **121,** 3786–3788 (2011).

16. Knobf, T. in *Psycho-Oncology* 134–138 (Oxford University Press, 2015). doi:10.1093/med/9780199363315.003.0020

17. Haque, R. *et al.* Impact of Breast Cancer Subtypes and Treatment on Survival: An Analysis Spanning Two Decades. *Cancer Epidemiol. Biomarkers Prev.* **21,** 1848–1855 (2012).

18. American Cancer Society. How is breast cancer treated? *American Cancer Society, Inc* (2016). Available at: http://www.cancer.org/cancer/breastcancer/detailedguide/breast-cancer-treating-general-info. (Accessed: 11th August 2016)

19. Ohgaki, H. & Kleihues, P. Genetic alterations and signaling pathways in the evolution of gliomas. *Cancer Sci.* **100,** 2235–2241 (2009).

20. Lefranc, F., Rynkowski, M., DeWitte, O. & Kiss, R. in *Advances and technical standards in neurosurgery* **34,** 3–35 (2009).

21. Weathers, S. & Gilbert, M. Advances in treating glioblastoma. *F1000Prime Rep.* **6,** 1–9 (2014).

22. Saha, T., Kar, R. K. & Sa, G. Structural and sequential context of p53: A review of experimental and theoretical evidence. *Prog. Biophys. Mol. Biol.* **117,** 250–263 (2015).

23. Baig, S. *et al.* Potential of apoptotic pathway-targeted cancer therapeutic research: Where do we stand? *Cell Death Dis.* **7,** e2058 (2016).

24. Koff, J., Ramachandiran, S. & Bernal-Mizrachi, L. A Time to Kill: Targeting Apoptosis in Cancer. *Int. J. Mol. Sci.* **16,** 2942–2955 (2015).

25. Grivicich, I., Regner, A. & Rocha, A. B. da. Apoptosis: Programmed Cell Death. *Rev. Bras. Cancerol.* **53,** 335–343 (2007).

26. Hassan, M., Watari, H., AbuAlmaaty, A., Ohba, Y. & Sakuragi, N. Apoptosis and Molecular Targeting Therapy in Cancer. *Biomed Res. Int.* **2014,** 1–23 (2014).

27. Favaloro, B., Allocati, N., Graziano, V., Di Ilio, C. & De Laurenzi, V. Role of Apoptosis in disease. *Aging (Albany. NY).* **4,** 330–349 (2012).

28. Bai, L. & Wang, S. Targeting apoptosis pathways for new cancer therapeutics. *Annu Rev Med* **65,** 139–155 (2014).

29. Wade, M., Wang, Y. V & Wahl, G. M. The p53 orchestra: Mdm2 and Mdmx set the tone. *Trends Cell Biol.* **20,** 299–309 (2010).

30. Joerger, A. C. & Fersht, A. R. The p53 Pathway: Origins, Inactivation in Cancer, and Emerging Therapeutic Approaches. *Annu. Rev. Biochem.* **85,** 375–404 (2016).

31. Shadfan, M., Lopez-Pajares, V. & Yuan, Z.-M. MDM2 and MDMX: Alone and together in regulation of p53. *Transl. Cancer Res.* **1,** 88–89 (2012).

32. Pei, D., Zhang, Y. & Zheng, J. Regulation of p53: a collaboration between Mdm2 and Mdmx. *Oncotarget* **3,** 228–235 (2012).

33. Shaw, D., Clamp, A. & Jayson, G. C. Angiogenesis as a target for the treatment of ovarian cancer. *Curr. Opin. Oncol.* **25,** 558–565 (2013).

34. Muller, P. A. J. & Vousden, K. H. Mutant p53 in Cancer: New Functions and Therapeutic Opportunities. *Cancer Cell* **25,** 304–317 (2014).

35. Yu, X., Narayanan, S., Vazquez, A. & Carpizo, D. R. Small molecule compounds targeting the p53 pathway: Are we finally making progress? *Apoptosis* **19,** 1055–1068 (2014).

36. Zawacka-Pankau, J. & Selivanova, G. Pharmacological reactivation of p53 as a strategy to treat cancer. *J. Intern. Med.* **277,** 248–259 (2015).

37. Kruse, J.-P. & Gu, W. Modes of p53 Regulation. *Cell* **137,** 609–622 (2009).

38. Hu, C.-Q. & Hu, Y.-Z. Small Molecule Inhibitors of the p53-MDM2. *Curr. Med. Chem.* **15,** 1720–1730 (2008).

39. Zhao, Y., Bernard, D. & Wang, S. Small Molecule Inhibitors of MDM2-p53 and MDMX-p53 Interactions as New Cancer Therapeutics. *Biodiscovery* **8,** 4 (2013).

40. Hoe, K. K., Verma, C. S. & Lane, D. P. Drugging the p53 pathway: understanding the route to clinical efficacy. *Nat. Rev. Drug Discov.* **13,** 217–236 (2014).

41. Nero, T. L., Morton, C. J., Holien, J. K., Wielens, J. & Parker, M. W. Oncogenic protein interfaces: small molecules, big challenges. *Nat. Rev. Cancer* **14,** 248–62 (2014).

42. Loregian, A. & Palù, G. Disruption of protein–protein interactions: Towards new targets for chemotherapy. *J. Cell. Physiol.* **204,** 750–762 (2005).

43. Li, Q. & Lozano, G. Molecular pathways: Targeting Mdm2 and Mdm4 in cancer therapy. *Clin. Cancer Res.* **19,** 34–41 (2013).

44. Graves, B. *et al.* Activation of the p53 pathway by small-molecule-induced MDM2 and MDMX dimerization. *Proc. Natl. Acad. Sci.* **109,** 11788–11793 (2012).

45. Joseph, T. L., Madhumalar, A., Brown, C. J., Lane, D. P. & Verma, C. Differential binding of p53 and nutlin to MDM2 and MDMX: Computational studies. *Cell Cycle* **9,** 1167–1181 (2010).

46. Popowicz, G. M. *et al.* Structures of low molecular weight inhibitors bound to MDMX and MDM2 reveal new approaches for p53-MDMX/MDM2 antagonist drug discovery. *Cell Cycle* **9,** 1104–1111 (2010).

47. Hu, L., Zhang, H., Bergholz, J., Sun, S. & Xiao, Z.-X. J. MDM2/MDMX: Master negative regulators for p53 and RB. *Mol. Cell. Oncol.* **3,** e1106635 (2016).

48. Vazquez, A., Bond, E. E., Levine, A. J. & Bond, G. L. The genetics of the p53 pathway, apoptosis and cancer therapy. *Nat. Rev. Drug Discov.* **7,** 979–987 (2008).

49. Chao, C. C.-K. Mechanisms of p53 degradation. *Clin. Chim. Acta* **438,** 139–147 (2015).

50. Wang, X. & Jiang, X. Mdm2 and MdmX partner to regulate p53. *FEBS Lett.* **586,** 1390–1396 (2012).

51. Karni-Schmidt, O., Lokshin, M. & Prives, C. The Roles of MDM2 and MDMX in Cancer. *Annu. Rev. Pathol. Mech. Dis.* **11,** 617–644 (2016).

52. Vu, B. *et al.* Discovery of RG7112: A Small-Molecule MDM2 Inhibitor in Clinical

Development. *ACS Med. Chem. Lett.* **4,** 466–469 (2013).

53. Koblish, H. K. *et al.* Benzodiazepinedione inhibitors of the Hdm2:p53 complex suppress human tumor cell proliferation in vitro and sensitize tumors to doxorubicin in vivo. *Mol. Cancer Ther.* **5,** 160–169 (2006).

54. Wang, S. *et al.* SAR405838: An Optimized Inhibitor of MDM2-p53 Interaction That Induces Complete and Durable Tumor Regression. *Cancer Res.* **74,** 5855–5865 (2014).

55. Rew, Y. & Sun, D. Discovery of a small molecule MDM2 inhibitor (AMG 232) for treating cancer. *J. Med. Chem.* **57,** 6332–6341 (2014).

56. Tovar, C. *et al.* MDM2 small-molecule antagonist RG7112 activates p53 signaling and regresses human tumors in preclinical cancer models. *Cancer Res.* **73,** 2587–2597 (2013).

57. Burgess, A. *et al.* Clinical Overview of MDM2/X-Targeted Therapies. *Front. Oncol.* **6,** 1–7 (2016).

58. Grasberger, B. L. *et al.* Discovery and cocrystal structure of benzodiazepinedione HDM2 antagonists that activate p53 in cells. *J. Med. Chem.* **48,** 909–912 (2005).

59. Zhao, Y., Aguilar, A., Bernard, D. & Wang, S. Small-Molecule Inhibitors of the MDM2 – p53 Protein – Protein Interaction (MDM2 Inhibitors) in Clinical Trials for Cancer Treatment. *J. Med. Chem.* **58,** 1038–1052 (2014).

60. U.S. National Institutes of Health. ClinicalTrials.gov. (2016). Available at: https://clinicaltrials.gov/ct2/show/study/NCT01636479. (Accessed: 13th September 2016)

61. Lee, J. H. *et al.* Novel pyrrolopyrimidine-based α-helix mimetics: Cell-permeable inhibitors of protein-protein interactions. *J. Am. Chem. Soc.* **133,** 676–679 (2011).

62. Santos, M. M. M. Recent advances in the synthesis of biologically active spirooxindoles. *Tetrahedron* **70,** 9735–9757 (2014).

63. Estrada-Ortiz, N., Neochoritis, C. G. & Dömling, A. How To Design a Successful p53-MDM2/X Interaction Inhibitor: A Thorough Overview Based on Crystal Structures. *ChemMedChem* **11,** 757–772 (2016).

64. Ribeiro, C. J. A., Amaral, J. D., Rodrigues, C. M. P., Moreira, R. & Santos, M. M. M. Spirooxadiazoline oxindoles with promising in vitro antitumor activities. *Med. Chem. Commun.* **7,** 420–425 (2016).

65. Ribeiro, C., Rodrigues, C., Moreira, R. & Santos, M. Chemical Variations on the p53 Reactivation Theme. *Pharmaceuticals* **9,** 25 (2016).

66. Yu, B., Yu, D.-Q. & Liu, H.-M. Spirooxindoles: Promising scaffolds for anticancer agents. *Eur. J. Med. Chem.* **97,** 673–698 (2015).

67. Arulananda Babu, S., Padmavathi, R., Ahmad Aslam, N. & Rajkumar, V. in *Studies in Natural Products Chemistry* **46,** 227–339 (2015).

68. Karabacak, M. *et al.* Synthesis and Evaluation of New Pyrazoline Derivatives as Potential Anticancer Agents. *Molecules* **20,** 19066–19084 (2015).

69. Ribeiro, C. J. a, Amaral, J. D., Rodrigues, C. M. P., Moreira, R. & Santos, M. M. M. Synthesis and evaluation of spiroisoxazoline oxindoles as anticancer agents. *Bioorganic Med. Chem.* **22,** 577–584 (2014).

70. Monteiro, Â., Gonçalves, L. M. & Santos, M. M. M. Synthesis of novel spiropyrazoline oxindoles and evaluation of cytotoxicity in cancer cell lines. *Eur. J. Med. Chem.* **79,** 266–272 (2014).

71. Ribeiro, C. J. A., Amaral, J. D., Rodrigues, C. M. P., Moreira, R. & Santos, M. M. M. Synthesis and evaluation of spiroisoxazoline oxindoles as anticancer agents. *Bioorg. Med. Chem.* **22,** 577–584 (2014).

72. Zak, K. *et al.* Mdm2 and MdmX inhibitors for the treatment of cancer: a patent review (2011 – present). *Expert Opin. Ther. Pat.* **23,** 425–448 (2013).

73. Dadiboyena, S. Cycloadditions and condensations as essential tools in spiropyrazoline synthesis. *Eur. J. Med. Chem.* **63,** 347–377 (2013).

74. Pavlovska, T. L., Redkin, R. G., Lipson, V. V. & Atamanuk, D. V. Molecular diversity of spirooxindoles. Synthesis and biological activity. *Mol. Divers.* **20,** 299–344 (2015).

75. Zhang, C.-Y., Liu, X.-H., Wang, B.-L., Wang, S.-H. & Li, Z.-M. Synthesis and Antifungal Activities of New Pyrazole Derivatives via 1,3-dipolar Cycloaddition Reaction. *Chem. Biol. Drug Des.* **75,** 489–493 (2010).

76. Ziarani, G. M., Gholamzadeh, P. & Lashgari, N. Oxindole as starting material in organic synthesis. **2013,** 470–535 (2013).

77. Sun, L. *et al.* Synthesis and Biological Evaluations of 3-Substituted Indolin-2-ones: A Novel Class of Tyrosine Kinase Inhibitors That Exhibit Selectivity toward Particular Receptor Tyrosine Kinases. *J. Med. Chem.* **41,** 2588–2603 (1998).

78. Mokhtari, S. *et al.* Synthesis and cytotoxic evaluation of novel 3-substituted derivatives of 2-indolinone. *Iran. J. Pharm. Res. IJPR* **11,** 411–21 (2012).

79. Balderamos, M. *et al.* Synthesis and Structure-Activity Relationship Studies of 3-Substituted Indolin-2-ones as Effective Neuroprotective Agents. *Exp. Biol. Med.* **233,** 1395–1402 (2008).

80. Zhou, Y. *et al.* Design, synthesis and biological evaluation of 3-benzylidene 4-bromo isatin derivatives. *J. Chem. Pharm. Res.* **5,** 1024–1028 (2013).

81. Wolkoff, P. A New Method of Preparing Hydrazonyl Halides. *Can. J. Chem.* **53,** 1333–1335 (1975).

82. Patel, H. V., Vyas, K. A., Pandey, S. P. & Fernandes, P. S. Facile synthesis of hydrazonyl halides by reaction of hydrazones with N-halosuccinimide-dimethyl sulfide complex. *Tetrahedron* **52,** 661–668 (1996).

83. Zhao, Y. *et al.* Diastereomeric Spirooxindoles as Highly Potent and Efficacious MDM2 Inhibitors. *J. Am. Chem. Soc.* **135,** 7223–7234 (2013).

84. Giono, L. E. & Manfredi, J. J. The p53 tumor suppressor participates in multiple cell cycle checkpoints. *J. Cell. Physiol.* **209,** 13–20 (2006).

85. Somasundaram, K. Tumor suppressor p53: regulation and function. *Front. Biosci.* **5,** D424-37 (2000).

86. Foucquier, J. & Guedj, M. Analysis of drug combinations: current methodological landscape. *Pharmacol. Res. Perspect.* **3,** e00149 (2015).

87. Chou, T.-C. Drug Combination Studies and Their Synergy Quantification Using the Chou-Talalay Method. *Cancer Res.* **70,** 440–446 (2010).

88. National Center for Biotechnology Information. 5-Fluorouracil. *PubChem - Open Chemistry Database* Available at: https://pubchem.ncbi.nlm.nih.gov/compound/5-Fluorouracil#section=Top. (Accessed: 26th August 2016)

89. 5-Fluorouracil. *Drug Bank* Available at: http://www.drugbank.ca/drugs/DB00544. (Accessed: 26th August 2016)

90. Amaral, J. D. *et al.* Live-cell imaging of p53 interactions using a novel Venus-based bimolecular fluorescence complementation system. *Biochem. Pharmacol.* **85,** 745–752 (2013).

91. Szatmari, T. *et al.* Detailed characterization of the mouse glioma 261 tumor model for experimental glioblastoma therapy. *Cancer Sci.* **97,** 546–553 (2006).

92. Bai, R.-Y., Staedtke, V. & Riggins, G. J. Molecular targeting of glioblastoma: Drug discovery and therapies. *Trends Mol. Med.* **17,** 301–312 (2011).

93. Rixe, O. & Fojo, T. Is Cell Death a Critical End Point for Anticancer Therapies or Is Cytostasis Sufficient? *Clin. Cancer Res.* **13,** 7280–7287 (2007).

94. Ribeiro, C. J. A. C. Design and synthesis of small molecule modulators of p53. (Universidade de Lisboa, 2015).

95. Saura, J., Tusell, J. M. & Serratosa, J. High-yield isolation of murine microglia by mild trypsinization. *Glia* **44,** 183–189 (2003).

96. Riss, T. L. *et al. Cell Viability Assays*. *Assay Guidance Manual* (Bethesda (MD): Eli Lilly & Company and the National Center for Advancing Translational Sciences, 2004).

97. Wlodkowic, D., Telford, W., Skommer, J. & Darzynkiewicz, Z. Apoptosis and Beyond: Cytometry in Studies of Programmed Cell Death. *Methods Cell Biol.* **104,** 55–98 (2011).

98. Guava Technologies. *Guava Nexin ® Reagent - For Labeling of Early Apoptotic Cells and Discriminating Between Early Apoptotic and Late Apoptotic/Dead Cells*. (2008).

99. eBioscience. *Flow Cytometry – BestProtocols. Viability Staining* (2010).

100. Invitrogen. *Propidium Iodide Nucleic Acid Stain*. *Molecular Probes - Invitrogen detection technologies* (2006).

101. Fried, J., Perez, A. G. & Clarkson, B. D. Flow cytofluorometric analysis of cell cycle distributions using propidium iodide. Properties of the method and mathematical analysis of the data. *J. Cell Biol.* **71,** 172–81 (1976).

102. Pereira, D. M. *et al.* MEK5/ERK5 signaling inhibition increases colon cancer cell sensitivity to 5-fluorouracil through a p53-dependent mechanism. *Oncotarget* **7,** (2014).

103. Simões, A. E. S. *et al.* Aberrant MEK5/ERK5 signalling contributes to human colon cancer progression via NF-κB activation. *Cell Death Dis.* **6,** e1718 (2015).

104. Progema. *Caspase-Glo(R) 3/7 Assay Technical Bulletin, TB323*. *Promega* (2015).

105. Maugg, D. *et al.* New Small Molecules Targeting Apoptosis and Cell Viability in Osteosarcoma. *PLoS One* **10,** e0129058 (2015).

106. Wang, D. *et al.* Two hour exposure to sodium butyrate sensitizes bladder cancer to anticancer drugs. *Int. J. Urol.* **15,** 435–441 (2008).

107. XU, S. *et al.* Synergistic effect of combining paeonol and cisplatin on apoptotic induction of human hepatoma cell lines. *Acta Pharmacol. Sin.* **28,** 869–878 (2007).

108. Tong, J. *et al.* Synergistic Antitumor Effect of Dichloroacetate in Combination with 5-Fluorouracil in Colorectal Cancer. *J. Biomed. Biotechnol.* **2011,** 1–7 (2011).

109. Jiang, Y. Nicotinamide-mediated inhibition of SIRT1 deacetylase is associated with the viability of cancer cells exposed to antitumor agents and apoptosis. *Oncol. Lett.* **6,** 600–604 (2013).

110. Torigoe, S., Ogata, Y., Matono, K. & Shirouzu, K. Molecular mechanisms of sequence-dependent antitumor effects of SN-38 and 5-fluorouracil combination therapy against colon cancer cells. *Anticancer Res.* **29,** 2083–2089 (2009).

111. Reynolds, C. P. & Maurer, B. J. in *Chemosensitivity* **110,** 173–184 (2005).

112. Zhou, X. *et al.* Azithromycin Synergistically Enhances Anti-Proliferative Activity of Vincristine in Cervical and Gastric Cancer Cells. *Cancers (Basel).* **4,** 1318–1332 (2012).

113. Chen, L. *et al.* Autophagy Inhibition Contributes to the Synergistic Interaction between EGCG and Doxorubicin to Kill the Hepatoma Hep3B Cells. *PLoS One* **9,** e85771 (2014).

114. Xu, S.-P. Antiproliferation and apoptosis induction of paeonol in HepG 2 cells. *World J. Gastroenterol.* **13,** 250 (2007).

115. Uphoff, C. C. & Drexler, H. G. *Cancer Cell Culture*. *Methods in molecular biology* **731,** (2011).

116. Igney, F. H. & Krammer, P. H. DEATH AND ANTI-DEATH: TUMOUR RESISTANCE TO APOPTOSIS. *Nat. Rev. Cancer* **2,** 277–288 (2002).

117. Meek, D. W. Regulation of the p53 response and its relationship to cancer. *Biochem. J.* **469,** 325–346 (2015).

Errata da Dissertação: The therapeutic potential of small molecules p53-MDM protein-protein interaction inhibitors

Na página 24 onde se lê: "As p53 tumour" deve ler-se: "p53 tumour".

Na página 27 onde se lê: "activation (Figure 4)." deve ler-se: "activation (Figure 3).".

Na página 37, em Scheme 3 onde se lê: "Synthesis of hydrazonoyl **7** and hydrazonyl chlorides **4**." deve ler-se: "Synthesis of hydrazonoyl **7** and hydrazonyl chlorides **4**. (a) aqueous ethanol 20%, r.t., 2-3h, 81-99%; (b) NCS, $S(CH_3)_2$, 0°C, 15 min; -78°C, 1h, then allowed to warm up to r.t., 62-88%.".

Na página 41 onde se lê: "**SI** – (...) ratio MDA-MB-231 IC_{50}/MCF-7 IC_{50}." deve ler-se: "[a] IC_{50} determined by the MTT method after 48h compound incubation. Each value is the mean (IC_{50} ± SD) of three independent experiments; [b] IC_{50} determined by the MTS method after 72h compound incubation. Each value is the mean (IC_{50} ± SD) of three independent experiments performed in duplicate. (...) **SI** – (...) ratio MDA-MB-231 IC_{50}/MCF-7 IC_{50}."

Na página 43, na **Figure 9** onde se lê: "(...) fibroblasts (CCD-10co) following 72 h incubation ith compounds" deve ler-se: "(...) fibroblasts (CCD-18co) following 72 h compound incubation".

Na página 48, na **Figure 14** onde se lê: "Threshold- CDI value threshold (CDI=1)." deve ler-se: "Threshold- CDI value threshold (CDI=1). **2e**IC_{10}=9.5μM; **2e**IC_{20}=10.7μM; **2e**IC_{50}=13.0μM and **5-FU**IC_{10}=1.7μM; **5-FU**IC_{20}=2.2μM; **5-FU**IC_{50}=3.2μM.".

Na página 52 onde se lê: **Table 5**" deve ler-se: "**Table 7**".

Na página 53 onde se lê: "and growth arrest (...) expression levels." deve ler-se: "and cell cycle arrest (...) expression levels in HCT-116 $p53^{(+/+)}$ cell line.".

Na página 59 onde se lê: "**Figure 22**- fibroblasts (CCD-10co)" deve ler-se: "**Figure 23** – fibroblasts (CCD-18co)", e onde se lê: "**Figure 23**" deve ler-se: "**Figure 24**".

Na página 60 onde se lê: "**Figure 24**" deve ler-se: "**Figure 25**".

Na página 61 onde se lê: "G2/M and a dose dependent increase" deve ler-se: "G2/M and a significant increase".

Na página 63 onde se lê: "Compounds **2a**, **2e**, **2g**, **2i**, **2j**, **2l** and **2m**" deve ler-se: "Compounds **2b**, **2e**, **2g**, **2i**, **2j**, **2l**, **2m** and **2q**".

Na página 65 onde se lê: "the MDM2-p53 interaction" deve ler-se: "the p53-MDM2 interaction" e onde se lê: "MDM2 expression levels." Deve ler-se: "MDM2 expression levels in HCT-116 $p53^{(+/+)}$ cell line."

Nas páginas 69 a 80 especificou-se o tipo de base utilizada para cada composto sintetizado, e onde se lê: "CDCl3" deve ler-se: "$CDCl_3$".

Na página 88 deve ler-se: 6.3.11.Statistical analysis - Data were analyzed statistically using the GraphPad software. All data are presented as mean ± standard error of the mean (SEM) or mean ± standard deviation (SD) of independent experiments. Differences between means were tested for significance using the Student's t-test (*$p < 0.05$; **$p < 0.01$; ***$p < 0.001$).